VOT 75112

STRESS ANALYSIS OF LAMINATED COMPOSITE PLATES WITH EMBEDDED SHAPE MEMORY ALLOY USING FINITE ELEMENT METHOD

(ANALISA TEGASAN KE ATAS PLAT RENCAM BERLAPIS DENGAN ALOI MEMORI BENTUK TERBENAM MENGGUNAKAN KAEDAH UNSUR TERHINGGA)

SHAMSUL BIN SARIP
ZAINUDIN BIN A.RASID
MOHD ZAKI BIN HASSAN

RESEARCH VOTE NO:
75112

Jabatan Mekanikal
Kolej Sains dan Teknologi
Universiti Teknologi Malaysia

2006

ABSTRACT

Shape memory alloy (SMA) wires are embedded within laminated composite plates to improve structural behaviours such as buckling and vibration. A simple linear finite element model and its source codes were developed to study the effect of SMA on these structural behaviours. Two methods of improvements are used here: The active property tuning (APT) and the active strain energy tuning (ASET). Studies are conducted on the antisymmetric angle ply SMA laminated composite plates. The effects of several parameters such as the geometric, mechanical and transformation effects on the SMA improvements of critical loads and eigen frequencies of the SMA composite plates are studied. The plate-bending model used in this study was developed based on the first order shear deformation theory (FSDT) and the finite element model used is the serendipity quadrilateral element with 40 degree of freedom per element. The results show a significant improvement of critical loads of the SMA composite plates for the simply supported boundary condition. In the case of eigen frequencies, the level of effect comes in couples where the improvements are more significant for frequency couples of modes I and IV and III and VI while frequency couple of modes II and V shows less significant effect.

ABSTRAK

Aloi memori bentuk (AMB) telah dibenam di dalam plat rencam berlapis dalam usaha memperbaiki kelakuan seperti ledingan and getaran bagi struktur tersebut. Satu permodalan kaedah unsur terhingga berserta kod puncanya telah dibangunkan untuk mengkaji kesan AMB ke atas kelakuan struktur berkenaan. Dua kaedah pembaikan telah dilaksanakan: Kaedah penalaan sifat aktif and kaedah penalaan tenaga terikan aktif. Kajian telah dijalankan ke atas plat rencam AMB berlapis dari jenis lapis sudut tak simetri. Kesan parameter-parameter seperti geometri, mekanikal dan penjelmaan ke atas pembaikan SMA terhadap beban kritikal dan frekuensi eigen telah dikaji. Permodelan plat-lenturan dalam kajian ini adalah berasaskan teori ubah bentuk ricih tertib pertama dan unsur lapan nod dengan 40 darjah kebebasan bagi setiap unsur telah digunakan. Keputusan dari kajian menunjukkan pembaikan yang memberangsangkan pada beban kritikal bagi keadaan sempadan yang disokong mudah. Bagi pembaikan frekuensi eigen pula, tahap kesan pembaikan adalah berpasang-pasang seperti pasangan frekuensi bagi mode I dan IV serta III dan IV menunjukkan pembaikan yang besar manakala pasangan frekuensi bagi mode II dan V, pembaikan adalah kecil.

DEDIKASI

BUAT MEREKA YANG SEDAR DAN TIDAK SEDAR,
AKAN HAKIKAT…..
DUNIA TELAH JAUH MENINGGALKAN KITA.

TABLE OF CONTENTS

LIST OF TABLES

LIST OF FIGURES

LIST OF SYMBOLS AND ABBREVIATIONS

FUNDAMENTAL OF MECHANICS OF COMPOSITES :

A_{ij} = Extensional stiffness matrix components (i,j = 1,2,3)
B_{ij} = Extensional-Bending coupling matrix components (i,j = 1,2,3)
D_{ij} = Bending stiffness matrix components (i,j = 1,2,3)
E_1 = Young Modulus in fibre direction
E_2 , E_3 = Young Modulus in matrix direction
G_{ij} = Modulus of Rigidity (i, j = 1,2,3)
M_n, M_y, M_{xy} = Moment resultant in x, y and xy direction respectively
N_n, N_y, N_{xy} = Force resultant in x, y and xy direction respectively
S_{ij}^1 = Transverse shear stiffness matrix components (i,j = 1,2)
$\underline{Q_{ij}}$ = Reduced Stiffness Matrix components (i,j = 1,…5)
$\overline{Q_{ij}}$ = Transformed Reduced Stiffness Matrix components (i,j = 1,…5)
S_{ij} = Compliance matrix components ((i , j = 1,…6)
V_{xz}, V_{yz} = Transverse shear force resultant in xz and yz direction respectively
k = i^{th} layer, starting from the bottom (Figure3.4)
x,y,z = plate coordinates in x,y and z direction
t = total height of the plate
t_i = z - coordinate of the plate of the i^{th} layer

α_1 ,α_2 ,α_3 and α_4 = Constants associated with the HSDT used

SMA BRINSON'S MODEL PARAMETER

ξ = Total martensite volume fraction
ξ_{so} = Stress induced martensite volume fraction
ξ_s = Initial stress induced martensite volume fraction
ξ_T = Temperature induced martensite volume fraction
ξ_{To} = Initial temperature induced martensite volume fraction
D = SMA Young's Modulus
θ = Thermoelastic tensor
Ω = Transformation tensor.
σ_S = Critical Stress Start
σ_F = Critical Stress Finish
E_M = Martensite Young's Modulus
E_A = Austenite Young's Modulus
ε_L = Maximum Residual Strain
ε_0 = Initial Strain
M_F = Martensite Finish Temperature
M_S =Martensite Start Temperature
A_S = Austenite Start Temperature
A_F = Austenite Finish Temperature
C_M =Stress Influence Coefficient
C_A =Stress Influence Coefficient

k =spring constant
L =length of the wire
S =cross-sectional area of the wire

SMA MODELLING :

ε_1 = total strain in 1-direction,

ε_{1m} = Matrix strain in 1-direction

ε_{1a} = SMA strain in 1-direction

V_m = Volume fractions of the matrix

V_a = Volume fractions of the SMA

σ_{1a} = Stress of SMA in the 1-direction

σ_{1m} = Stress of the matrix material in 1-direction

E_a = SMA Young's modulus

E_{1m} = Young's modulus of matrix in 1-direction

α_s = Thermal expansion coefficient of the SMA

α_{1m} = Thermal expansion coefficient of the matrix in 1-directio

ΔT = Change of temperature

$\sigma_r = \sigma_1^r$ = Recovery stress obtained through SMA activation

$\{\sigma_1^r\}$ = Matrix of recovery stress in material direction

$\{\sigma_x^r\}$ = Matrix of recovery stress in arbitrary direction

FINITE ELEMENT MODELLING :

$[\overline{B}]$ = Matrix of total strain displacement matrix
$[B_b]$ = Matrix of bending strain displacement matrix
$[B_m]$ = Matrix of extensional strain displacement matrix
$[\overline{B}_m]$ = Matrix of total extensional strain displacement matrix
$[B_l]$ = Matrix of non-linear strain displacement matrix
$[B_o]$ = Matrix of linear strain displacement matrix
$[B_s]$ = Matrix of shear strain displacement matrix
$\{F\}$ = Matrix of external forces
$[K_o]$ = Matrix of linear stiffness matrix of the finite element model
$[K_\sigma]$ = Matrix of geometric stiffness matrix of the finite element model
$[K_L]$ = Matrix non-linear large displacement stiffness matrix of the finite element model
$[N_i]$ = Matrix of shape functions
$\overline{N_x}$, $\overline{N_y}$, $\overline{N_{xy}}$ = Force resultants of initial stress

$\overline{L_x}$, $\overline{L_y}$, $\overline{L_{xy}}$ = Force resultants of initial stress

$\overline{M_x}$, $\overline{M_y}$, $\overline{M_{xy}}$ = Moment resultants of initial stress

$\overline{L_x^1}$, $\overline{L_y^1}$, $\overline{L_{xy}^1}$ = Force resultants of initial stress

$\overline{M_x^1}$, $\overline{M_y^1}$, $\overline{M_{xy}^1}$ = Moment resultants of initial stress

$\overline{M_x^2}$, $\overline{M_y^2}$, $\overline{M_{xy}^2}$ = Moment resultants of initial stress

$N_{i,x}$, $N_{i,y}$ $= \frac{\partial N_i}{\partial x}, \frac{\partial N_i}{\partial y}$

P = Load

P_{CR} = Critical load

$\{a\}$ = Generalised displacement of any nodes

$\{\overline{a_i}\}$ = Nodal displacement

$\delta\{\overline{a}\}$ = Variations in nodal displacement

h = Total thickness of a plate

u,v,w = Displacement of a generic point in x,y and z directions respectively

u_o ,v_o ,w_o = Displacement of a mid-plane point in x,y and z directions respectively

$u_{o,x}$, $v_{o,x}$, $w_{o,x}$ $= \frac{\partial u_o}{\partial x}$, $\frac{\partial v_o}{\partial x}$, $\frac{\partial w_o}{\partial x}$

z = Coordinate value in thickness (z) direction

β = A constant to differentiate between two plate theories : FSDT and HSDT

ε_{ij} = Strain components

$\{\varepsilon\}$ = Matrix of total strain of a point

$\{\varepsilon_o\}$ = Matrix of linear strain of a point

$\{\varepsilon_m\}$ = Matrix of extensional strain of a point

$\{\varepsilon_b\}$ = Matrix of flexural strain of a point

$\{\varepsilon_s\}$ = Matrix of shear strain of a point

$\{\varepsilon_l\}$ = Matrix of non- linear strain of a point

ψ = Force function

λ = Critical load

λ_{ND} = Non-Dimensionalised critical load

χ = Load Parameter

θ_x , θ_y = Rotation about x and y axis, respectively

$\theta_{x,x}$, $\theta_{y,x}$ $= \frac{\partial \theta_x}{\partial x}$, $\frac{\partial \theta_y}{\partial x}$

σ_{ij} = Stress components

σ_{ij}^o = Initial stress components

RESULT :

E_1 = Young Modulus of fibre

E_2 = Young Modulus of matrix

G_{ij} = Modulus of rigidity (i,j = 1,2,3)

a	= Length of a plate
b	= Width of a plate
h	= Thickness of a plate
v_{ij}	= Poisson's Ratios (i,j = 1,2,3)
P	= Load
χ	= Load parameter
P_0	= Amount of load if $\chi = 1$

1. INTRODUCTION

1.1. Background and Motivation

The importance of fibre reinforced composite (FRC) related products cannot be denied in today's world. FRC has been used to replace traditional materials in many industries such as automotive, aerospace, marine and architectural structures [1]. We also frequently come across to FRC products such as sporting goods like tennis racquets and golf clubs in our daily life. The main advantages of the FRC is its outstanding high strength and stiffness to weight ratios which can result in weight saving. Furthermore the properties of composites such as thermal expansion and damping characteristic can be controlled by changing the fibre orientation and the stacking sequences of the laminated composites to suit designers' need [2]. One area that the weight efficiency and controllable properties of the FRC are crucial is the aerospace industry. This is because much portions of the structure in aircraft structures designed to be load carrying capacity components are made of thin flat or curved panels. Examples of these components are aircraft stabilizers, fuselage sections, missile nose and body sections. These components are subjected to both mechanical loads such as lateral pressure and edge compression loads and thermal load. As these loads are responsible for failures such as yielding and buckling failure, it is important to study the state of stress beside other behaviours such as vibration, buckling and post buckling of FRC plates.

The structural behaviours of FRC can be optimised by using the correct combination of FRC parameters such as lamination angle, number of layers, aspect ratios etc. However the improvement based on this optimization procedure is rather fully utilised. One method that can give improvement to structural behaviours is by employing passive treatment such as using structural stiffeners. This however can

override the weight efficiency advantage obtained from using the FRC. Researchers in the last decade have turn to new material technology such as the smart materials as an active treatment for improving structural behaviours of FRC plates.

Smart material is a class of materials that has inherent intelligence to react toward external stimuli such as heat, electrical field and electromagnetic field. This reaction will produce the desired functions such as changing the shape and modifying structural behaviours of a structure. Smart materials that react by inducing an amount of strain can be classified into several types: piezoelectric material, shape memory alloys (SMA), magnetostrictive materials, electrorheulogical fluids, electro-optic materials, electroacoustic materials and electromagnetic materials. SMA is a new type of functional materials that has been a subject of intensive researches in the last decade. This is due to its unique properties of one way shape memory effect (SME), two way shape memory effect, pseudoelasticity and high damping capacity. These properties allow the SMA to have functional abilities such as the high strain and stress recoveries that no conventional materials can provide [3].

Since the well-known finding of the Nickel-Titanium SMA in 1963 by Buehler and coworkers [5], intensive researches have made it possible for practical and theoretical applications of the SMA that cover a diversity of areas such as aerospace, automotive, medical, commercial appliance, sports, toys and apparels. Today, SMA has attracted much interest due to its ability to function as sensors and actuators simultaneously [6]. This property leads the SMA to the application of the smart or intelligent structure. A smart structure as shown schematically in figure 1 combines actuators, sensors and a control mechanism that allow them to sense external stimuli and response in a predetermined manner [7].

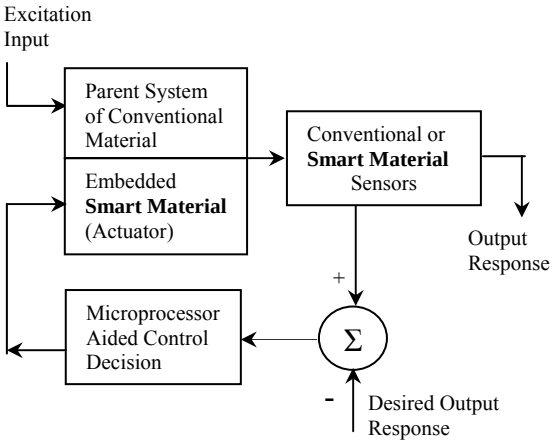

Fig. 1 : Schematic of a smart structure [4]

SMA is a widely preferred smart material since through its shape memory effect (SME) property it offers the advantage of high recovery stress and/or strain upon heating the material above a critical temperature. Generally the high recovery strain provides shape change while the high recovery stress increases strain energy and thus improves structural behaviours of a structure. A high recovery strain of up to 10% and recovery stress of up to 800 MPa can be obtained for nitinol SMA [8].

Table 1 shows the advantages and disadvantages of the SMA as compared to the piezoelectric and magnetostrictive materials. It shows that the SMA is better for high stress or strain applications while the others are more suited in high frequency applications.

Table 1: Comparing SMA, piezoelectric (PZE) and magneto restrictive (MR) material (5).

	SMA	PZE	MR
Stress (Mpa)	200	35	35
Strain	0.1	0.001	0.002
Frequency (Hz)	0-5	1-20000	1-20000
Efficiency, η (%)	5	50	80

However there are setbacks of the SMA for having a slow response time and low working efficiency. To overcome this and other weaknesses, the shape memory alloy composite has generated much interest [2]. By embedding SMA wires within laminated composites, the behaviour of the SME can be applied in the following ways. Restraining the SMA to recover its strain will allow the shape control of the structure it is embedded into. Constraining the strain recovery however will induce the internal stress that can strengthen structures while improving structural problems such as vibration, buckling and post buckling, impact loading, fracture, noise and acoustic.

SMA composite is either a polymer laminated composite or a metal-matrix composite that has SMA embedded into it in a form of wires or ribbons. The current technology allows the processing of a high quality SMA with diameter below 0.2 mm for wire form and 25 μm thickness for film which allows direct integration without disturbing the structural integrity of the composite material [9]. Most importantly the constraint of the matrix allows the generation of the high recovery stress.

It is inevitable that the new generation of smart material and structures technologies will not only have a tremendous impact upon the design, development and manufacture of the next generation products in diverse industries but also the economic climate in the international marketplace [10]. As to be seen in the literature review next, the study on the structural behaviour improvements of SMA plates are still considerably few. More studies on several parameters are still required for further understanding on these subjects. The study of structural behaviours of composite plates usually starts with the calculation of stress and deflection. It then follows with the studies on vibrations and buckling, with the linear part comes first followed by the nonlinear vibrations and post-buckling. Realizing the importance of the smart material

technology as the future design base provides the motivation for this research to be conducted. In this research the study on the structural behaviours of SMA plates are at the initial stage of calculating the stress and deflections effects of SMA on composite plates. Several parameter studies are conducted. At the end it is hope that this study will improve the overall understanding of the postbuckling behaviour of SMA plates.

1.2. Literature reviews

This literature review will give an overview on what has been done on the subjects that lead to the current work. Five areas of researches will be reviewed: Structural behaviours of composite plates, history of the SMA, constitutive models of the SMA, structural applications of the SMA and the structural applications of the SMA plates.

1.2.1 Structural behaviours of composite plates

In this section a review is given on the development of the study of the structural behaviours of composite plates especially in the development of the displacement theories of laminated composites. Studies on structural behaviours of laminated composite plates has been studied since the early nineteen sixties. During the early studies, the analytical method was employed. Jones [1] in 1973 gave the exact solutions of the buckling loads and vibration frequencies for the unsymmetrically laminated cross-ply rectangular plates that consider the effects of bending and extension couplings. These early studies of buckling of plates with rather simpler geometry, boundary conditions and loading are well documented in Jones [3] and Whitney [4]. With the advent of computers and the development of displacement based laminated plate theories ranging from the classical lamination theory (CLT) to the higher order shear deformation theory, the approximate methods especially the finite element method has gained the most attention.

It is well known that the behaviour of laminated plates can be accurately predicted if each layer is analysed by the three dimensional theory of elasticity. For example, buckling analysis based on this theory was conducted by Srinivas and Rao [5] and Pagano [6] where the results were comparable to the results of the analytical method. However due to its computational complication and cost, the equivalent single layer 2D theory was developed. In this theory, the displacements are expanded as a linear combination of the thickness co-ordinate and a laminated composite plate is represented as an equivalent single layer with anisotropic properties. This theory started with the classical lamination theory (CLT), which is the extension of the Kirchoff's classical plate theory. The CLT assumes the plane sections prior to deformation remain plane and normal to the deflected reference surface and the thickness does not change during deformation. This implies that it ignores transverse shear deformation, which is actually significant especially in thick laminated composites due to the high ratio between in-plane elastic modulus and transverse shear modulus. As a result, the CLT over predicts the critical loads and under predicts the stress and free vibrations compared to the exact values. This condition is improved by considering the transverse shear deformation in the shear deformation theories.

The first order shear deformation theories (FSDT) or Mindlin's plate theory is based on the assumption that normal to the mid-plane remains straight during plate deformation, but not necessarily normal. However since transverse shear strains are constant throughout the thickness of the plate, this theory does not comply with the actual physical case where the shear strain at the top and bottom surfaces must be zero. This inaccuracy of the solution can be improved by introducing the shear correction factor. Kam and Chang [7] derived the shear correction factor from the exact expression for orthotropic material for the buckling and vibration analysis of

laminated plates using the FSDT and obtained results that were closed to the exact values. In this study, the shear correction factor of 5/6 is used as Leissa [8] mentioned, this factor is generally accepted for laminated composite plates. Another problem is that the solutions from the numerical methods can be too stiff especially for thin plates. This so called shear locking phenomenon though can be solved partly by applying selective or reduced integration, it is still a problem in many cases. With these problems in the FSDT, the higher order shear deformation theories (HSDT) that expands further the displacement in terms of the thickness direction were developed. Various theories of HSDT were proposed such as the third order theories of Lo et al [9], Reddy [10,11], Moita et al [12] and Zabaras and Pervez [13]. The theories of Lo et al and Moita et al consider the second order displacement but the theories of Reddy and Pervez omitted that term. The third order theory of Reddy accommodates the parabolic distribution of transverse shear stress along the thickness of the plate and thus forces the transverse shear stresses on the top and bottom of the laminate to vanish which results in the omitting of the second order displacement term. The third order theory of Zabaras and Pervez however explained the third order displacement as the warping of the normal in the x and y directions and the second order displacements are omitted to meet the condition that the transverse shear stresses σ_{xz} and σ_{yz} vanish on the top and bottom surfaces of plate as in Reddy's theory. Studies on structural behaviours such as stress, deflection, vibration and buckling of laminated composite plates using several HSDT were conducted by researchers such as Moita et al [12], Phan and Reddy [14], Noor and Peter [15], Reddy and Khdeir [16] and Kozma and Ochoa [17]. In most cases the studies were conducted by varying the effects such as the level of anisotropy, plate thickness, the number of layers etc. Luccioni and Dong [2] conducted an intensive study on vibration and buckling of

rectangular plates using the semi-analytical (Levy-type) finite element method. The study on linear buckling that includes the thermo-mechanical effects are also studied such as by Shankera and Iyenger [18] and Chen and Mei [19].

The extension to the geometric non-linear effect on the study of the composite plates was however studied by few researchers. Reddy [20] included the von Karman's non-linear effect in his study to calculate stresses and frequencies of composite plates while Chandrashekhara and Bangera [21] used the same method for their study on beams. Understanding the post-buckling behaviour of laminated plates is important in order to know the load carrying capacity of plates after buckling. By this, the strength of the plate can be fully utilised and the weight of the plate can be reduced. Kapania and Raciti [22], Noor [23] and Liessa [8] investigated the methods and aspects of post-buckling study in their review of the buckling and post-buckling of the laminated plates. Most post-buckling studies concerned to the relation of in-plane compressive force versus transverse deflection assuming no changes in the buckled pattern of the plate. Stein [24] studied the post buckling behaviour of simply supported and clamped, on long, rectangular orthotropic plates using the finite difference method. Zhang and Matthews [25] investigated the effect of shear direction on post-buckling behaviour of plates under combined shear and compressive loading. Shiau and Wu [26] conducts the detailed analysis of the plate response over a wide post-buckling load range while considering changes in buckled pattern of the plate using the simplified FSDT. Barbero and Reddy [27] using the generalised laminated plate theory showed that, inclusion of the effect of geometric non-linearity, do not exhibit any bifurcation in certain composite laminates with bending-extensional coupling in contrast to the prediction of the eigen-value problem when it is loaded under compression. In this study, the effect of the geometric non-linearity using the

von Karman strain terms is studied to compare the critical load obtained from the eigen-value problem. The effect of geometric non-linearity has been studied based on the HSDT of Zabaras and Pervez.

1.2.2 History of SMA

The understanding of SMA started relatively late as compared to traditional materials such as metals and concrete. The first reported SMA behaviour is the pseudoelastic behaviour of the gold-cadmium SMA that was discovered by a Swedish scientist in 1932 [34]. Chang and Read later discovered the shape memory effect behaviour of the gold-cadmium in 1951 [35]. It is however not until 1963 when Buehlers and coworkers at the Naval Ordnance Laboratory, USA discovered the shape memory effect of the nickel-titanium (Nitinol) that the understanding and the use of the SMA started to flourish [36]. The SMA behaviours was later found in many other alloys such as CU-Zn, Cu-Zn-Al, Cu-Zn-Sn, Ni-Al and Fe-Pt. A great deal of effort was expanded after this time to characterize the property of the SMA and to exploit those properties to the applications of the SMA. As the understanding on the subject grows, various constitutive relationship were proposed and tremendous amount of applications were suggested. Since the first large scale application of SMA which was a coupling to connect titanium hydraulic tubing in the Grumman F-14 aircraft in 1971 [37-humbeek], the SMA products has grown vastly in the field of actuators, coupling and fastners, medical applications, smart composites, earthquake-supression related applications, fashion, decoration and gadgets, appliances and many others. Reviews on this subjects can be obtained in books such as Funakubo [38] and papers such as Humbeek [37], Birman [39],Wada et al [40] and C.S.Rogers [41].

1.2.3 SMA constitutive models

This section is to give a review of some of the SMA constitutive models that are available in the literature. The aim of the constitutive model is to formulate mathematically the unified behaviours of SMA such as shape memory effect, quassiplasticity and pseudoelasticity. Several constitutive models have been and are still proposed to predict the thermomechanical response of the SMA. One of the earliest model is the one dimensional Tanaka's model [42]. It is the macroscopic model that is derived from thermodynamic concepts and through experimental observations. The SMA behaviours in this model are constituted into two equations: constitutive equations and kinetic equations. The constitutive equation is obtained by minimization of free energy using the energy equation and the Clausius-Duhem inequality. Martensitic transformation is considered progressive and this progress can be explained thru an internal variable, the volume fraction of martensite, ξ,. The evolutionary equation is determined by considering transformation micro-mechanism and it is expressed using exponential function in the form of $\xi=\xi(\sigma,T)$. Tanaka's model was found to be able to characterize most of the behaviours of the SMA. Liang and Rogers [43] improved the Tanaka's model by directly matching experimental result to get the evolutionary equation and this equation is expressed using the cosine function. The constitutive equation remains the same while parameters of the equations can be determined through experiments. A major improvement of the Tanaka's model was made by Brinson [44,45]. Brinson recognized that not all martensite that are converted to austenite will produce the recovery stress. Only the stress induced martensite that is responsible for the shape memory effect. As such, martensite fraction is divided into two: stress induced and temperature induced martensite. This model also does not assume constant material functions in the constitutive relationship. Furthermore Brinson's made some amendment so that the

constitutive equation will be valid at any temperature. This model was found to give a better representation of the SMA behaviours than the Liang and Rogers's model [46, ford,hebda,white].

In a different approach, the so called thermodynamic model was developed by Boyd and Lagoudas [47]. This model start with a free energy equation and by utilizing a dissipation potential in conjunction with the second law of thermodynamic, the evolution law for the internal state variable i.e. the volume fraction can be derived. This model is a 3-dimensional model that can be reduced to a 1-dimensional model [48]. This model has been used to solve the problem of SMA actuators embedded in metal matrix composites where a multi-axial stress state exist [49,50-logoudas,bo,qidwai].

The Muller-Achenbach model was initially proposed by Achenbach [51], Achenbach & Muller [52] and Muller & Xu [53]. The earlier model can capture the pseudoelastic phenomena only. The model was then improved to include the thermoelastic and reorientation processes by Seelecke [54] and Huo & Xu [55]. This model views SMA mesoscopically since the basic elements involve are lattices of martensite and austenite. It is also actually a phenomenological model since the postulates made are basically based on experimental observations. As in Bo and Lagoudas [47] model, this model is based on thermodynamic principles of free energy and dissipation potential. For any phase to be in equilibrium, the free energy must be minimum and the dissipation potential must be satisfied. This model then goes into deep in utilising statistical thermodynamics principles in order to determine the rate of transformation and finally by equating the energy balance equation for the SMA, the solution of the force-deformation plot can be obtained. An important finding of this model is that the pseudoelastic process is an unstable process for having equilibrium

downward slope force-deformation curve. A conjecture was made that hysteresis occurs due to this. This downward slope line is actually a diagonal that determine the turning point for the internal yield and recovery processes. Even though this model can accurately represent thermoelastic behaviour, the disadvantage of this model is its highly mathematical formulation that make it difficult to be incorporated to finite element method.

1.2.4 Structural applications of SMA

The improvement made by the SMA on structures can be classified into two categories: active property tuning (APT), and active strain energy tuning (ASET) [56]. APT refers to the increase of the Young's modulus, yield strength and other properties of the SMA during the transformation of martensite to austenite phase. However the damping capacity is reduced upon transformation [57]. On the other hand, ASET involves the embedment of the prestrained martensite into laminated composite. This pseudo-plastic SMA is therefore an integral part of the composite. When the heat is increased, the fibers are constrained from returning to their memorized length and thus creating the recovery force. This recovery force is used to increase the strain energy and the stiffness of the structure and thus improving structural problems such as shifting natural frequency, suppress vibration, increase critical and thermal buckling loads, control post-buckling and thermal post-buckling deflections and prevent cracks and fatigues. If the fibers is located eccentrically to the natural exist, the recovery force of the SMA will provides the structure a bending moment that can change the shapes or positions of SMA structures. This type of ASET is called the active shape control (ASC). Note that the APT is always there for each occurrence of the ASC and ASET and it was found that the effect of APT is

much smaller as compared to the effect of the other two [56]. Researches on this SMA structures especially beams are rather extensive. Though each research is to prove the effect of SMA in improving structural behaviours, all are differs in terms of structural configuration, form of SMA, number of SMA training cycles conducted and the method of analysis.

C.A.Rogers et al [56] was one of the earliest researchers to formulate several concepts of structural improvement of SMA composite plates. In their paper, they discuss the concepts of ASET and APT and then suggest the geometric form of the SMA composite plates. After proposing the constitutive relationship, they developed the general dynamic model and formulation of the SMA composite plates. Finally they solve the linear problems of bending deflection, free vibration, buckling analysis and acoustic transmission using the Raleigh-Ritz method. The results on effectiveness of the concepts of APT and ASET in improving structural behaviour of the SMA plates were encouraging.

Zak et al [58] studied several parameters such as the orientation and location of SMA wires, the orientation and relative volume fraction of reinforcing fibres, the thickness to length and length to width ratios and boundary conditions that effect the free vibration and critical load performances of SMA composite plates. Both concepts of APT and ASET were studied. It was found that the greatest changes in the natural frequencies and the critical loads are observed not for the lowest modes of vibration but generally for those modes where the nodal lines are perpendicular to the orientation angle of the SMA wires. Furthermore it was found that the changes in natural frequencies and critical loads also a function of the orientation of the SMA wires as well as the length to width ratio.

Positioning pre-strained SMA wires or strips eccentrically to the neutral axis of a beam or plate will give the SMAHC a moment recovery upon activation of the SMA. SMA wires can also be placed on the neutral axis of the beam if the wires have been trained to deflect upon activation. The amount of the recovered bending moment will depend on several factors such as the amount of transformation, the amount of pre-strain and the volume fraction of the SMA wires. The concept of the ASC can be used in applications such as the strict precision pointing requirement of the spacecraft, space-based radar and laser, stern shape control for submarines and the adaptive hydro- or aerodynamic lifting surface [59]. Shape control of beams was applied to have large deflections in flexible beams [60-66] or small deflections in beams [67] or SMA composite beams [68-74]. Icardi [41] in his recent paper gave the analytical modeling, numerical simulation and experimental validation of the analysis of a flexible composite beam having bending moment actuated by SMA wires. He then applied his model to the elastomeric SMA beam that upon heating will act as large bending actuators. Similarly, Wang and Shahinpoor [42] modeled a structure that consisted of SMA wires embedded externally between a flexible beam and a soft plastic tube. A moment equation was derived based on a flexible cantilever beam with a concentrated follower load at the free end and a uniformly distributed follower load along the beam. This moment equation was incorporated to the Euler-Bernoulli beam equation to give the mathematical model of the problem. Wang and Shahinpoor proved that SMA wires could be used to cause large bending in elastomeric beams.

Baz et al [50] embedded nitinol strips that were trained to deflect at temperature higher than A_s inside sleeves, which are placed on the natural axis of the beam. A mathematical model via FEM was developed to study the dynamic effect of the SMA. Also a thermal finite element model was developed to study the thermal gradient

across the cross-section of the beam. Most theoretical results showed close agreement with the experiment finding. Choi et al [51-52] conducted an analytical and experimental study to control the shape of a SMA composite beam. They used Euler's formulation of lateral deflection and the 'cut and paste' method to determine the deflection due to the bending of the SMA. Kim et al [53] enhanced the effect of the SMA on the active shape control of beams by applying the concept of elastic tailoring to give the coupling effect such as bending-twisting and extension–bending that will act as passive shape control of the beams. The recovery forces were calculated independently using the procedures developed by Brinson and Lammering [75]. Ghomsei et al [76] however combined constitutive equation of the Brinson's SMA model with displacement fields of a polymer beam loaded axially and laterally to obtain the finite element model for the composite actuator.

By the ASET of SMA composite structure, critical natural frequencies can be increased away from the operative frequencies [77-80]. Furthermore the mode shape can be shifted away from the critical positions [81]. Increasing the stiffness thru ASET control can also suppress vibrations [82-84]. However vibrations can also be suppressed by increasing the damping capacity of the SMA. This can be done thru active or passive ways [85-87]. The critical buckling and thermal buckling load can be increased while the post- and thermal post buckling can be controlled thru ASET control [88-90].

Epps & Chandra [58] modeled the SMA composite beam as a beam on elastic foundation where the characteristic of this elastic foundation depended on the recovery forces. The governing equations of a uniform composite beam on an elastic foundation undergoing bending vibration were solved using Galerkin's method. It was found that the natural frequencies depended upon the beams stiffness, mass, length

and the recovery forces. The recovery forces were predicted using the Liang and Rogers model [58]. Experiments were carefully conducted considering the effect of curing temperature. The results showed that the first natural frequency could be increased by 22% if one 20 mils diameter wire is used. The increase grew to 176% if 50 wires of 10 mils diameter wire were used.

Baz et al [59] studied the control capability of the nitinol SMA on the natural frequencies of clamped-clamped composite beams. SMA wires were embedded on the natural planes thru a vulcanised rubber sleeves. Two sets of SMA were used; one with 250 cycles of SME training and the other was without training. The Euler-Bernoulli's thin beam was assumed neglecting shear deformation and rotary inertias. The individual contribution to the beam stiffness was determined and formulated. The contribution includes the flexural rigidity of the beam, geometric stiffness of the axial and thermal loading and the elasticity stiffness of the nitinol. The finite element analysis was conducted and the results were validated thru experiment. It was shown that the natural frequencies could be shifted to higher values by activating nitinol wires.

Lau et al [60] in their research determined analytically and experimentally the natural frequencies of clamped-clamped smart composite beams without considering the effect of the curing temperature of the matrix and SMA temperature on surrounding. Combining the stress recovery equation of the Brinson's model [60] and lateral vibration equation of the beam, the differential equation was solved analytically to give the roots of the natural frequency of the beams. The experimental results showed close agreement with the analytical results. It was found that at low volume fraction of SMA, natural frequencies decreased because of the thermal

compressive stress that existed. As the volume fraction increased, tension recovery stress overrode the compressive stress and thus increasing the natural frequencies.

A study by Baz et al [63] demonstrated theoretically and experimentally the feasibility of using SMA in suppressing the flexural vibrations of a flexible cantilevered beam. Connecting the nitinol actuators externally between two points of the beam, the SMA of the actuators were utilized to memorize the desired distance between the two points. At the instance when the deviation of the desired spacing occurred, the activation of the SMA will create recovery forces and moments that will bring back the beam to the memorized shape. By placing the actuators external to the beams, natural cooling of the actuators to ambient temperature will return the SMA to martensite phase. The problem was modelled using the finite element method where the effect of the SMA came as the control moment developed by the nitinol actuator. The phase transformation process was assumed to be sudden. Thus the Young's modulus of the SMA was assumed to shift instantaneously from the Young's modulus of the martensite to the Young's modulus of the austenite. The results obtained showed close agreement between theory and experiments. The result showed that two nitinol actuators were required for effective vibration damping for each degree of freedom to be controlled.

Chen and Levy [67] studied the effect of changing the Young's modulus of isotropic beams by overlaying the beams with SMA layers. It was demonstrated that the approach could change the natural frequencies and adjusting the excitation of the beams. The method was aimed for completed structures where there was no possible modification can be made. Thermal bending moment was derived from the 1D unsteady heat condition problem of the beam. Assuming Euler's beam, the governing equation of the beam was developed and modified to equations constituted the

transverse displacement terms using coefficient of non-dimensional parameters. Transverse displacements were then solved assuming the variable separable solution.

Baz et al [69] studied the buckling characteristic of flexible fiberglass composite beams that were controlled by SMA wires. Nitinol wires inside rubber sleeves were embedded along the neutral axis of a composite beam. Prior to that nitinol wires were trained to memorize the shape of the unbuckled beam. Once buckling occurs, the SMA wires were activated and tried to bring the beam to return to its original shape. Finite element model was developed and individual contribution of fiberglass-resin laminate, nitinol wires, thermal stress and the SME to the buckling of the beam was analysed. The stiffness matrix consists of the conventional transverse and geometric stiffness matrices. The external axial and thermal loads contributed negatively to the total stiffness matrix while the geometric stiffness matrix due to nitinol wires added positively to the stiffness matrix. It was shown that for the given SMA beam, embedding eight SMA wires would increase the buckling load three times. The result from experiments correlated well to the finite element results.

The study on the post buckling of the composite SMA plates due to compressive load is rather few even though more studies on the thermal postbuckling were conducted in the last decade. In their research, Thompson and Loughlan [91,92] proved that by embedding pre strained SMA wires into laminated plates, the out of plane displacement can be reduced. Two concepts of SMA control were used. Firstly, SMA wires were embedded at the outermost layer of the symmetric cross-ply composite laminate ($[0_2/90_2]_s$) and secondly the wires were located within tubing at the neutral axis of the composite plate. The results obtained from the finite element commercial software were compared to their experimental results. It was found that the post buckling deflection can be reduced for even a small volume fraction of the

SMA. The second concept were found to give more effect on the elevation of the post buckling response as compared to the first concept.

The study on the effect of SMA on the thermal buckling and postbuckling behaviour of laminated composites was first studied by Zhong et al [93]. The SMA properties and stress recovery were taken from experimental data conducted by Cross et al [94]. The displacement field of the composite was based on the Kirchoff's classical lamination theory. The nonlinear finite element equation was solved using updated Lagrangian formulation. The effect of several parameters such as the use of the non-orthotropic and unsymmetric laminate and boundary conditions were studied. Result showed that SMA can greatly reduce or completely eliminate the postbuckling deflection at certain elevated temperature.

Duan [95], Duan et al [96] and Tawfik et al [97] later used a different finite element approach to solve the thermal postbuckling of SMA quassi-isotropic plates. Using incremental updated lagrangian formulation and the marching method, the study prove that SMA fibres can significantly improve the postbuckling behaviour of laminated composite. Similarly, Park et al [98] solve the postbuckling of SMA composite plates using the incremental updated lagrangian formulation and the marching method. He however use the first order shear deformation theory to describe the displacement field of the laminated composites. Guo et al [99] improve the marching method technique by taking strain as a cumulative physical quantity while the stress is an instant one. As a result the method does not need the many small increments as in the marching method. Lee et al [100] studied the postbuckling of SMA composite shells. Using the Brinson's model the constitutive equation was incorporated into the finite element software of ABACUS to solve the psotbuckling of

SMA shells. It was found that the lateral deflection of shell was reduced due to the effect of SMA.

From the literature review it shows that various displacement theories have been developed to be applied in the studies of structural behaviours of composite plates. The trend now is to incorporate the SMA into composite layers as to improve the performance of the structural behaviours of composite plates through APT and ASET improvement methods. This is possible with the development of constitutive theories of SMA where the behaviours of SMA embedded within composite layers can be predicted. In this research these developments are used to study the effect of SMA on stress and deflection of composite plates.

1.3 Objectives

The objectives of this research are:

1. To develop a linear finite element model of the shape memory alloy composite plates.
2. To develop source codes for the above model.
3. To study the effect of SMA on several structural behaviours of composite plates such as stress, deflection, free vibration and buckling.
4. To conduct parametric studies on the effect of SMA on the above structural behaviours.

1.4 Scope

This research is to develop a linear FEM model for the SMA composite plates and use this model to study the effect of SMA on several structural behaviours. This study is limited to the following scope and assumptions.

- The SMA wires are nicely embedded within epoxy matrix and as for the composite fibres, the bonding of the SMA wires is assumed to be perfect so that the rule of mixture can be applied.
- The amount of recovery stresses are predetermined using the Brinson's model where the constitutive and evolutionary equations of the model are solved for the cases of shape memory effect, pseudoelasticity ad quassiplastcity..
- The study is limited to the linear analysis where for example the buckling and free vibration improvements made by SMA are studied through the well known eigen-value problems.
- The first order displacement theory is used as the kinematic assumption of the displacement behaviour of the composite plates.
- The plates understudy are square laminated plates where each layer may be considered homogeneous and orthotropic in the macroscopic sense. The plates can be symmetric or anti-symmetric in terms of material properties and geometry where layers are of equal thickness. The unsymmetrical plate are not considered in this study.
- The deformation behaviour of the composite matrix and fibres are assumed to be linear.
- Boundary conditions applied to the plates are the combinations of simply supported and clamped boundary conditions.

1.5 Research organization

The report of this research is divided into six chapters:

1. Chapter 1: Introduction
2. Chapter 2: Composite plate and SMA theories
3. Chapter 3: Finite Element Formulation of SMA composite plates

4. Chapter 4: Code developement
5. Chapter 5: Structural analysis of SMA plates
6. Chapter 6: Conclusions and recommendations

2.0 COMPOSITE PLATES AND SMA THEORIES.

2.1 Theory of laminated composite plate

The behaviour of laminated composite plate is interesting as the material properties and the response to the external loading can be tailored. How laminates response to loads depends on many factors such as fibre angles, stacking arrangements, material properties, span to thickness ratios etc. As an example, referring to figure 2.1 when two laminated composites subjected to the same level of bending moment, M, the first laminate will bend much less than the second one because the stacking sequence of the first composite allows it to have a larger bending stiffness.

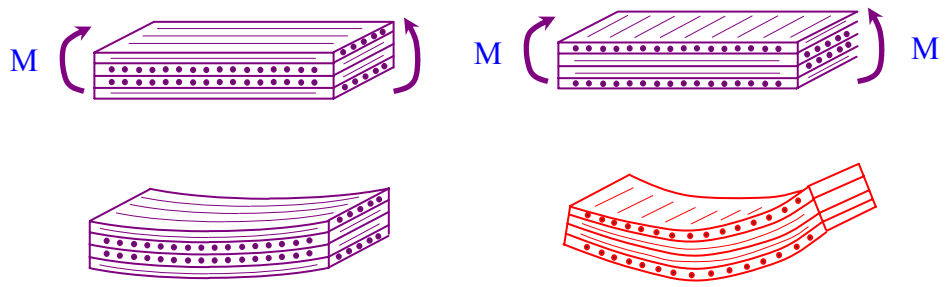

(a) $[0/90]_s$ laminates **(b) $[90/0]_s$ laminates**

Figure 2.1: Differences in bending deformation between $[0/90]_s$ and $[90/0]_s$ laminates [Hyer,1998].

The material properties of a laminated composite plate such as the Young Modulus, Poisson ratio and thermal coefficient can be tailored. Not just that, by controlling the stacking arrangement, the coupling phenomenon can be controlled also. To understand the effect of these factors, we have to understand the constitutive relationship of a laminated composite plate. This constitutive relationship is derived by combining the

constitutive relationship of a laminae and the kinematic equations of the laminated composite plate into the equations that define the stress resultants that occur in composites. Understanding the physical meaning of the constitutive relationship of a laminae and the kinematic behaviour of laminated composite plates is thus crucial before we can understand the behaviour of laminated composite plates as a whole. As such we go into reviewing the mechanics of a laminae first.

2.1.1 Mechanics of a laminae

The behaviour of laminated composites in this study is viewed globally rather than locally where the interaction of constituents of composites is of interest. This so called macro mechanical approach uses the average apparent mechanical properties to study global responses such as deflections, vibration frequencies, vibration damping and buckling loads.

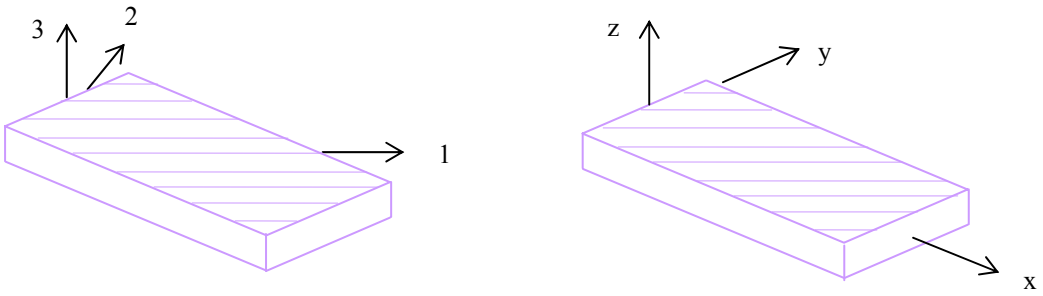

a. Principal Coordinate System
1 – Direction of Fibres
2,3 – Direction transverse to fibre

b. Global Coordinate System

Figure 2.2: The principal and global coordinate systems

The fibres and the matrix materials are assumed to be smeared into one equivalent homogeneous material. Since this material is to have different properties in three mutually perpendicular directions, a laminated composite is called an orthotropic

material. Setting the coordinate system based on the right hand rule, the principal material and the global coordinate systems are shown in figure 2.2.

With the assumption of the orthotropic properties, the compliance matrix of the laminae has been reduced to nine independent constants. So we have a stress-strain relationship, in the material coordinate system,

$$\begin{Bmatrix} \varepsilon_1 \\ \varepsilon_2 \\ \varepsilon_3 \\ \gamma_{12} \\ \gamma_{13} \\ \gamma_{23} \end{Bmatrix} = \begin{bmatrix} S_{11} & S_{12} & S_{13} & 0 & 0 & 0 \\ S_{12} & S_{22} & S_{23} & 0 & 0 & 0 \\ S_{13} & S_{23} & S_{33} & 0 & 0 & 0 \\ 0 & 0 & 0 & S_{44} & 0 & 0 \\ 0 & 0 & 0 & 0 & S_{55} & 0 \\ 0 & 0 & 0 & 0 & 0 & S_{66} \end{bmatrix} \begin{Bmatrix} \sigma_1 \\ \sigma_2 \\ \sigma_3 \\ \tau_{12} \\ \tau_{13} \\ \tau_{23} \end{Bmatrix} \qquad (2.1a)$$

where

$$S_{11} = \frac{1}{E_1} \qquad S_{12} = -\frac{\nu_{12}}{E_1} \qquad S_{13} = -\frac{\nu_{13}}{E_1}$$

$$S_{22} = \frac{1}{E_2} \qquad S_{23} = -\frac{\nu_{23}}{E_2} \qquad S_{33} = \frac{1}{E_3} \qquad (2.1b)$$

$$S_{44} = \frac{1}{G_{12}} \qquad S_{55} = \frac{1}{G_{13}} \qquad S_{66} = \frac{1}{G_{23}}$$

or

$$\{\varepsilon\} = [S]\{\sigma\} \qquad (2.1c)$$

where $\{\sigma\}$ is the stress matrix, $\{\varepsilon\}$ is the strain matrix and $[S]$ is the compliance matrix.

In the case of a plate laminae, since in-plane stresses are usually much higher than stresses perpendicular to the plane, it is reasonable to make the plane-stress assumption.

However, leaving the effect of transverse shear will be inaccurate especially in the case of thick plates. Thus taking into account the transverse shear stresses and strains along with the plane stress assumption, we have,

$$\begin{Bmatrix} \varepsilon_1 \\ \varepsilon_2 \\ \gamma_{12} \\ \gamma_{13} \\ \gamma_{23} \end{Bmatrix} = \begin{bmatrix} S_{11} & S_{12} & 0 & 0 & 0 \\ S_{12} & S_{22} & 0 & 0 & 0 \\ 0 & 0 & S_{33} & 0 & 0 \\ 0 & 0 & 0 & S_{44} & 0 \\ 0 & 0 & 0 & 0 & S_{55} \end{bmatrix} \begin{Bmatrix} \sigma_1 \\ \sigma_2 \\ \tau_{12} \\ \tau_{13} \\ \tau_{23} \end{Bmatrix} \qquad (2.2a)$$

or

$$\{\varepsilon\} = [S]\{\sigma\} \qquad (2.2b)$$

where $[S]$ is the reduced compliance matrix.

Inverting this stress-strain relationship, we have

$$\begin{Bmatrix} \sigma_1 \\ \sigma_2 \\ \tau_{12} \\ \tau_{13} \\ \tau_{23} \end{Bmatrix} = \begin{bmatrix} Q_{11} & Q_{12} & 0 & 0 & 0 \\ Q_{12} & Q_{22} & 0 & 0 & 0 \\ 0 & 0 & Q_{33} & 0 & 0 \\ 0 & 0 & 0 & Q_{44} & 0 \\ 0 & 0 & 0 & 0 & Q_{55} \end{bmatrix} \begin{Bmatrix} \varepsilon_1 \\ \varepsilon_2 \\ \gamma_{12} \\ \gamma_{13} \\ \gamma_{23} \end{Bmatrix} \qquad (2.3a)$$

or

$$\{\sigma\} = [Q]\{\varepsilon\} \qquad (2.3b)$$

where $[Q]$ is the reduced stiffness matrix

And,

$$Q_{11} = \frac{E_1}{1-\nu_{12}\nu_{21}} \qquad Q_{22} = \frac{E_2}{1-\nu_{12}\nu_{21}}$$

$$Q_{12} = \frac{\nu_{12}E_2}{1-\nu_{12}\nu_{21}} = \frac{\nu_{21}E_1}{1-\nu_{12}\nu_{21}} \qquad (2.3c)$$

$$Q_{33} = G_{12} \qquad Q_{44} = G_{13} \qquad Q_{55} = G_{23}$$

Transforming into any arbitrary global coordinate system where material coordinate axes are at θ degree from the global coordinate axes such as shown in figure 2.3, we have the stress strain relationship as followed,

$$\begin{Bmatrix} \sigma_x \\ \sigma_y \\ \tau_{xy} \\ \tau_{xz} \\ \tau_{yz} \end{Bmatrix} = \begin{bmatrix} \overline{Q}_{11} & \overline{Q}_{12} & \overline{Q}_{13} & 0 & 0 \\ \overline{Q}_{12} & \overline{Q}_{22} & \overline{Q}_{23} & 0 & 0 \\ \overline{Q}_{13} & \overline{Q}_{23} & \overline{Q}_{33} & 0 & 0 \\ 0 & 0 & 0 & \overline{Q}_{44} & \overline{Q}_{45} \\ 0 & 0 & 0 & \overline{Q}_{45} & \overline{Q}_{55} \end{bmatrix} \begin{Bmatrix} \varepsilon_x \\ \varepsilon_y \\ \gamma_{xy} \\ \gamma_{xz} \\ \gamma_{yz} \end{Bmatrix} \qquad (2.4a)$$

or $\{\sigma\} = \left[\overline{Q}\right] \{\varepsilon\}$

where $\left[\overline{Q}\right]$ is the transformed reduced stiffness matrix.

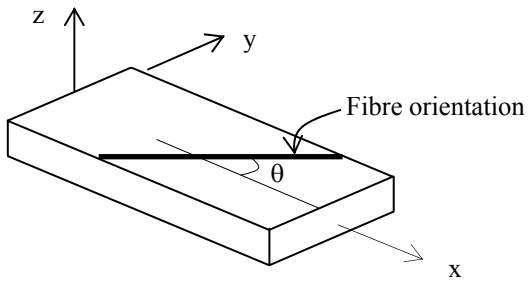

Figure 2.3: Angle of fibre orientation, θ

Taking m = cos θ and n = sin θ, we have,

$$\overline{Q}_{11} = Q_{11}m^4 + 2(Q_{12} + 2Q_{44})\, n^2m^2 + Q_{22}n^4$$

$$\overline{Q}_{12} = (Q_{11} + Q_{22} - 4Q_{44})\, n^2m^2 + Q_{12}(n^4 + m^4)$$

$$\overline{Q}_{13} = (Q_{11} - Q_{12} - 2Q_{44})\, nm^3 + (Q_{12} - Q_{22} + 2Q_{44})\, n^3m$$

$$\overline{Q}_{22} = Q_{11}n^4 + 2(Q_{12} + 2Q_{44})\, n^2m^2 + Q_{22}m^4$$

$$\overline{Q}_{23} = (Q_{11} - Q_{12} - 2Q_{44})\, n^3 m + (Q_{12} - Q_{22} + 2Q_{44})\, nm^3 \qquad (2.4b)$$

$$\overline{Q}_{33} = (Q_{11} + Q_{22} - 2Q_{12} - 2Q_{44})\, n^2 m^2 + (Q_{44})\,(n^4 + m^4)$$

$$\overline{Q}_{44} = Q_{44} m^2 + Q_{55} n^2$$

$$\overline{Q}_{45} = (Q_{44} - Q_{55})\, mn$$

$$\overline{Q}_{55} = Q_{44} n^2 + Q_{55} m^2$$

Here it is clear that the constitutive relationship of a laminae depends not only on the properties of the fibre and the matrix but also the angle of orientation of the fibre.

The kinematics response is totally a geometric movement of composites when loads are applied. The analysis of laminated composite can be based on three dimensional elasticity theories or lamination theories. The 3D elasticity theory treats each layer as an elastic continuum with possibly distinct material properties from adjacent layer. Between two layers are related by continuity of displacements and stress equations. However as the number of layers increases, the analysis becomes complicated. A better alternative is the lamination theory where the laminated plate is treated as a single layer.

2.1.2 Classical Lamination Theory

Kirchoff in the mid 1800s made assumption that has greatly simplified the analysis of plates, shells and beams. This later so called the classical lamination theory has been successfully applied to the analysis of composite plates especially for thin plates. Referring to figure 2.4, a laminated plate can be acted upon by loads such as bending moment, M, distributed load, q, in-plane load, N and point load, P.

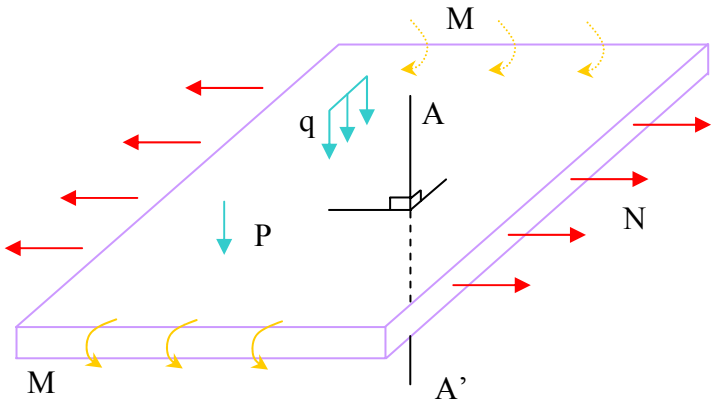

Figure 2.4: Laminated plate acted upon by loads

The Kirchoff's hypothesis stated that the line AA' remains straight and normal to the geometric mid-plane after deformation as in figure 2.5 and also the length of the line AA' remains the same.

The first assumption implied that the line AA' does not deform but instead it only rotates and translates. In other words, the effect of transverse shear is neglected. The fact that the length remains the same means that there is no strain in z direction. With these two implications, the strains and displacements at any points can be expressed in terms of the displacements of points on the composite midplane. This also implied that the problem has been reduced from three dimensional to the two dimensional problem.

The total displacements can then be summarised in the following equations.

$$u(x,y,z) = u_0(x,y) - z\left(\frac{\partial w_0(x,y)}{\partial x}\right)$$

$$v(x,y,z) = v_0(x,y) - z\left(\frac{\partial w_0(x,y)}{\partial y}\right) \qquad (2.5)$$

$$w(x,y,z) = w_0(x,y)$$

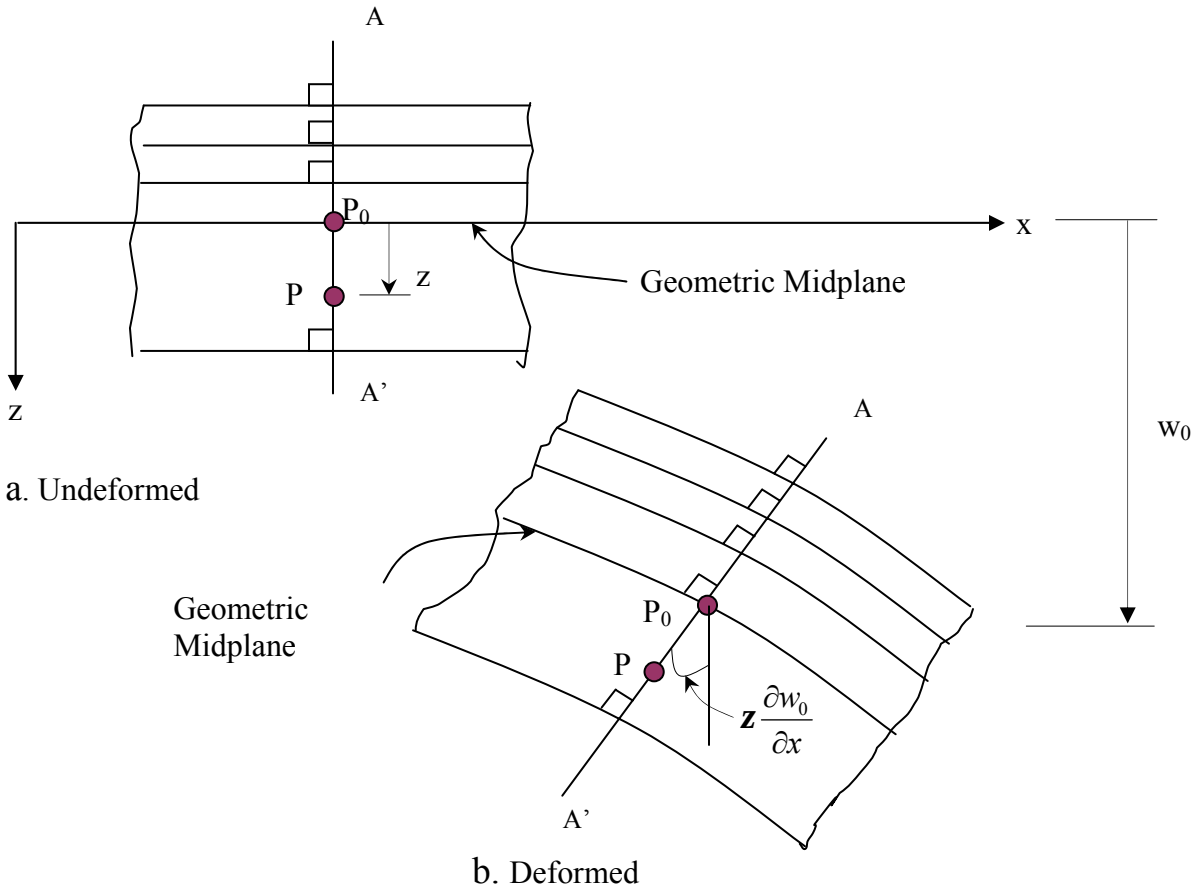

Figure 2.5: Kinematics of deformation in the x-z plane - CLT

The classical lamination theory is accurate for thin plates where the plate thickness to span ratio tends to zero. However, for moderately thick plates the thickness to span ratio is not small enough to neglect transverse shear deformation and the Kirchoff assumption is no longer applicable.

2.1.3 First Order Shear Deformation Theory

The first order shear deformation theory maintains the Kirchoff's assumptions except that the line AA' in figure 2.6 does not have to be normal to the geometric mid-plane after deformation occurs. This implies that constant transverse shear stresses throughout plate

thickness are included in the kinematic equations. However since the normal stress in z direction remains disregard, the analysis will remain a two dimensional problem.

Total displacement in x and y directions will remain the combination of displacements due to translation and rotation.

$$u(x,y,z) = u_0(x,y) - z\left(\frac{\partial \theta_0(x,y)}{\partial x}\right)$$

$$v(x,y,z) = v_0(x,y) - z\left(\frac{\partial \theta_0(x,y)}{\partial y}\right) \qquad (2.6)$$

$$w(x,y,z) = w_0(x,y)$$

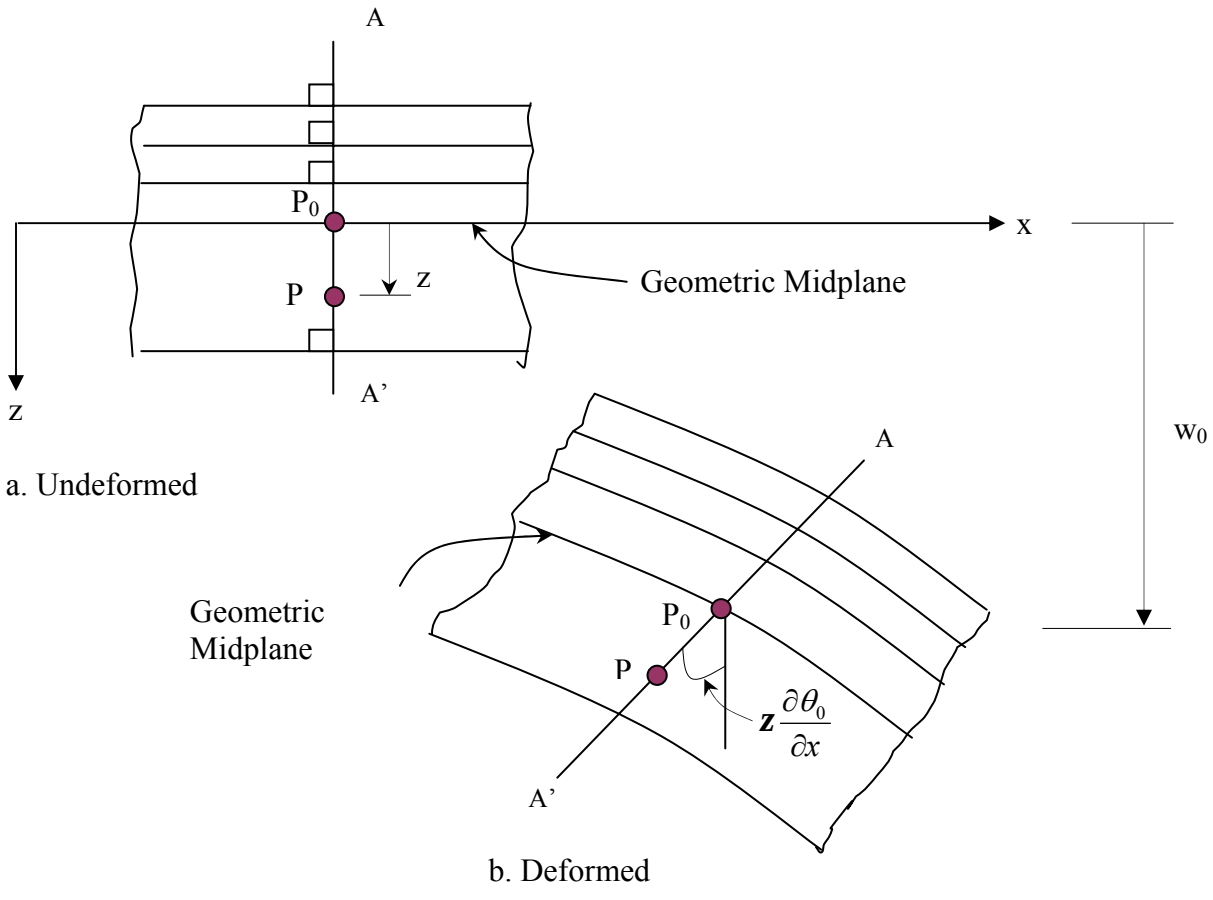

Figure 2.6: Kinematics of deformation in the x-z plane - FSDT

The FSDT provides accurate results for moderately thin plates. For the span to thickness ratio becomes less than 20, the accuracy of the result will become lesser. Furthermore for very thin plates, the FSDT will give overly stiff results for the solutions that are obtained from the finite element method. This so called the shear locking phenomenon is due to the domination of the shear stiffness in the total stiffness as compared to the bending stiffness when the full integration of the total potential energy is done. Even though shear locking can be reduced by implementing the reduced or selective integration, the results in many cases are still overly stiff. Another problem of the FSDT is that the assumption of constant transverse shear stress is actually not correct since it is known that the shear stresses on the top and bottom surfaces of the plate are zero. To improve this condition, the shear correction factor is added to the out of plane terms of the FSDT equations. The shear correction factor of $\frac{5}{6}$ is a generally accepted value even though the more accurate value must be calculated in a case by case manner. For all these problems, researchers have developed higher order theories in getting more accurate results.

2.1.4 Higher Order Shear Deformation Theory

The higher order theory of the laminated composite was developed for thick plates and at the same time improving the FSDT. This development however must maintain the two dimensional form of the FSDT. The improvement of the FSDT can be done by adding higher order terms of displacement based on the existing deformation parameters such as u_0 , v_0 , θ_x and θ_y or just adding new deformation parameters. Several deformation theories can be gathered in a generalised displacement field as followed.

$$u(x,y,z) = u_0(x,y) + z\left(\alpha_1 \frac{\partial \omega}{\partial x} + \alpha_2 \theta_x\right) + z^3\left(\alpha_3 \zeta_x + \alpha_4 \frac{4}{3h^2}\left(\theta_x + \frac{\partial \omega}{\partial x}\right)\right)$$

$$v(x,y,z) = v_0(x,y) + z\left(\alpha_1 \frac{\partial \omega}{\partial y} + \alpha_2 \theta_y\right) + z^3\left(\alpha_3 \zeta_y + \alpha_4 \frac{4}{3h^2}\left(\theta_y + \frac{\partial \omega}{\partial y}\right)\right) \quad (2.7)$$

$$w(x,y,z) = w_0(x,y)$$

where

α_1 ,α_2 ,α_3 and α_4 are constants associated with the HSDT used

u_0, v_0 = Displacement in x and y direction respectively

θ_x, θ_y = Rotations about x and y axis respectively

ω = Displacement in z direction

ζ_x, ζ_y = New displacement parameters in x and y direction

Assigning the values of α_1 ,α_2 ,α_3 and α_4 constants as in the following table 2.1, the generalised displacement field will become a specific theory developed by different researchers.

Table 2.1: Constants correspond to FSDT and HSDT.

α_1	α_2	α_3	α_4	Theory
-1	0	0	0	Kirchoff's CLT
0	-1	0	0	Mindlin's FSDT
0	1	0	-1	Reddy's HSDT (11)
0	-1	1	0	***Zabaras's and Pervez's HSDT (13)***

Assigning the values of constant appropriately, the HSDT of Zabaras and Pervez is as followed.

$$u(x,y,z) = u_0(x,y) - z\ \theta_x + z^3\ (\zeta_x\ )$$

$$v(x,y,z) = v_0(x,y) - z\ \theta_y + z^3\ (\zeta_y\ ) \qquad (2.7)$$

$$w(x,y,z) = w_0(x,y)$$

where this HSDT add a new displacement parameter , ζ. ζ_x is defined as warping of laminated plates about the x-axis.

Understanding the constitutive relationship of a laminae and the kinematic of laminated composite plates, the constitutive relationship of a laminated plate can be derived.

2.1.5 Layerwise Theory

2.1.6 Mechanic of laminated composite plates

Some laminates may consist of three to four layers while others may have more than a hundred of layers. Constructing the constitutive relationship of a laminated composite plate, the constitutive relationship for a laminae is incorporated into the kinematic equations of the HSDT of Zabaras and Pervez through the stress resultant equations of laminated composites. The simplified generalised kinematic equations of laminated composite plates are,

$$u(x,y,z) = u_o\ (x,y) + z\ \theta_x\ (x,y)\ +\ z^3\beta\zeta_x$$

$$v(x,y,z)\ = v_o\ (x,y) + z\ \theta_y\ (x,y)\ +\ z^3\beta\zeta_y \qquad (2.8)$$

$$w(x,y,z)\ = w_o\ (x,y)$$

Where,

u, v, w = displacement of a generic point (x,y,z) in x, y and z direction respectively

u_o, v_o, w_o = displacement of mid-plane in x, y and z direction respectively

z = coordinate in thickness direction

θ_x, θ_y = rotations of the normal of the reference planes about y-axis and x-axis respectively

ζ_x, ζ_y = third order displacements or warping functions

β = a constant to differentiate the two plate theories

= 0 for FSDT and

= 1 for HSDT

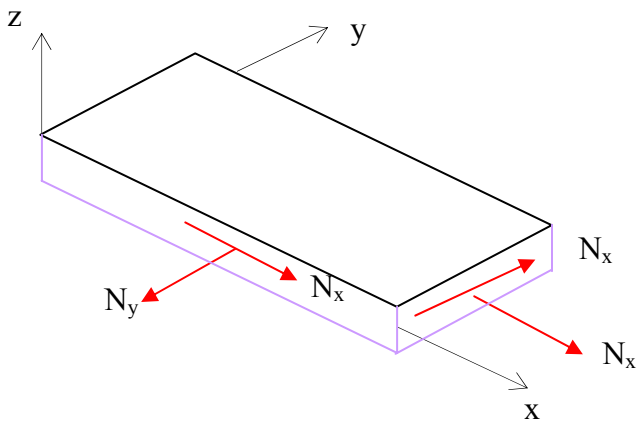

Figure 2.7 : Membrane Stresses

So strain can be expressed as

$$\varepsilon_x = \frac{\partial u}{\partial x} = \frac{\partial u_o}{\partial x} + z\frac{\partial \theta_x}{\partial x} + z^3 \beta \frac{\partial \zeta_x}{\partial x}$$

$$\varepsilon_y = \frac{\partial v}{\partial y} = \frac{\partial v_o}{\partial y} + z\frac{\partial \theta_y}{\partial y} + z^3 \beta \frac{\partial \zeta_y}{\partial y} \qquad (2.9)$$

$$\varepsilon_{xy} = \frac{\partial u}{\partial y} + \frac{\partial v}{\partial x} = \frac{\partial u_o}{\partial y} + \frac{\partial v_o}{\partial x} + z\left(\frac{\partial \theta_x}{\partial y} + \frac{\partial \theta_y}{\partial x}\right) + z^3 \beta \left(\frac{\partial \zeta_x}{\partial y} + \frac{\partial \zeta_y}{\partial x}\right)$$

$$\varepsilon_{xz} = \frac{\partial u}{\partial z} + \frac{\partial w}{\partial x} = \frac{\partial w_o}{\partial x} + \theta_x + 3z^2 \beta \zeta_x$$

$$\varepsilon_{yz} = \frac{\partial v}{\partial z} + \frac{\partial w}{\partial x} = \frac{\partial w_o}{\partial y} + \theta_y + 3\, z^2\, \beta\, \zeta_y$$

The concept of stress resultants is employed in deriving the constitutive relationship of laminated composites plates. Stress resultants are membrane forces or moments that act along member axes and tangent to plate mid-surfaces, as shown in Figure 2.7.

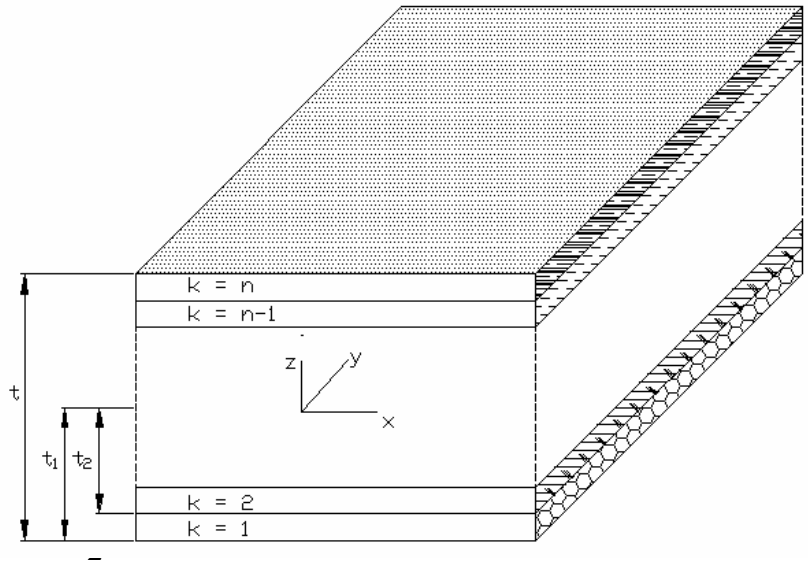

Figure 2.8 : Geometry of a laminated plate

Referring to the geometry of a laminated plate such as shown in Figure 2.8, force and moment resultants are defined as follows :

For the in-plane resultant forces and moments,

$$[N] = \begin{Bmatrix} N_x \\ N_y \\ N_{xy} \end{Bmatrix} = \int_{-t/2}^{t/2} \begin{Bmatrix} \sigma_x \\ \sigma_y \\ \tau_{xy} \end{Bmatrix} dz$$

$$[M] = \begin{Bmatrix} M_x \\ M_y \\ M_{xy} \end{Bmatrix} = \int_{-t/2}^{t/2} \begin{Bmatrix} \sigma_x \\ \sigma_y \\ \tau_{xy} \end{Bmatrix} z dz \qquad (2.10a)$$

$$[P] = \begin{Bmatrix} P_x \\ P_y \\ P_{xy} \end{Bmatrix} = \int_{-t/2}^{t/2} \begin{Bmatrix} \sigma_x \\ \sigma_y \\ \tau_{xy} \end{Bmatrix} z^3 \, dz$$

where *[N]* is the matrix of resultant force, *[M]* is the matrix of resultant moment and *[P]* is the matrix of higher order force.

For the out of plane forces,

$$[V] = \begin{Bmatrix} V_{xz} \\ V_{yz} \end{Bmatrix} = \int_{-t/2}^{t/2} \begin{Bmatrix} \tau_{xz} \\ \tau_{yz} \end{Bmatrix} dz \qquad (2.10b)$$

$$[W] = \begin{Bmatrix} W_{xz} \\ W_{yz} \end{Bmatrix} = \int_{-t/2}^{t/2} \begin{Bmatrix} \tau_{xz} \\ \tau_{yz} \end{Bmatrix} z^2 \, dz$$

where *[V]* is the matrix of resultant shear force and *[W]* is the matrix of the higher order shear force.

So,

$$\begin{Bmatrix} N_x \\ N_y \\ N_{xy} \end{Bmatrix} = \Sigma [\overline{Q}_{ij}] \int_{-t/2}^{t/2} \begin{Bmatrix} \varepsilon_{x0} \\ \varepsilon_{y0} \\ \varepsilon_{xy0} \end{Bmatrix} dz + \int_{-t/2}^{t/2} \begin{Bmatrix} \kappa_x \\ \kappa_y \\ \kappa_{xy} \end{Bmatrix} z \, dz + \int_{-t/2}^{t/2} \begin{Bmatrix} \dfrac{\partial \zeta_x}{\partial x} \\ \dfrac{\partial \zeta_y}{\partial y} \\ \dfrac{\partial \zeta_x}{\partial y} + \dfrac{\partial \zeta_y}{\partial x} \end{Bmatrix} z^3 \, dz \quad (2.11a)$$

or,

$$[N] = [A]\{\varepsilon_p\} + [B]\{\varepsilon_f\} + [E]\{\varepsilon_w\} \qquad (2.11b)$$

Similarly,

$$\begin{Bmatrix} M_x \\ M_y \\ M_{xy} \end{Bmatrix} = \Sigma [\overline{Q}_{ij}] \left[\int_{-t/2}^{t/2} \begin{Bmatrix} \varepsilon_{x0} \\ \varepsilon_{y0} \\ \varepsilon_{xy0} \end{Bmatrix} z dz + \int_{-t/2}^{t/2} \begin{Bmatrix} \kappa_x \\ \kappa_y \\ \kappa_{xy} \end{Bmatrix} z^2 \, dz + \int_{-t/2}^{t/2} \begin{Bmatrix} \dfrac{\partial \zeta_x}{\partial x} \\ \dfrac{\partial \zeta_y}{\partial y} \\ \dfrac{\partial \zeta_x}{\partial y} + \dfrac{\partial \zeta_y}{\partial x} \end{Bmatrix} z^4 \, dz \quad (2.12a)$$

or

$$[M] = [B]\{\varepsilon_p\} + [D]\{\varepsilon_f\} + [F]\{\varepsilon_w\} \qquad (2.13b)$$

and

$$\begin{Bmatrix} P_x \\ P_y \\ P_{xy} \end{Bmatrix} = \sum [\overline{Q}_{ij}] \left[\int_{-t/2}^{t/2} \begin{Bmatrix} \varepsilon_{x0} \\ \varepsilon_{y0} \\ \varepsilon_{xy0} \end{Bmatrix} z^3 \, dz + \int_{-t/2}^{t/2} \begin{Bmatrix} \kappa_x \\ \kappa_y \\ \kappa_{xy} \end{Bmatrix} z^4 \, dz + \int_{-t/2}^{t/2} \begin{Bmatrix} \dfrac{\partial \zeta_x}{\partial x} \\ \dfrac{\partial \zeta_y}{\partial y} \\ \dfrac{\partial \zeta_x}{\partial y} + \dfrac{\partial \zeta_y}{\partial x} \end{Bmatrix} z^6 \, dz \right] \qquad (2.14)$$

or

$$[P] = [E]\{\varepsilon_p\} + [F]\{\varepsilon_f\} + [G]\{\varepsilon_w\}$$

Combining all terms, the constitutive relationship for a laminated composite plate becomes,

$$\begin{Bmatrix} N_x \\ N_y \\ N_{xy} \\ M_x \\ M_y \\ M_{xy} \\ P_x \\ P_y \\ P_{xy} \\ V_x \\ V_y \\ W_x \\ W_y \end{Bmatrix} = \begin{bmatrix} A_{11} & A_{12} & A_{13} & B_{11} & B_{12} & B_{13} & E_{11} & E_{12} & E_{13} & 0 & 0 & 0 & 0 \\ A_{12} & A_{22} & A_{23} & B_{12} & B_{22} & B_{23} & E_{12} & E_{22} & E_{23} & 0 & 0 & 0 & 0 \\ A_{13} & A_{23} & A_{33} & B_{13} & B_{23} & B_{33} & E_{13} & E_{23} & E_{33} & 0 & 0 & 0 & 0 \\ B_{11} & B_{12} & B_{13} & D_{11} & D_{12} & D_{13} & F_{11} & F_{12} & F_{13} & 0 & 0 & 0 & 0 \\ B_{12} & B_{22} & B_{23} & D_{12} & D_{22} & D_{23} & F_{12} & F_{23} & F_{23} & 0 & 0 & 0 & 0 \\ B_{13} & B_{23} & B_{33} & D_{13} & D_{23} & D_{33} & F_{13} & F_{23} & F_{33} & 0 & 0 & 0 & 0 \\ E_{11} & E_{12} & E_{13} & F_{11} & F_{12} & F_{13} & G_{11} & G_{12} & G_{13} & 0 & 0 & 0 & 0 \\ E_{12} & E_{22} & E_{23} & F_{12} & F_{22} & F_{23} & G_{12} & G_{22} & G_{23} & 0 & 0 & 0 & 0 \\ E_{13} & E_{23} & E_{33} & F_{13} & F_{23} & F_{33} & G_{13} & G_{23} & G_{33} & 0 & 0 & 0 & 0 \\ 0 & 0 & 0 & 0 & 0 & 0 & 0 & 0 & 0 & S_{11}^1 & S_{12}^1 & S_{11}^2 & S_{12}^2 \\ 0 & 0 & 0 & 0 & 0 & 0 & 0 & 0 & 0 & S_{12}^1 & S_{22}^1 & S_{12}^2 & S_{22}^2 \\ 0 & 0 & 0 & 0 & 0 & 0 & 0 & 0 & 0 & S_{11}^2 & S_{12}^2 & S_{11}^3 & S_{12}^3 \\ 0 & 0 & 0 & 0 & 0 & 0 & 0 & 0 & 0 & S_{12}^2 & S_{22}^2 & S_{12}^3 & S_{22}^3 \end{bmatrix} \begin{Bmatrix} \varepsilon_x^m \\ \varepsilon_y^m \\ \varepsilon_{xy}^m \\ \varepsilon_x^b \\ \varepsilon_y^b \\ \varepsilon_{xy}^b \\ \varepsilon_x^w \\ \varepsilon_y^w \\ \varepsilon_{xy}^w \\ \varepsilon_{xz}^s \\ \varepsilon_{yz}^s \\ \varepsilon_{xz}^{sw} \\ \varepsilon_{yz}^{sw} \end{Bmatrix} \qquad (2.15a)$$

or,

$$\begin{Bmatrix} \{N\} \\ \{M\} \\ \{P\} \\ \{V\} \\ \{W\} \end{Bmatrix} = \begin{bmatrix} [A] & [B] & [E] & 0 & 0 \\ [B] & [D] & [F] & 0 & 0 \\ [E] & [F] & [G] & 0 & 0 \\ 0 & 0 & 0 & [S_1] & [S_2] \\ 0 & 0 & 0 & [S_2] & [S_3] \end{bmatrix} \qquad (2.15b)$$

where the in-plane coefficients are,

$$\{ [A], [B], [D], [E], [F], [G]\} = \sum_{k=1}^{n} \int \overline{Q_{ij}} \ (1, z, z^2, z^3, z^4, z^6) \, dz \qquad (2.15c)$$

and the out of plane coefficients are,

$$\{ [S_1], [S_2], [S_3] \} = \sum_{k=1}^{n} \int \overline{R_{ij}} \ (1, z^2, z^4) \, dz \qquad (2.15d)$$

2.2 SMA theory

In this section, the properties of the shape memory effect, quassiplasticity and pseudoelasticity of the non-embedded SMA are first described. It is then followed by the description of the property of the embedded SMA. The explanations on the SMA composite structures in terms of its configuration and construction where the former depends on the control strategy of the structure are given. Finally the detail description on the Brinson's model is given and the constitutive and the evolutionary equations of this model are solved to give the plots that represent the properties of shape memory effect, quassiplasticity and pseudoelasticity of the SMA. This Brinson's model parameters used in this study are experimental values taken from Zak et al (2001).

2.2.1 Properties of the SMA

SMA posses unique properties of shape memory effect, quassiplasticity and pseudoelasticity as mentioned in section 1.2.3. At the heart of these novel properties is the SMA ability to undergo a solid-solid first order transformation process that is called

the thermoelastic transformation. Thermoelastic transformation is a reversible diffusionless solid transition between the parent phase austenite and the product phase martensite. Cooling an austenite phase will cause the movement of its crystal lattices in order to accommodate the minimum free energy state [Otsaka and Wayman 1998]. Rather than a long distance movement, atoms start to form new orientations thru a shear dominant mechanism called twinning. In the twinning process a strain caused by a martensite variant will be accommodated by its surrounding variants causing the orientation of alternate variants such as in figure 2.9a. The transformation is thus called the self-accommodated transformation and this martensite is called the temperature induced martensite (TIM). The first nucleation of martensite occurs at temperature M_s which is lower than temperature T_0 where the free energy of martensite equal to the free energy of austenite (Funakubo 1987). By the end of transformation process at temperature M_f, a maximum of 24 orientations of martensite can be formed making it less symmetry and lower in mechanical properties as compared to the parent phase. These 24 orientations can be divided into two variants, M^+ and M^- (Huo et al. 1993). As this thermoelastic transformation occurs within the austenite crystal frame as shown in figure 2.9, the process is reversible and the macroscopic shape of the martensite is the same as the macroscopic shape of the austenite. Heating the martensite, thermoelastic transformation will occur to change the multivariant martensite back to the single variant austenite thru a temperature hysteresis path. There are thus four transition temperatures, M_s, M_f, A_s and A_f where letters s and f refer to the start and final respectively. These transformation temperatures are usually assumed to be linearly related to stress in Tanaka's [1990], Liang and Rogers (1990) and Brinson's model (1990). The transition

temperatures can be controlled by changing the SMA alloy composition and conducting the heat treatment. For commonly available SMAs, the transformation temperatures can remain within a fully controllable temperature range from as low as -53^0C to -5^0C to as high as 59^0C to 121^0C with a total hysteresis span of 26^0C to 46^0C in the case of binary alloys. The hysteresis span can be further reduced to 10^0C by the addition of copper, or alternatively enhanced to 100^0C by the addition of niobium (Zak et al. 2003).

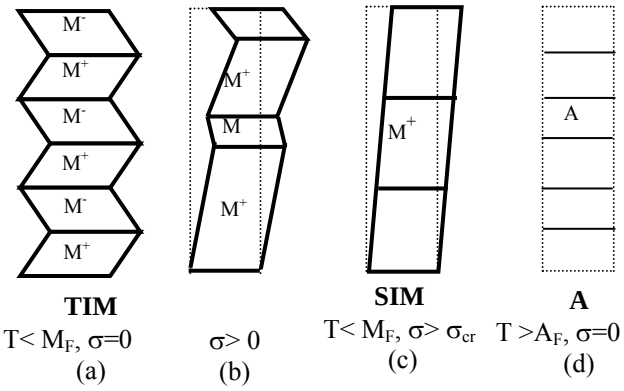

Figure 2.9: The effect of temperature and stress on the SMA (Hornbogen 1991)

The effect of stress on the SMA is important due to the displacive nature of the transformation. Referring to figure 2.9c, applying an amount of force to the TIM at $T < M_f$ will reorient the twinned martensite to the stress preferrential oriented martensite (SIM). Releasing the load will see the permanent strain in the martensite in a behaviour called the quasiplasticity (Müller, S. Seelecke 2001) as in figure 2.10a. The strain can be recovered by heating the SIM to a temperature higher than A_f. At this temperature all martensite will change to austenite that has a macroscopic shape equivalent to the original temperature induced martensite thus recovering the original shape. This phenomena shown in figure 2.10a is called the shape memory effect (SME). Recovery strain of up to 6-8% can be achieved for nitinol (Gandhi and Thompson 2000).

Restraining the strain recovery will induce the internal stress gradually. Recovery stress of up to 800 Mpa can be achieved for NiTi (Thompson and Loughlan 1997). Giving a load to austenite phase at a higher temperature, the austenite will be converted to SIM after a critical stress is reached. As in figure 2.10b, releasing the load then will return the SMA to its austenite phase thus recovering strain up to 8%. At a temperature above T_d, austenite will behave like any typical metals where yielding occurs to indicate the start of plasticity.

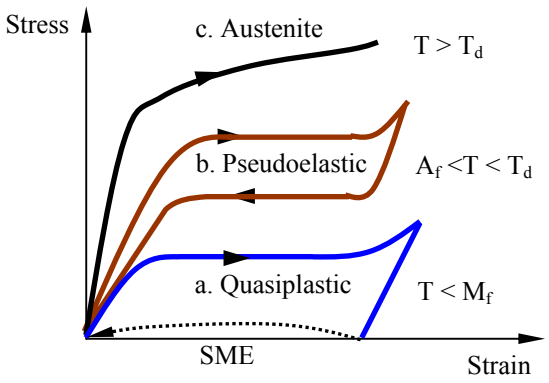

Figure 2.10: Quasiplasticity, SME and Pseudoelasticity

2.2.2 Properties of the embedded SMA

Numerous studies have been conducted on the transformational behaviour of the free SMA but the same studies on the SMA composite are rather limited (Jonnalagada 1998). A review on the stress recovery behaviour of the SMA when it is embedded is given here. From the studies of Sittner and Stalmans (2000), Zheng et al. (2001) and Tsoi et al. (2002), the transformational behaviour of the SMA composite is directly related to the existence of the TIM and SIM and the effect of the constraining matrix on them. Both martensites transform to austenite upon heating but in a different manner. Referring to figure 2.11, the transformation of TIM to austenite require no macroscopic shape change,

in contrast to the transformation of SIM. As a result the constraining matrix has no effect on the transformation of TIM but the same matrix impedes the transformation of SIM. This impeding of the SIM transformation will result in the gradual inducement of the recovery stress.

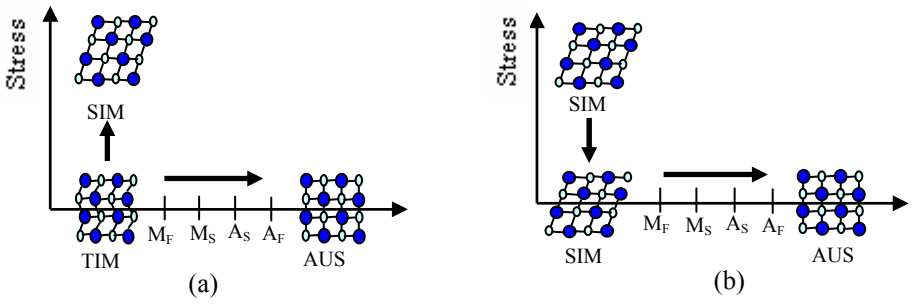

Figure 2.11: Transformation of (a) free TIM and (b) SIM to austenite.

The transformational behaviour of the SMAHC can be studied thru the differential scanning calorimetry (DSC) and isolength tests (Sittner and Stalmans 2000, Zheng et al. 2001 and Tsoi et al. 2002). A comparison between the free and constrained recoveries of nickel rich Ni-Ti for different values of pre-strains is now explained. While the free recovery represents the isolated SMA, the constraint recovery here represents the SMAHC. With reference to figure 2.12, for 0% SMA pre-strain, there is no difference in the reverse transformation between the free and constrained recoveries because in both recoveries, the present martensite is the TIM and TIM is not affected by the constraint. A transformation in both cases releases the same amount of heat as detected by the DSC test. However with a pre-strain, the existence of both the TIM and SIM in the martensite will see them to be transformed to austenite in the case of free recovery but for the constrained case, only TIM is transformed to austenite resulting in the less amount of endothermic heat detected. Increasing the pre-strain to 8% which is the maximum

recoverable strain for NiTi SMA, the heat detected by the free recovery remain the same while in the case of the constrained recovery, zero endothermic heat is detected. This is because at the maximum recoverable strain, ε_L = 8%, all SMA have been converted to SIM which is impeded from transforming to austenite upon heating.

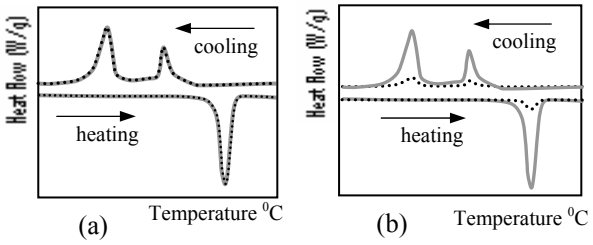

Figure 2.12: A DSC test on (a) Free TIM (b) 8% pre-constraint TIM (free recovery, constraint recovery)

Table 2.2 shows the result of the iso-length tests on the constrained NiTi SMA for different pre-strain levels. At 0% pre-strain there is no recovery stress since there is no SIM. At 8% pre-strain, the SMA contains both the TIM and SIM. While matrix constraining of the SIM will result in stress recovery, the amount of SIM to be converted finishes before the A_F temperature is reached.

Table 2.2: Comparing free and constraint recovery for 0% and 8% pre-strained TIM.

Free Recovery	Constraint Recovery
0% pre-strain	
TIM TIM AUS TIM	TIM TIM AUS TIM
8% pre-strain	
TIM TIM + SIM AUS TIM	TIM TIM + SIM AUS + SIM TIM + SIM

2.2.3 SMA composite structure

a. Control strategies

The structure of the SMA composite plate is characterised by the location of the SMA fibres or wires and the way SMA wires are attached to the composites. The location of the SMA wires depends on the required control strategy. Referring to section 1.2.4, the control strategy depends on the types of SMA improvement needed: APT, ASC and ASET. APT is about increasing the mechanical property of the SMA such as the Young's modulus and the coefficient of thermal expansion when transformation from martensite to austenite occurs. SMA is best situated along the neutral axis of the plates for this purpose. ASC requires the SMA to induce bending moment upon its activation. This can be achieved in two ways: Attaching or embedding SMA wires eccentrically to the neutral axis as in figure 2.13b and 2.13c and training the SMA to deflect upon activation while embedding it at the neutral axis (Baz et el. 1998). Finally in ASET, the recovery stress induced when SMA is activated is used to increase the stiffness of the composite. For this purpose SMA wires should be situated either along the neutral axis (figure 2.13a) or symmetrically through thickness of the plate (figure 2.13c). Notice that SMA wires can be directly embedded within the matrix of the SMAHC or thru sleeves as in figures 2.13d and 2.13e. In the direct embedding, the recovery stress is dependent on the compliance of the surrounding matrix. The lower the compliance, the higher the level of induced force (Thompson and Loughlan 2001). Direct embedding has a disadvantage of destroying the matrix in the case of overheating while embedding thru sleeves prevent resistive heat to

directly transferred to the matrix. However embedding thru sleeves requires the SMA wires to be clamped at both ends in order to get any recovery stress. This is however in reality impractical (Thompson and Loughlan 2001).

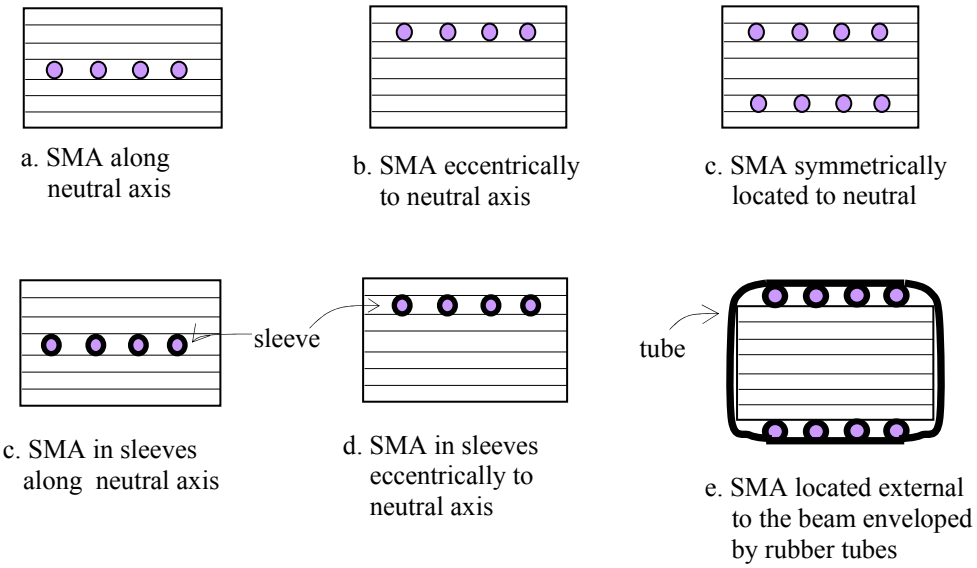

Figure 2.13: SMA plate cross-sections for different control strategies

b. SMA composite structures

Rogers et (1991) proposed three layer SMA composite plates where SMA composite layer were located in the middle of the plates. Referring to figure 2.13, graphite-epoxy layers (G/E) are stacked symmetrically on top and bottom of the nitinol/epoxy (N/E) layer which is the SMA composite layer. The direction of the nitinol fibres can be in the E11 or E22 direction. The orientations of graphite epoxy plies was not specified. Both APT and ASET were studied. The effect of APT and ASET were studied by Zak et al (2003) on SMA composite plates of the configuration as in figure 2.13c. The plates consists of 12 layers: 2 Nitinol-epoxy layers and 10 graphite-epoxy layers in a configuration of $[0^0/(\pm\alpha)_s/0^0]$. This SMA composite plate is shown in figure 2.14.

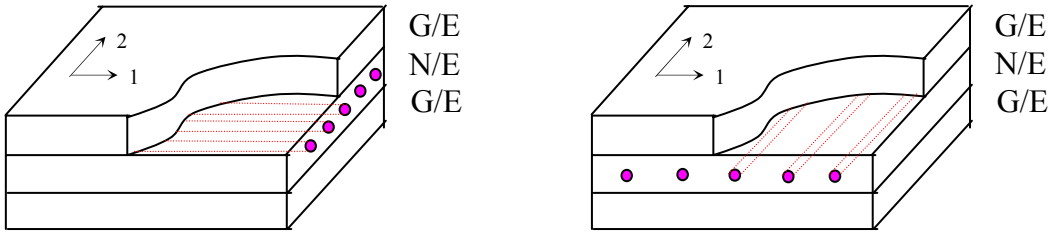

Figure 2.13 : SMA composite structures with SMA fibres in 2 different directions:

a) E11 direction b) E22 direction

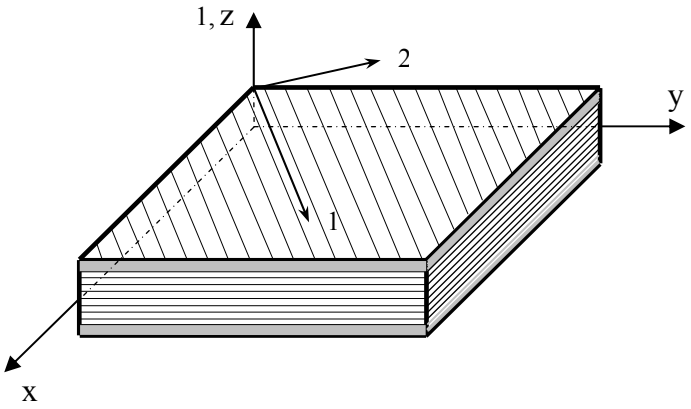

Figure 2.14: SMA composite plates (: N-E layer, :G-E layer)

The SMA plates in figure 2.13 and 2.14 have relatively small number of SMA layers compared to composite layers. The purpose behind this is to minimize the electrical wiring required to activate the SMA wires. However for aerospace applications, the activation required can be obtained through environmental heating. As such SMA fibres or wires can be embedded parallel to graphite fibres within each layer of graphite-epoxy layer such as shown in figure 2.15. Studies on thermal buckling and postbuckling of SMA composite plates using this types of SMA composite were conducted by Zhong et al (1994), Tawfik et al (1998), Duan et al (2000), Pak et al (2003) and Heli (2003).

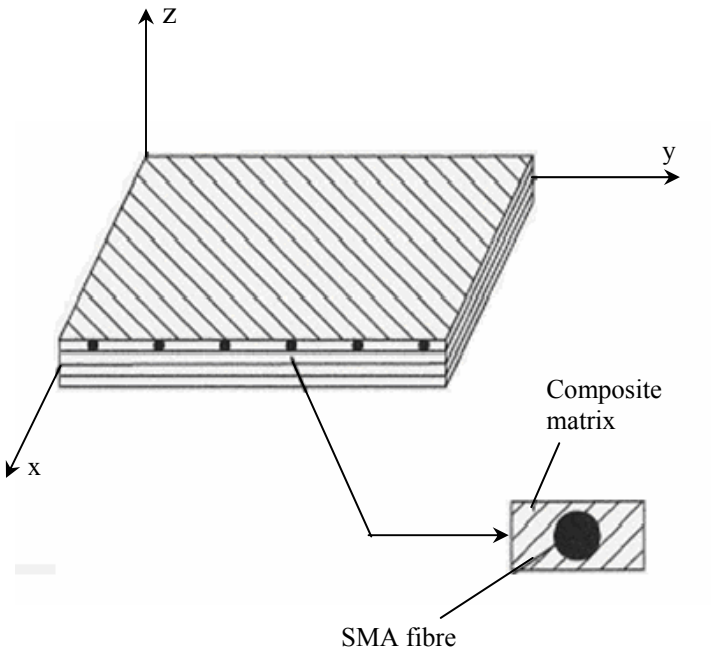

Figure 2.15. The SMA composite plates in thermal applications (Park 2003)

2.2.4 SMA Brinson's Model

The Brinson's model (Brinson 1991) made a significant improvement to Tanaka's model (Tanaka 1990) and the Liang and Rogers's model (Liang and Rogers 1990). It recognises the SIM as the only martensite that gives the functional property of SME and pseudoelasticity rather than the total martensite that contains both the TIM and the SIM. Brinson's model assumes that the transformation depends only on temperature and stress and the amount of transformation that occurs is described using the volume fraction martensite, ξ_S. Thus solution to the Brinson's model as in Tanaka's and Liang and Rogers's model simply involve solving 2 equations namely the constitutive equation and the evolutionary equations. Brinson's model is quite popular for engineering applications since it is simple, accurate and easy to be implemented into numerical applications such as the finite element method.

This section will describe the Brinson's model (Brinson 1990) in terms of its constitutive relation and evolutionary relationship for constant material functions. The experimental material parameters taken from Zak et al (2003) are specified. With this material parameters, the plots of behaviours of shape memory effect, pseudoelasticity, free recovery, restrained and constrained recovery are plotted.

a. Brinson's model

Brinson (1990) made a modification so that this model can be used at low temperature by dividing martensitic fraction into two parts.

$$\xi = \xi_s + \xi_T \qquad (2.16)$$

where ξ_s corresponds to the fraction of the SIM and ξ_T refers to the fraction of the TIM. Furthermore, this division is logical considering the result of the studies mentioned in section 2.3.2 where only SIM that is responsible for recovery stress. From Tanaka (1990) and equation (1), we have

$$\sigma = \sigma(\varepsilon, \xi_s, \xi_T, T) \qquad (2.17)$$

and after simple derivation and applying a forced condition we have a constitutive relationship of Brinson's model for constant material parameter.

$$\sigma - \sigma_o = D(\varepsilon - \varepsilon_o) + \Omega\ (\xi_s - \xi_{so}) + \theta(T - T_o) \qquad (2.18)$$

where D is theYoung Modulus, θ is thermoelastic tensor and Ω is transformation tensor. The effect of stress on transition temperature now must consider the conversion of TIM to SIM. This process of conversion starts after a TIM is given a stress up to a critical value, σ_s^{cr} and finish at a stress value of σ_f^{cr}. The values of these critical stresses can be determined thru experiments or theoretically by developing a model based on the potential energy necessary to overcome the chemical energy barrier for conversion of

twins as in the work of Achenbach and Muller (1990). The stress temperature coefficients, C_A and C_M in Brinson's model are not assumed to be equal and both are determined thru experiments. Figure 2.16 shows the effect of stress on the critical temperature.

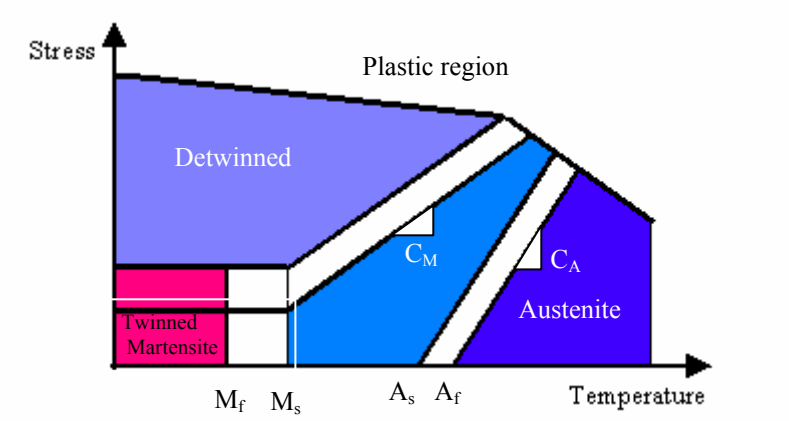

Figure 2.16: The effect of stress on the transformation temperature.

So the evolution equations are:

1. Twinned Martensite ↔ detwinned martensite

   a. T>M_s and $\sigma_s^{cr} + C_m(T - M_s) < \sigma < \sigma_f^{cr} + C_m(T - M_s)$

$$\xi_s = \frac{1-\xi_{so}}{2}\cos\left[\frac{\pi}{\sigma_s^{cr} - \sigma_f^{cr}}\left(\sigma - \sigma_f^{cr} - C_m(T - M_s)\right)\right] + \frac{1+\xi_{so}}{2} \qquad (2.19a)$$

$$\xi_t = \xi_{to} - \frac{\xi_{To}}{1-\xi_{so}}(\xi_s - \xi_{so}) \qquad (2.19b)$$

   b. T<M_s and $\sigma_s^{cr} < \sigma < \sigma_f^{cr}$

$$\xi_s = \frac{1-\xi_{so}}{2}\cos\left[\frac{\pi}{\sigma_s^{cr} - \sigma_f^{cr}}\left(\sigma - \sigma_f^{cr}\right)\right] + \frac{1+\xi_{so}}{2} \qquad (2.19c)$$

$$\xi_t = \xi_{to} - \frac{\xi_{To}}{1-\xi_{so}}(\xi_s - \xi_{so}) + \Delta_{T\xi} \qquad (2.19d)$$

   where, if M_f < T<M_s and T<T_o,

$$\Delta_{T\xi} = \frac{\xi_{so}}{2}\cos\left[\frac{\pi}{A_f - A_s^{cr}}\left(T - M_f\right)\right] + 1 \qquad (2.19e)$$

   else, $\Delta_{T\xi} = 0$

2. Martensite ↔ Austenite.

For $T>A_s$ and $C_A(T-A_f) < \sigma < C_A(T-A_S)$

$$\xi = \frac{\xi_o}{2}\left(\cos\left[\frac{\pi}{A_f - A_s}\left(T - A_s - \frac{\sigma}{C_A}\right)\right]+1\right) \quad (2.20a)$$

$$\xi_S = \xi_{So} - \frac{\xi_{So}}{\xi_o}(\xi_o - \xi) \quad (2.20b)$$

$$\xi_T = \xi_{To} - \frac{\xi_{To}}{\xi_o}(\xi_o - \xi) \quad (2.20c)$$

b. Material parameters

Table 2.3 shows the parameters correspond to the constitutive and evolutionary equations of the Brinson's model. These parameters are experimental values taken from experiments conducted by Zak et al (2003). These parameters will be used throughout this study.

Table 2.3: Parameters of the Shape Memory Alloy Brinson's Model (Zak et al 2003)

Parameters	Values
Critical Stress Start,σ_S (Pa)	80E6
Critical Stress Finish,σ_F (Pa)	155.0E6
Martensite Young's Modulus (Pa)	33.0E9
Austenite Young's Modulus (Pa)	69.6E9
Maximum Residual Strain, ε_L	0.058
Initial Strain, ε_0	0.001
Martensite Finish Temperature (^{0}C)	20.7
Martensite Start Temperature (^{0}C)	26.8
Austenite Start Temperature (^{0}C)	37.2
Austenite Finish Temperature (^{0}C)	47.0
Stress Influence Coefficient C_M (Pa $^0C^{-1}$)	10.6E6
Stress Influence Coefficient C_A (Pa $^0C^{-1}$)	9.7E6

c. Brinson's model result

With these material parameters, the Brinson's Model constitutive and evolutionary equations are solved in order to study the properties of quassiplasticity and SME that gives both full and partial stress recoveries. It starts by giving the Nitinol SMA an

amount of stress that reaches above critical finish stress, σ_F for a complete detwinning process to occur (ξ_s=1). This Nitinol SMA can be fully martensite ($T<M_f$) or fully austenite ($M_s<T<A_s$). A complete unloading thereafter for each case will give the maximum residual strain, ε_L of about 0.058 m/m. These behaviours of quassiplasticity are shown in figure 2.17.

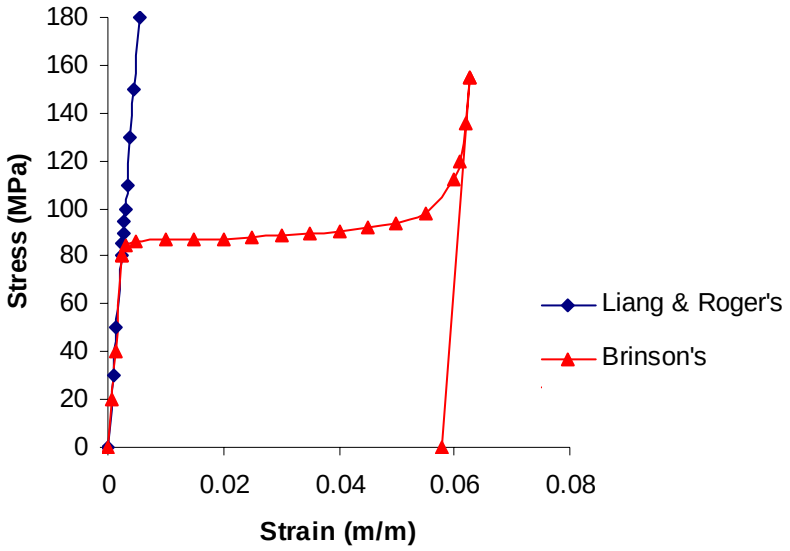

Figure 2.17: Quassiplasticity of fully martensite Nitinol SMA

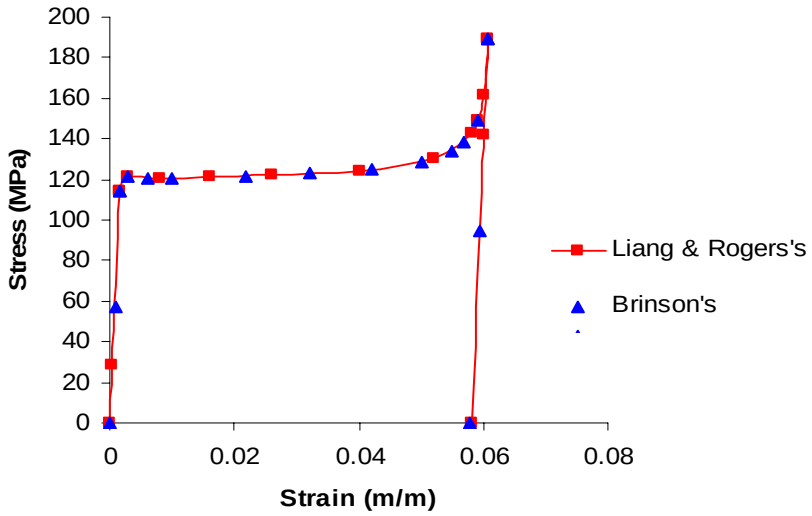

Figure 2.18: Quassiplasticity of fully austensite Nitinol SMA

Notice that in figure 2.17, Liang and Rogers's model cannot represent the detwinning process of martensite where the loading process becomes the infinite linear elastic loading. However for fully austenite case, both models provide a similar response such as in figure 2.18.

The same type of SMA with a certain amount of pre-strained is now heated above the austenite start temperature, A_s while it is prohibited from recovering its strain. The full stress recovery or restrained recovery occurs when the SMA wires are totally prohibited to recover its strain i.e. there is no change in strain (Liang and Rogers 1990). As a result a huge amount of recovery stress can be generated even for a small amount of pre-strain given. Figure 2.19 provides the amount of recovery stress over an increase in temperature for different values of SMA initial strains, e. Notice that in figure 2.19, the incomplete Liang and Rogers's curve is shown where in the complete one, an enormous amount of recovery stress of more than 4000 MPa can be recovered.

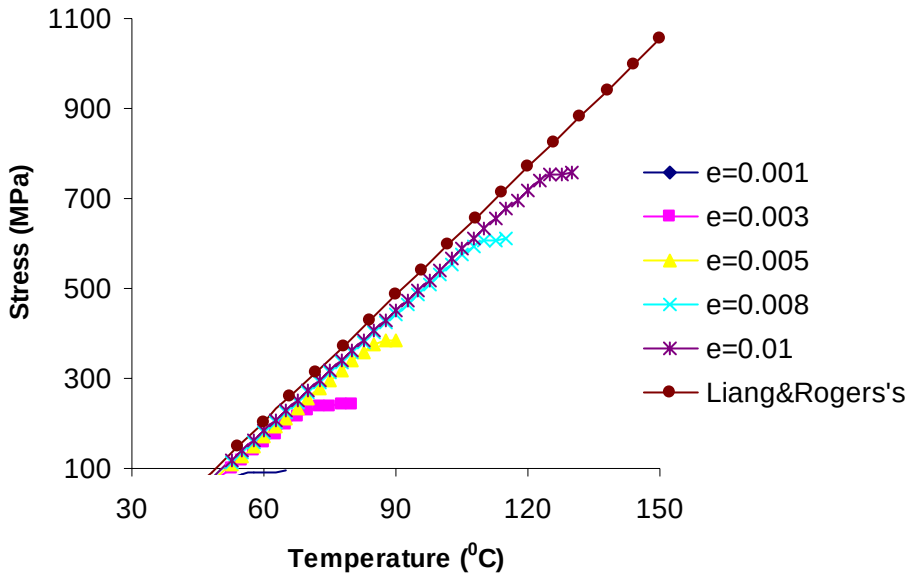

Figure 2.19. Full stress recovery of SMA for different initial strains.

This full recovery assumption is suitable if SMA wires are fixed at both ends. A better assumption for the SMA composite plates is the controlled recovery where some recovery strain may occur during the heating process of the SMA wires. The SMA and the composite can be modeled as a SMA-spring structure such as in figure 2.20 where the amount of recovery strain allowed to occur depends on the stiffness of spring.

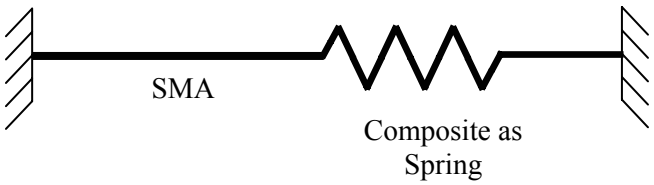

Figure 2.20: SMA-spring representation of SMA composite plates.

Figure 2.21 shows the reduction of the recovery stress in the control recovery for different values of SMA-spring property, kL/s where k is the spring constant, L is the length of the wire and s is the cross-sectional area of the wire (Liang and Rogers 1990).

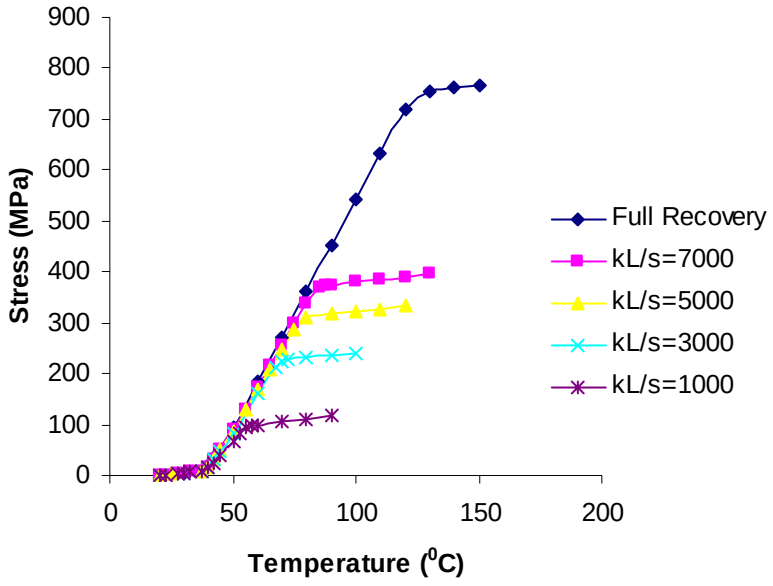

Figure 2.21: Controlled stress recovery of SMA for different spring parameters.

2.2.5 Approach to SMA structure's mathematical formulation

The mathematical formulation for composite plates is rather established. For example in the case of finite element method, the formulation involves combining the assumed displacement field and the constitutive relation into the principle of virtual work equation (Cook 1985). By embedding SMA into composite plates, the effect on the material constants and the addition of the recovery stress in the case of ASET applications need to be considered. For two constituent SMA composite layers such as the nitinol-epoxy layer in figure 2.14, the layer is treated as an orthotropic layer similar to typical graphite/epoxy layer (Rogers et al. 1990). There are two approaches in incorporating SMA recovery stress to the formulation. Firstly the recovery stress values are inserted into the governing equation either as the external force (Zak et al 2003) or internal stress (Zhong et al (1994), Tawfik et al (1998), Duan et al (2000), Pak et al (2003) and Heli (2003) while secondly the constitutive relation of the SMA such as the equation 2.3 for Brinson's model is incorporated to the constitutive equation (Ghomsei et al 2004, Rasani 2003). In the first approach, the recovery stress values can be either taken from experiment or form the model such as Brinson's model. This approach is used in the majority cases and also will be used in the present study.

2.3 Closure

3.0 FINITE ELEMENT FORMULATION OF SMA COMPOSITE PLATES

3.1 Introduction

The approach to the finite element formulation in this study as mentioned in section 2.2.5, is of the first type where the recovery stress values are inserted into the governing equation either as the external force or the internal stress. This approach was initially proposed by Jia and Rogers [1993] and later refined by several researchers (Zhong et al. 1994, Tawfik et al. 1998, Duan et al. 2000, Park et al. 2003 and Heli 2003). The Brinson's model is used to obtain the recovery stress correspond the temperature given to the SMA composite plates. As for the SMA layer, the effective properties are determined through employing the rule of mixture. Since the tensional recovery load will be in the direction along the SMA wire, the orientation of the SMA wire should be in the principle-1 direction. Using the effective properties, the global transformed reduced stiffness matrix $\left[\overline{Q}\right]$ and the material stiffness ABD matrix of the SMA composite plates can be determined through the usual way as in the derivation for the same stiffness of the FRC. The kinematic of the SMA composite plates in this study is based on the FSDT where the von Karman's nonlinear moderate strain term is added to the strain equation. Combining the kinematics and constitutive relations of the SMA composite into the Hamilton's principle using the FEM approach, the governing equations that dictate the structural behaviours of SMA plates can be obtained. Note that even though the derivation of the FEM formulation here is to include the non-linear structural analysis where the total Lagrangian formulation is used., the scope of this research is limited to the linear analysis only. Furthermore, the thermal effect of heating is neglected in this

study. As such, the obtained formulation will be reduced to specifically meet the required linear analysis such as the stress, deflection, free vibration and buckling analysis.

3.2 Effective properties

Referring to figure 3.1 [23], assuming a perfect bonding, both SMA and matrix stretches the same amount in the 1-direction. A perfect bonding results in only a global strain that involves SMA or actuator and matrix together. The local strain of the SMA will be prohibited by surrounding matrix thus resulting in recovery stress. So

$$\varepsilon_1 = \varepsilon_{1m} = \varepsilon_{1a} \qquad (3.1)$$

where ε_1, ε_{1m} and ε_{1a} are the total strain, matrix strain and actuator strain in 1-direction respectively.

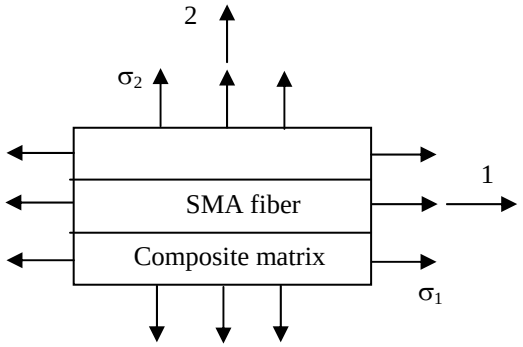

Figure 3.1. A volume representation of a SMA layer [Zhong et al 1994]

Since total force in 1-direction is contributed by both the matrix and SMA,

$$F_1 = F_{1m} + F_{1a}$$

$$= A_m\sigma_{1m} + A_a\sigma_{1a} \qquad (3.2a)$$

$$\sigma_1 = \frac{F_1}{A} = \frac{A_m\sigma_{1m} + A_a\sigma_{1a}}{A}$$

$$= V_m\sigma_{1m} + V_a\sigma_{1a} \qquad (3.2b)$$

where V_m and V_a are the volume fractions of the matrix and SMA respectively.

The calculation for volume fractions of SMA and matrix can be calculated, for example in a lamina of SMA-matrix such as shown in figure 3.2, total area A

$$A = ab \tag{3.3a}$$

So

$$V_a = n\pi \frac{d_a{}^2}{A} \quad \text{and} \quad V_m = 1 - V_a \tag{3.3b}$$

where n and d_a are the number of SMA wires and the diameter of the SMA wire respectively.

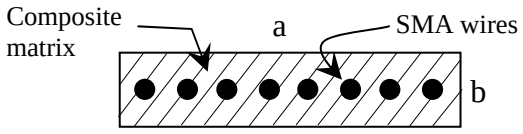

Figure 3.2 A SMA composite layer

In 1-direction, the stress-strain relation can be defined as

$$\sigma_{1a} = E_a(\varepsilon_1 - \alpha_a \Delta T) + \sigma_r \tag{3.4}$$

where σ_{1a} is the stress in the SMA direction, E_a is the SMA Young's modulus which can be obtained from Brinson's model, ε_1 is the strain in 1-direction, α_s is the thermal expansion coefficient of the SMA, ΔT is the change of temperature and σ_r is the recovery stress obtained through SMA activation. The values of σ_r can be obtained from Brinson's model. For matrix material,

$$\sigma_{1m} = E_{1m}(\varepsilon_1 - \alpha_{1m} \Delta T) \tag{3.5}$$

where σ_{1m} is the stress of the matrix material in 1-direction, E_{1m} is the matrix Young's modulus in 1-direction and α_{1m} is the thermal expansion coefficient of the matrix in 1-

direction. Inserting equations *(3.4)* and *(3.5)* into *(3.2)*, we have a stress-strain relationship for 1D SMA-matrix system.

$$\begin{aligned}\sigma_1 &= V_m\sigma_{1m} + V_a\sigma_{1a} \\ &= V_m E_m\left(\varepsilon_1 - \alpha_{1m}\Delta T\right) + V_a\left(E_a\left(\varepsilon_1 - \alpha_a\Delta T\right) + \sigma_r\right) \\ &= E_1(\varepsilon_1 - \alpha_1\Delta T) + \sigma_r V_a \end{aligned} \qquad (3.6)$$

where the effective properties,

$$E_1 = V_m E_{1m} + V_a E_a \qquad (3.7a)$$

$$\alpha_1 = \left(V_m E_{1m}\alpha_{1m} - V_a E_a \alpha_a\right)/E_1 \qquad (3.7b)$$

where σ^r_1 is the recovery stress.

For Poisson's ratio, by definition

$$\upsilon_{12} = -\frac{\Delta w/w}{\Delta L/L} \qquad or \qquad \frac{\Delta w}{w} = -\upsilon_{12}\left(\frac{\Delta L}{L}\right) \qquad (3.8)$$

where w is width of the lamina. Thus

$$w = w_m + w_a \qquad and \qquad \Delta w = \Delta w_m + \Delta w_a \qquad (3.9)$$

With the perfect bonding assumption,

$$\Delta L_m = \Delta L_a \qquad (3.10)$$

$$\frac{\Delta w_a}{w_a} = -\upsilon_{12a}\left(\frac{\Delta L}{L}\right) \text{ and } \Delta w_a = -\upsilon_{12a} w_a \frac{\Delta L}{L} \qquad (3.11a)$$

$$\frac{\Delta w_m}{w_m} = -\upsilon_m\left(\frac{\Delta L}{L}\right) \text{ and } \Delta w_m = -\upsilon_m w_m \frac{\Delta L}{L} \qquad (3.11b)$$

Inserting into *(3.9)*,

$$\Delta w = -\left(-\upsilon_{12a} w_a + -\upsilon_m w_m\right)\frac{\Delta L}{L}$$

Dividing both side by w,

$$\frac{\Delta w}{w} = \left(-\upsilon_{12}\frac{w_a}{w} + \upsilon_m \frac{w_m}{w}\right)\frac{\Delta L}{L}$$

So,

$$\upsilon_{12} = \upsilon_a V_a + \upsilon_m V_m \qquad (3.12)$$

The effective properties in 2-direction are determined using the same concept. Stress are equal for SMA and matrix in 2-direction. So we have

$$\sigma_2 = \sigma_{2a} = \sigma_{2m} \qquad (3.13)$$

$$\sigma_{2a} = E_{2a}\left(\varepsilon_{2a} - \alpha_{2a}\Delta T\right) \quad \text{or} \quad \varepsilon_{2a} = \frac{\sigma_2}{E_{2a}} + \alpha_{2a}\Delta T \qquad (3.14)$$

$$\sigma_{2m} = E_{2m}\left(\varepsilon_{2m} - \alpha_{2m}\Delta T\right) \quad \text{or} \quad \varepsilon_{2m} = \frac{\sigma_2}{E_m} + \alpha_{2m}\Delta T \qquad (3.15)$$

Total elongation is a combination of the matrix and SMA elongation.

$$\Delta L_2 = \Delta L_m + \Delta L_a \qquad (3.16)$$

$$\Delta A_2 = \Delta A_m + \Delta A_a \quad \text{but} \quad \varepsilon = \frac{\Delta L}{L} = \frac{\Delta A}{A} \qquad (3.17)$$

$$A_2\varepsilon_2 = A_m\varepsilon_{2m} + A_a\varepsilon_{2a} \qquad (3.18)$$

So,

$$\varepsilon_2 = V_m\varepsilon_{2m} + V_a\varepsilon_{2a}$$

$$= V_m\left(\frac{\sigma_2}{E_m} + \alpha_{2m}\Delta T\right) + V_a\left(\frac{\sigma_2}{E_{2a}} + \alpha_{2a}\Delta T\right) \qquad (3.19)$$

$$= \left(\frac{V_m}{E_{2m}} + \frac{V_a}{E_{2a}} \right) \sigma_2 + \left(V_m \alpha_{2m} + V_a \alpha_{2a} \right) \Delta T$$

$$= E_2 \sigma_2 + \alpha_2 \Delta T \qquad (3.20a)$$

where,

$$E_2 = \frac{E_{2m} E_a}{V_m E_a + V_a E_{2m}} \qquad (3.20b)$$

$$\alpha_2 = V_m \alpha_{2m} + V_a \alpha_{2a} \qquad (3.20c)$$

Similarly for modulus of rigidity,

$$G_{12} = \frac{G_m G_a}{V_m G_a + V_a G_m} \qquad (3.20d)$$

3.3 Stress-strain Relationship

Based on the above analysis and the plane stress assumption of the plate, the constitutive relationship for a SMA laminated composite plate is

$$= \begin{Bmatrix} \sigma_1 \\ \sigma_2 \\ \sigma_{12} \end{Bmatrix} = \begin{bmatrix} Q_{11} & Q_{12} & 0 \\ Q_{12} & Q_{22} & 0 \\ 0 & 0 & Q_{33} \end{bmatrix} \left(\begin{Bmatrix} \varepsilon_1 \\ \varepsilon_2 \\ \varepsilon_{12} \end{Bmatrix} - \begin{Bmatrix} \alpha_1 \\ \alpha_2 \\ \alpha_{12} \end{Bmatrix} \Delta T \right) + V_a \begin{Bmatrix} \sigma_1^r \\ 0 \\ 0 \end{Bmatrix} \qquad (3.21a)$$

or in short form,

$$\sigma_1 = [Q] \left(\{\varepsilon_1\} - \{\alpha_1\} \Delta T \right) + Va \{\sigma_1^r\} \qquad (3.21b)$$

where *[Q]* is the reduced stiffness matrix whose elements are as followed.

$$Q_{11} = E_1 / 1 - \nu_{12} \nu_{21} \qquad Q_{12} = \nu_{12} E_2 / 1 - \nu_{12} \nu_{21} = \nu_{21} E_1 / 1 - \nu_{12} \nu_{21}$$

$$Q_{22} = E_2 / 1 - \nu_{12} \nu_{21} \qquad (3.21c)$$

$$Q_{33} = G_{12}$$

For transverse shear strain,

$$\begin{Bmatrix}\tau_{13}\\ \tau_{23}\end{Bmatrix}=\begin{vmatrix}Q_{44} & 0\\ 0 & Q_{55}\end{vmatrix}\begin{Bmatrix}\varepsilon_{13}\\ \varepsilon_{23}\end{Bmatrix} \qquad (3.22)$$

where $Q_{44}=G_{13}$ and $Q_{55}=G_{22}$.

The constitutive relation for a general orthotropic layer can be obtained by transforming the orthotropic stress using the transformation matrix. We have

$$\{\sigma_x\}=[T]^{-1}\{\sigma_1\} \quad \text{or} \quad [T]\{\sigma_x\}=\{\sigma_1\}$$

$$\{\varepsilon_x\}=[T]^{-1}\{\varepsilon_1\} \quad \text{or} \quad [T]\{\varepsilon_x\}=\{\varepsilon_1\} \qquad (3.23a)$$

$[T]$ is the transformation matrix,

$$[T]=\begin{bmatrix}c^2 & s^2 & 2cs\\ s^2 & c^2 & -2cs\\ cs & cs & c^2-s^2\end{bmatrix} \quad \text{and} \quad [T]^{-1}=\begin{bmatrix}c^2 & s^2 & -2cs\\ s^2 & c^2 & 2cs\\ cs & -cs & c^2-s^2\end{bmatrix} \qquad (3.23b)$$

where c=cos θ and s = sin θ.

For the generally orthotropic layer, transforming equation *(21b)*,

$$[T]\{\sigma_x\}=[Q][T](\{\varepsilon_x\}-\{\alpha_x\}\Delta T)+Va[T]\{\sigma_{x1}^r\} \qquad (3.24a)$$

$$[T]^{-1}[T]\{\sigma_x\}=[T]^{-1}[Q][T](\{\varepsilon_x\}-\{\alpha_x\}\Delta T)+Va[T]^{-1}[T]\{\sigma_x^r\} \qquad (3.24b)$$

$$\{\sigma_x\}=[T]^{-1}[Q][T](\{\varepsilon_x\}-\{\alpha_x\}\Delta T)+Va\{\sigma_{x1}^r\} \qquad (3.24c)$$

or

$$\begin{Bmatrix}\sigma_x\\ \sigma_y\\ \sigma_{xy}\end{Bmatrix}=\begin{bmatrix}\overline{Q}_{11} & \overline{Q}_{12} & \overline{Q}_{13}\\ \overline{Q}_{12} & \overline{Q}_{22} & \overline{Q}_{23}\\ \overline{Q}_{13} & \overline{Q}_{23} & \overline{Q}_{33}\end{bmatrix}\left(\begin{Bmatrix}\varepsilon_x\\ \varepsilon_y\\ \varepsilon_{xy}\end{Bmatrix}-\begin{Bmatrix}\alpha_x\\ \alpha_y\\ \alpha_{xy}\end{Bmatrix}\Delta T\right)+\begin{Bmatrix}\sigma_x^r\\ \sigma_y^r\\ \sigma_{xy}^r\end{Bmatrix}V_a \qquad (3.24d)$$

where $[\overline{Q}]$ is the transformed reduced stiffness matrix and

$$\{\alpha_x\} = [T]^{-1}\{\alpha_1\} \tag{3.25a}$$

or

$$\begin{Bmatrix}\alpha_x\\ \alpha_y\\ \alpha_{xy}\end{Bmatrix} = \begin{bmatrix}c^2 & s^2 & -cs\\ s^2 & c^2 & cs\\ cs & -cs & c^2-s^2\end{bmatrix}\begin{Bmatrix}\alpha_1\\ \alpha_2\\ 0\end{Bmatrix} = \begin{Bmatrix}c^2\alpha_1 + s^2\alpha_2\\ s^2\alpha_1 + c^2\alpha_2\\ cs\alpha_1 - cs\alpha_2\end{Bmatrix} \tag{3.25b}$$

$$\{\sigma_x^r\} = [T]^{-1}\{\sigma_1^r\} \tag{3.25c}$$

or

$$\begin{Bmatrix}\sigma_x\\ \sigma_y\\ \sigma_{xy}\end{Bmatrix} = \begin{bmatrix}c^2 & s^2 & -cs\\ s^2 & c^2 & cs\\ cs & -cs & c^2-s^2\end{bmatrix}\begin{Bmatrix}\sigma_1\\ \sigma_2\\ 0\end{Bmatrix} = \begin{Bmatrix}c^2\sigma_1 + s^2\sigma_2\\ s^2\sigma_1 + c^2\sigma_2\\ cs\sigma_1 - cs\sigma_2\end{Bmatrix} \tag{3.25d}$$

3.4 Displacement field and strains

Using the Mindlin's first order shear deformation theory [Mindlin 1970] i.e. equation *(2.8)* for β=0, displacement at any points on a laminated composite plate can be expressed as,

$$\begin{aligned} u(x,y,z,t) &= u_o(x,y,t) - z\,\theta_x(x,y,t)\\ v(x,y,z,t) &= v_o(x,y,t) - z\,\theta_y(x,y,t)\\ w(x,y,z,t) &= w_o(x,y,t)\end{aligned} \tag{3.26}$$

Strain can be expressed as

$$\{\varepsilon\} = \begin{Bmatrix}\varepsilon_{xx}\\ \varepsilon_{yy}\\ \gamma_{xy}\end{Bmatrix} = \begin{Bmatrix}\dfrac{\partial u}{\partial x}\\ \dfrac{\partial v}{\partial y}\\ \dfrac{\partial u}{\partial y}+\dfrac{\partial v}{\partial x}\end{Bmatrix} + \frac{1}{2}\begin{Bmatrix}\left(\dfrac{\partial w}{\partial x}\right)^2\\ \left(\dfrac{\partial w}{\partial y}\right)^2\\ 2\left(\dfrac{\partial w}{\partial x}\right)\left(\dfrac{\partial w}{\partial y}\right)\end{Bmatrix} + z\begin{Bmatrix}-\dfrac{\partial \theta_x}{\partial x}\\ -\dfrac{\partial \theta_y}{\partial y}\\ -\left(\dfrac{\partial \theta_x}{\partial y}+\dfrac{\partial \theta_y}{\partial x}\right)\end{Bmatrix} \tag{3.27}$$

or $\{\varepsilon\} = \{\varepsilon_m\} + \{\varepsilon_{nl}\} + z\{\varepsilon_b\}$ *(3.28)*

where $\{\varepsilon_m\}$, $\{\varepsilon_{nl}\}$and $\{\varepsilon_b\}$ are the inplane linear strain vector, the inplane nonlinear strain vector and the curvature strain vector, respectively. Furthermore, *u, v* and *w* are the displacements in the x, y and z directions respectively.

The incremental transverse shear strain vector is as follows

$$\{\gamma\} = \begin{Bmatrix} \gamma_{xz} \\ \gamma_{yz} \end{Bmatrix} = \begin{Bmatrix} \frac{\partial w}{\partial x} + \theta_y \\ \frac{\partial w}{\partial y} + \theta_y \end{Bmatrix} \tag{3.29}$$

3.5 Stress Resultant Constitutive Relationship

Stress resultants are defined as

$$\begin{Bmatrix} N_x \\ N_y \\ N_{xy} \end{Bmatrix} = \int_{-\frac{t}{2}}^{\frac{t}{2}} \begin{Bmatrix} \sigma_x \\ \sigma_y \\ \sigma_{xy} \end{Bmatrix} dz \qquad \begin{Bmatrix} M_x \\ M_y \\ M_{xy} \end{Bmatrix} = \int_{-\frac{t}{2}}^{\frac{t}{2}} \begin{Bmatrix} \sigma_x \\ \sigma_y \\ \sigma_{xy} \end{Bmatrix} z dz \qquad \begin{Bmatrix} Q_{xz} \\ Q_{yz} \end{Bmatrix} = \int_{-t/2}^{t/2} \begin{Bmatrix} \tau_{xz} \\ \tau_{yz} \end{Bmatrix} dz \tag{3.30}$$

Combining equations *(3.24d), (3.27), (3.29) and (3.30)* we have the constitutive relation for the SMA composite plates.

$$\begin{Bmatrix} N \\ M \end{Bmatrix} = \begin{bmatrix} A & B \\ B & D \end{bmatrix} \left(\begin{Bmatrix} \varepsilon_l \\ \kappa \end{Bmatrix} + \begin{Bmatrix} \varepsilon_{nl} \\ 0 \end{Bmatrix} \right) + \begin{Bmatrix} N_r \\ M_r \end{Bmatrix} \tag{3.31}$$

and

$$\{Q\} = \begin{Bmatrix} Q_{xz} \\ Q_{yz} \end{Bmatrix} = \begin{bmatrix} A_{44} & A_{45} \\ A_{45} & A_{55} \end{bmatrix} \{\gamma\} = [A'] \{\Delta\gamma\} \tag{3.32}$$

where [A], [A'], [B] and [D] are the laminate stiffness matrices. *{N},{M}* and*{Q}* are the in-plane, moment and transverse shear resultant vectors, respectively. $\{N_r\}$ and $\{M_r\}$ are the resultant force and moment due to recovery stress respectively, i.e.

$$(\{N_r\}, \{M_r\}) = \sum_{k=1}^{n} \int_{-\frac{t}{2}}^{\frac{t}{2}} \{\sigma_x^r\} V_a(1, z) dz \tag{3.33}$$

3.6 Finite element implementation

A continuum square plate is discretised into several elements. The optimum number of elements is determined through the convergent tests. Eight noded isoparametric quadrilateral elements are used in this study. The elements and nodes are numbered locally and globally in a way such as shown in figure 3.3. Each node carries 5 degrees of freedoms per node. The generalized displacement matrix for each node is :

$$\{a\} = \sum_{i=1}^{8} N_i \{d_i\} \qquad (3.34a)$$

where $\{a\}$ and $\{d_i\}$ are the generalised and nodal displacements and N_i is the ith shape function.

$$\{a\} = \{u \; v \; w \; \theta_x \; \theta_y\}^T$$

$$\{\bar{a}_i\} = \{u_{oi} \; v_{oi} \; w_{oi} \; \theta_{xi} \; \theta_{yi}\}^T \qquad (3.34b)$$

$$N_1 = -\frac{1}{4}(1-\zeta)(1-\eta)(1+\zeta+\eta)$$

$$N_2 = \frac{1}{2}(1-\zeta^2)(1-\eta)$$

$$N_3 = -\frac{1}{4}(1+\zeta)(1-\eta)(1-\zeta+\eta)$$

$$N_4 = \frac{1}{2}(1+\zeta)(1-\eta^2) \qquad (3.34c)$$

$$N_5 = -\frac{1}{4}(1+\zeta)(1+\eta)(1-\zeta-\eta)$$

$$N_6 = \frac{1}{2}(1-\zeta^2)(1+\eta)$$

$$N_7 = -\frac{1}{4}(1-\zeta)(1+\eta)(1+\zeta-\eta)$$

$$N_8 = \frac{1}{2}(1-\zeta)(1-\eta^2)$$

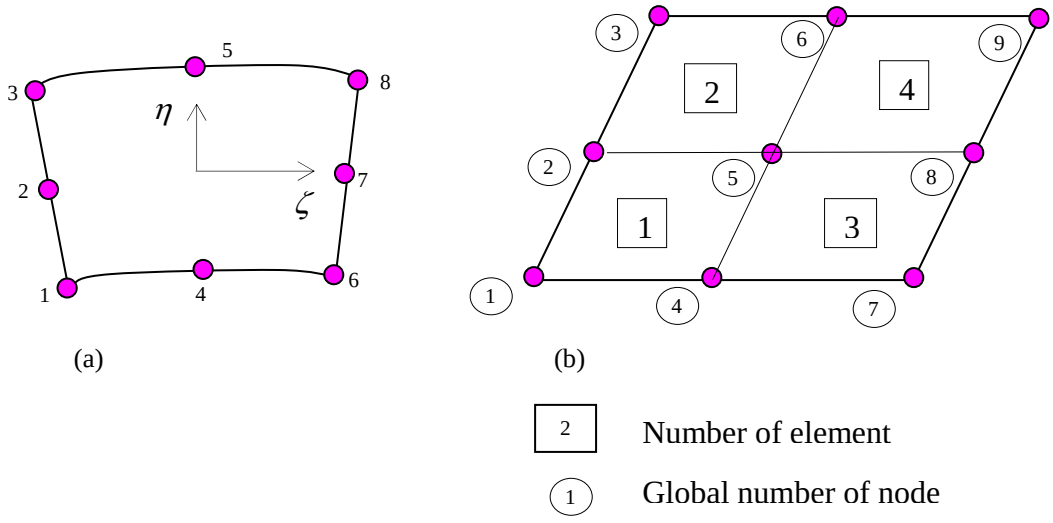

Figure 3.3 : Quadratic quadrilateral element with natural coordinate system

The strain-displacement relationships are:

$$\{\varepsilon_m\} = [B_m]\{\bar{a}_i\} \qquad (3.35a)$$

$$\{\varepsilon_b\} = [B_b]\{\bar{a}_i\} \qquad (3.35b)$$

$$\{\varepsilon_s\} = [B_s]\{\bar{a}_i\} \qquad (3.35c)$$

where $[B_m]$ is the extensional strain displacement matrix, $[B_b]$ is the flexural strain displacement matrix and $[B_s]$ is the shear strain displacement matrix.

$$[B_m] = \begin{bmatrix} \frac{\partial N_i}{\partial x} & 0 & 0 & 0 & 0 & 0 & 0 \\ 0 & \frac{\partial N_i}{\partial y} & 0 & 0 & 0 & 0 & 0 \\ \frac{\partial N_i}{\partial y} & \frac{\partial N_i}{\partial x} & 0 & 0 & 0 & 0 & 0 \end{bmatrix} \begin{Bmatrix} u_i \\ v_i \\ w_i \\ \theta_{xi} \\ \theta_{yi} \\ \zeta_{xi} \\ \zeta_{yi} \end{Bmatrix} \qquad (3.36a)$$

$$[B_b] = \begin{bmatrix} 0 & 0 & 0 & \frac{\partial N_i}{\partial x} & 0 & 0 & 0 \\ 0 & 0 & 0 & 0 & \frac{\partial N_i}{\partial y} & 0 & 0 \\ 0 & 0 & 0 & \frac{\partial N_i}{\partial y} & \frac{\partial N_i}{\partial x} & 0 & 0 \end{bmatrix} \begin{Bmatrix} u_i \\ v_i \\ w_i \\ \theta_{xi} \\ \theta_{yi} \\ \zeta_{xi} \\ \zeta_{yi} \end{Bmatrix} \qquad (3.36b)$$

$$[B_s] = \begin{bmatrix} 0 & 0 & \frac{\partial N_i}{\partial x} & N_i & 0 & 0 & 0 \\ 0 & 0 & \frac{\partial N_i}{\partial y} & 0 & N_i & 0 & 0 \end{bmatrix} \begin{Bmatrix} u_i \\ v_i \\ w_i \\ \theta_{xi} \\ \theta_{yi} \\ \zeta_{xi} \\ \zeta_{yi} \end{Bmatrix} \qquad (3.36c)$$

The non-linear strain can be grouped such as,

$$\{\varepsilon_l\} = \frac{1}{2} \begin{bmatrix} \frac{\partial w}{\partial x} & 0 \\ 0 & \frac{\partial w}{\partial y} \\ \frac{\partial w}{\partial y} & \frac{\partial w}{\partial x} \end{bmatrix} \begin{Bmatrix} \frac{\partial w}{\partial x} \\ \frac{\partial w}{\partial y} \end{Bmatrix} = \frac{1}{2} [A] \{\theta\} \qquad (3.37a)$$

where matrix $\{\theta\}$ is such as,

$$\{\theta\} = \begin{Bmatrix} \frac{\partial w}{\partial x} \\ \frac{\partial w}{\partial y} \end{Bmatrix} = \begin{bmatrix} 0 & 0 & N_{i,x} & 0 & 0 \\ 0 & 0 & N_{i,y} & 0 & 0 \end{bmatrix} \begin{Bmatrix} u_{oi} \\ v_{oi} \\ w_{oi} \\ \theta_{xi} \\ \theta_{yi} \end{Bmatrix} = [G] \{a_i\} \qquad (3.37b)$$

In variational terms, equation *(3.35a-c)* and *(3.37a), (3.38a)* become

$\{\delta\varepsilon_m\}=[B_m]\{\delta d\}$

$\{\delta\kappa\} =[B_b] \{\delta d\}$

$$\{\delta\gamma\} = [B_s]\ \{\delta d\}] \qquad (3.38)$$

$$\{\delta\varepsilon_{nl}\} = [A_L]\ [G]\{\ \delta d\}$$

Using equation *(3.31)*, resultant vectors *{N}*, *{M}* and *{Q}* can be written as

$$\{N\} = [A]\{\varepsilon_m+\varepsilon_{nl}\}+ [B]\{\varepsilon_b\} + \{N_r\}$$

$$= ([A][B_m]+ \tfrac{1}{2}[A][\Delta A_L][G] + [B][B_b])\{d\}+\{N_r\} \qquad (3.39)$$

$$\{M\} = [B]\{\varepsilon_m+\varepsilon_{nl}+\varepsilon_o\}+ [D]\{\varepsilon_b\} + \{M_r\}$$

$$= ([B][B_m]+ \tfrac{1}{2}[A][\ A_L][G] + [B][B_b])\{d\}+\{M_r\} \qquad (3.40)$$

$$\{Q\} = [A']\ \{\Delta\gamma\}$$

$$= ([A'][B_s]\{d\} \qquad (3.41)$$

Specifically for later purpose, we definej

$$\{N_m\} = [A][Bm]\{d\} \qquad (3.42a)$$

$$\{N_b\} = [B][Bb]\{d\} \qquad (3.42b)$$

3.7 Principle of virtual works

The Hamilton's principle is used to formulate the governing equation for linear structural behaviours. Hamilton's principle requires that

$$\int_{t_1}^{t_2} (\delta(T-U)+\delta W)dt = 0 \qquad (3.43)$$

where T and U are the kinetic and strain energy of an element and W is the external work. Inserting the formulations for T, U and W for a plate bending element,

$$\int \left\{ \frac{1}{2}\delta\left[\int_v \sigma_{ij}\varepsilon_{ij}\,dV + \int_v \sigma_{ij}^0 u_{s,i}\,u_{s,j}\,dV \right] - \frac{1}{2}\delta\int_v \left\{\dot{u}\right\}^T \rho\left\{\dot{u}\right\}dV - \delta W \right\} dt = 0 \qquad (3.44)$$

where σ_{ij} and ε_{ij} are stress and strain components, σ_{ij}^{0} is initial stress components and u_s refer to displacements u, v and w.

a. Evaluating the first term of variational statement:

The inclusion of the non-linear terms into the variational principle for isotropic plates is derived in Zienkiewicz & Taylor [30] and simplified here.

$$\delta U_1 = \frac{1}{2}\delta \int_V \sigma_{ij}\, \varepsilon_{ij}\, dV \qquad (3.45a)$$

$$= \frac{1}{2}\delta \int_A \{\varepsilon_m\}^T \{N\} + \{\varepsilon_{nl}\}^T \{N\} + \{\varepsilon_b\}^T \{M\} + \{\varepsilon_s\}^T \{Q\}\, dA \qquad (3.45b)$$

From *(3.38-41)*, we have

$$\frac{1}{2}\delta\{d\}^T \int_A [B_m]^T \left[\left([A][B_m] + \frac{1}{2}[A][A_L][G] + [B][B_b] \right)\{d\} + \{N_r\} \right] dA +$$

$$\frac{1}{2}\delta\{d\}^T \int_A [G]^T [A_L]^T \left[\left([A][B_m] + \frac{1}{2}[A][A_L][G] + [B][B_b] \right)\{d\} + \{N_r\} \right] dA +$$

$$\frac{1}{2}\delta\{d\}^T \int_A [G]^T [A_o]^T \left[\left([A][B_m] + \frac{1}{2}[A][A_L][G] + [B][B_b] \right)\{d\} + \{N_r\} \right] dA +$$

$$\frac{1}{2}\delta\{d\}^T \int_A [B_b]^T \left[\left([B][B_m] + \frac{1}{2}[B][A_L][G] + [D][B_b] \right)\{d\} + \{M_r\} \right] dA +$$

$$\frac{1}{2}\delta\{d\}^T \int_A [B_s]^T [([S_1][B_s])\{d\}] dA \qquad (3.46)$$

$$= \frac{1}{2}\delta\{d\}^T \int_A \left([B_m]^T [A][B_m] + [B_m]^T [B][B_b] + [B_b]^T [B][B_m] + [B_b]^T [D][B_b] \right)\{d\} dA + \qquad (3.47a)$$

$$\frac{1}{2}\delta\{d\}^T \int_A \left([B_s]^T [S_1][B_s] \right)\{d\} dA + \qquad (3.47b)$$

$$\frac{1}{2}\delta\{d\}^T \int_A \left(\frac{1}{2}[B_m]^T[A][A_L][G]+[G][A_L]^T[A][B_m]+\right.$$

$$\left.[G][A_L]^T[B][B_b]+\frac{1}{2}[B_b]^T[B][A_L][G]\right)\{d\}dA+ \qquad (3.47c)$$

$$\frac{1}{2}\delta\{d\}^T \frac{1}{3}\int_A \frac{3}{2}[G]^T[A_L]^T[A][A_L][G]\{d\}dA+ \qquad (3.47d)$$

$$\frac{1}{2}\delta\{d\}^T \int_A [G]^T[A_L]^T\{N_r\}dA+ \qquad (3.47e)$$

$$\frac{1}{2}\delta\{d\}^T \int_A \left([B_m]^T\{N_r\}+[B_b]^T\{M_r\}\right)dA+ \qquad (3.47f)$$

$$\frac{1}{2}\delta\{d\}^T \int_A [G]^T[A_o]^T\{N_r\}dA \qquad (3.47g)$$

Equation *(3.47c)* will cause unsymmetric matrix and need to be rearranged.

$$[G][A_L]^T[A][B_m]\{d\}=\frac{1}{2}[G][A_L]^T[A][B_m]\{d\}+\frac{1}{2}[G][A_L]^T[A][B_m]\{d\}$$

$$=\frac{1}{2}[G][A_L]^T[A][B_m]\{d\}+\frac{1}{2}[G][A_L]^T\{N_m\}$$

$$=\frac{1}{2}[G][A_L]^T[A][B_m]\{d\}+\frac{1}{2}[G]^T[N_m]^T[G]\{d\} \qquad (3.48)$$

where referring to equation *(3.42a)*, $\{N_m\}=\begin{Bmatrix} N_{mx} \\ N_{my} \\ N_{mxy} \end{Bmatrix}=[A][B_m]\{d\}$ and $[N_m]=\begin{bmatrix} N_{mx} & N_{mxy} \\ N_{mxy} & N_y \end{bmatrix}$

Similarly,

$$[G][A_L]^T[B][B_b]\{d\}=\frac{1}{2}[G][A_L]^T[B][B_b]\{d\}+\frac{1}{2}[G][A_L]^T[B][B_b]\{d\}$$

$$=\frac{1}{2}[G][A_L]^T[B][B_b]\{d\}+\frac{1}{2}[G][A_L]^T\{N_b\}$$

$$=\frac{1}{2}[G][\Delta A_L]^T[B][B_b]\{d\}+\frac{1}{2}[G]^T[N_b]^T[G]\{d\} \qquad (3.49a)$$

where referring to equation *(3.42b)*,

$$\{N_b\} = \begin{Bmatrix} N_{bx} \\ N_{by} \\ N_{bxy} \end{Bmatrix} = [B][B_b]\{d\} \text{ and } [N_b] = \begin{bmatrix} N_{bx} & N_{bxy} \\ N_{bxy} & N_{by} \end{bmatrix}. \quad (3.49b)$$

Equation *(3.47e)* can be arranged such as,

$$[G]^T[A_L]^T\{N_r\} = [G]^T[N_r][G]\{d\} \quad (3.50a)$$

where,

$$\{N_r\} = \begin{Bmatrix} N_{rx} \\ N_{ry} \\ N_{rxy} \end{Bmatrix} \text{ and } [N_r] = \begin{bmatrix} N_{rx} & N_{rxy} \\ N_{rxy} & N_{ry} \end{bmatrix}. \quad (3.50b)$$

Naming the stiffness and forces terms, we have

from *(3.47a)*, the linear stiffness matrix

$$[K_L] = \int_A \left([B_m]^T[A][B_m] + [B_m]^T[B][B_b] + [B_b]^T[B][B_m] + [B_b]^T[D][B_b]\right)dA \quad (3.51a)$$

From *(3.47b)*, the shear stiffness matrix,

$$[K_s] = \int_A [B_s]^T[S_1][B_s]dA \quad (3.51b)$$

From *(3.47c)* and *(3.48)*, the first order nonlinear stiffness matrix,

$$[N1] = \int_A \Big([B_m]^T[A][A_L][G] + [G]^T[A_L]^T[A][B_m] + [G][A_L]^T[B][B_b] + [B_b]^T[B][A_L][G] + [G]^T[N_m]^T[G] + [G]^T[N_b]^T[G]\Big)dA \quad (3.51c)$$

From *(3.47d)*, the second order nonlinear stiffness matrix,

$$[N2] = \int_A \frac{3}{2}[G]^T[A_L]^T[A][A_L][G]dA \quad (3.51d)$$

From *(3.47e)* and *(3.50)*, the geometric stiffness matrix due to recovery stress,

$$[K_r] = \int_A [G]^T [N_r][G] dA \qquad (3.51e)$$

From *(3.47f)*, the recovery load vector,

$$\{P_r\} = \int_A \left([B_m]^T \{N_r\} + [B_b]^T \{M_r\} \right) dA + \qquad (3.51f)$$

Combining all terms, the first strain energy term is

$$= \frac{1}{2} \delta \{d\}^T \left([K_L] + [K_s] + [K_r] + \frac{1}{2}[N1] + \frac{1}{3}[N2] \right) \{d\} + \{\delta d\}^T \{P_o\} \qquad (3.52)$$

b. Evaluating the second term of the Hamilton's principle:

$$\delta U_2 = \frac{1}{2} \delta \int_V \sigma_{ij}^0 u_{s,i} u_{s,j} \, dV \qquad (3.53)$$

$$= \frac{1}{2} \delta \int_V \sigma_{xj} \frac{\partial U_s}{\partial x} \frac{\partial U_s}{\partial j} + \sigma_{yj} \frac{\partial U_s}{\partial y} \frac{\partial U_s}{\partial j} + \sigma_{zj} \frac{\partial U_s}{\partial z} \frac{\partial U_s}{\partial j} \qquad (3.54)$$

$$= \frac{1}{2} \delta \int_V \sigma_{xx} \frac{\partial U_s}{\partial x} \frac{\partial U_s}{\partial x} + \sigma_{xy} \frac{\partial U_s}{\partial x} \frac{\partial U_s}{\partial y} + \sigma_{xz} \frac{\partial U_s}{\partial x} \frac{\partial U_s}{\partial z}$$

$$+ \quad \sigma_{yx} \frac{\partial U_s}{\partial y} \frac{\partial U_s}{\partial x} + \sigma_{yy} \frac{\partial U_s}{\partial y} \frac{\partial U_s}{\partial y} + \sigma_{yz} \frac{\partial U_s}{\partial y} \frac{\partial U_s}{\partial z}$$

$$+ \quad \sigma_{zx} \frac{\partial U_s}{\partial z} \frac{\partial U_s}{\partial x} + \sigma_{zy} \frac{\partial U_s}{\partial z} \frac{\partial U_s}{\partial y} + \sigma_{zz} \frac{\partial U_s}{\partial z} \frac{\partial U_s}{\partial z} \qquad (3.55)$$

$$= \frac{1}{2} \delta \int_V \sigma_{xx} u_{,x} u_{,x} + \sigma_{xx} v_{,x} v_{,x} + \sigma_{xx} w_{,x} w_{,x} + \sigma_{xy} u_{,x} u_{,y} + \sigma_{xy} v_{,x} v_{,y}$$

$$+ \quad \sigma_{xy} w_{,x} w_{,y} + \sigma_{xz} u_{,x} u_{,z} + \sigma_{xz} v_{,x} v_{,z} + \sigma_{xz} w_{,x} w_{,z}$$

$$+ \quad \sigma_{yx} u_{,y} u_{,x} + \sigma_{yx} v_{,y} v_{,x} + \sigma_{yx} w_{,y} w_{,x} + \sigma_{yy} u_{,y} u_{,y} + \sigma_{yy} v_{,y} v_{,y}$$

$$+ \quad \sigma_{yy} w_{,y} w_{,y} + \sigma_{yz} u_{,y} u_{,z} + \sigma_{yz} v_{,y} v_{,z} + \sigma_{yz} w_{,y} w_{,z}$$

$$+ \quad \sigma_{zx} u_{,z} u_{,x} + \sigma_{zx} v_{,z} v_{,x} + \sigma_{zx} w_{,z} w_{,x} + \sigma_{zy} u_{,z} u_{,y} + \sigma_{zy} v_{,z} v_{,y}$$

$$+ \quad \sigma_{zy} w_{,z}\, w_{,y} + \sigma_{zz} u_{,z}\, u_{,z} + \sigma_{zz} v_{,z}\, v_{,z} + \sigma_{zz} w_{,z}\, w_{,z} \qquad (3.56)$$

But the generalized displacement,

$$u = u_o\,(x,y) + z\,\theta_x\,(x,y)$$

$$v = v_o\,(x,y) + z\,\theta_y\,(x,y)$$

$$w = w_o\,(x,y)$$

$$= \frac{1}{2}\,\delta \int_A \sigma_{xx}(u_{o,x} - z\,\theta_{x,x} + z^3\,\zeta_{x,x})(u_{o,x} - z\,\theta_{x,x} + z^3\,\zeta_{x,x}) + \sigma_{xx}\,(v_{o,x} + z\,\theta_{v,x}$$

$$+ \quad z^3\,\zeta_{y,x})\,(v_{o,x} + z\,\theta_{v,x} + z^3\,\zeta_{y,x}) + \sigma_{xx}\, w_{,x}\, w_{,x}$$

$$+ \quad 2\sigma_{xy}(u_{o,x} + z\,\theta_{x,x} + z^3\,\zeta_{x,x})\,(u_{o,x} + z\,\theta_{x,x} + z^3\,\zeta_{x,x})$$

$$+ \quad 2\sigma_{xy}\,(v_{o,x} + z\,\theta_{v,x} + z^3\,\zeta_{y,x})\,(v_{o,x} + z\,\theta_{v,x} + z^3\,\zeta_{y,x})$$

$$+ \quad 2\sigma_{xy}\, w_{,x}\, w_{,y} + 2\sigma_{xz}(u_{o,x} - z\,\theta_{x,x} + z^3\,\zeta_{x,x})(3z^2\zeta_x - \theta_x)$$

$$+ \quad 2\sigma_{xz}(v_{o,x} + z\,\theta_{y,x} + z^3\,\zeta_{y,x})(3z^2\zeta_y + \theta_y) + \sigma_{yy}(u_{o,y} + z\,\theta_{x,y}$$

$$+ \quad z^3\,\zeta_{x,y})\,(u_{o,y} + z\,\theta_{x,y} + z^3\,\zeta_{x,y}) + \sigma_{yy}\,(v_{o,y} + z\,\theta_{v,y} + z^3\,\zeta_{y,y})\,(v_{o,y} +$$

$$+ \quad z\,\theta_{v,y} + z^3\,\zeta_{y,y}) + \sigma_{yy}\, w_{,y}\, w_{,y} + 2\sigma_{yz}(u_{o,y} - z\,\theta_{x,y} + z^3\,\zeta_{x,y})\,(3z^2\zeta_x - \theta_x)$$

$$+ \quad 2\sigma_{yz}(v_{o,y} - z\,\theta_{y,y} + z^3\,\zeta_{y,y})\,(3z^2\zeta_y - \theta_y) \qquad (3.57)$$

Defining,

$$\begin{bmatrix} \overline{N}_x & \overline{L}_x & \overline{M}_x & \overline{L}^1_x & \overline{M}^1_x & \overline{M}^2_x \\ \overline{N}_y & \overline{L}_y & \overline{M}_y & \overline{L}^1_y & \overline{M}^1_y & \overline{M}^2_y \\ \overline{N}_{xy} & \overline{L}_{xy} & \overline{M}_{xy} & \overline{L}^1_{xy} & \overline{M}^1_{xy} & \overline{M}^2_y \end{bmatrix} = \int_{-t/2}^{t/2} \begin{Bmatrix} \sigma^0_x \\ \sigma^0_y \\ \sigma^0_{xy} \end{Bmatrix} [\,1\; z\; z^2\; z^3\; z^4\; z^6\,] \qquad (3.58a)$$

and

$$\begin{bmatrix} \overline{Q}_x & \overline{S}_x & \overline{P}_x & \overline{S}^1_x & \overline{S}^2_x \\ \overline{Q}_y & \overline{S}_y & \overline{P}_y & \overline{S}^1_y & \overline{S}^2_y \end{bmatrix} = \int_{-t/2}^{t/2} \begin{Bmatrix} \tau_{xz} \\ \tau_{yz} \end{Bmatrix} [\,1\; z\; z^2\; z^3\; z^5\,]\, dz \qquad (3.58b)$$

So we have,

$$= \frac{1}{2}\,\delta\int_A \overline{N}_x(u_{o,x}^2 + v_{o,x}^2 + w_{,x}^2) + 2\overline{N}_{xy}(u_{o,x}u_{o,y} + v_{o,x}v_{o,y} + w_{,x}w_{,y})$$

$$+ \overline{N}_y(u_{o,y}^2 + v_{o,y}^2 + w_{,y}^2) + 2\overline{L_x}(u_{o,x}\theta_{x,x} + v_{o,x}\theta_{v,x})$$

$$+ 2\overline{L_{xy}}(-u_{o,x}\theta_{x,y} - u_{o,y}\theta_{x,x} - v_{o,x}\theta_{v,y} - v_{o,y}\theta_{y,x}) + 2\overline{L_y}(u_{o,y}\theta_{x,y} + v_{o,y}\theta_{v,y})$$

$$+ \overline{M}_x(\theta_{x,x}^2 + \theta_{v,x}^2) + 2\overline{M}_{xy}(\theta_{x,x}\theta_{x,y} + \theta_{v,x}\theta_{y,y}) + 2\overline{M}_y(\theta_{x,y}^2 + \theta_{v,y}^2)$$

$$+ 2\overline{L}^1_x(u_{o,x}\zeta_{x,x} + v_{o,x}\zeta_{y,x}) + 2\overline{L}^1_{xy}(u_{o,x}\zeta_{x,y} + u_{o,y}\zeta_{x,x} + v_{o,x}\zeta_{y,y} + v_{o,y}\zeta_{y,x})$$

$$+ 2\overline{L}^1_y(u_{o,y}\zeta_{x,y} + v_{o,y}\zeta_{y,y}) + 2\overline{M}^1_x(\theta_{x,x}\zeta_{x,x} + \theta_{y,x}\zeta_{y,x})$$

$$+ 2\overline{M}^1_{xy}(\theta_{x,x}\zeta_{x,y} + \theta_{x,y}\zeta_{x,x} + \theta_{y,x}\zeta_{y,y} + \theta_{y,y}\zeta_{y,x}) + 2\overline{M}^1_y(\theta_{x,y}\zeta_{x,y} + \theta_{y,y}\zeta_{y,y})$$

$$+ \overline{M}^2_x(\zeta_{x,x}^2 + \zeta_{y,x}^2) + 2\overline{M}^2_{xy}(2\zeta_{x,x}\zeta_{x,y} + \zeta_{y,x}\zeta_{y,y}] + 2\overline{M}^2_y(\zeta_{x,y}^2 + \zeta_{y,y}^2)$$

$$+ 2\overline{Q_x}(u_{o,x}\theta_x + v_{o,x}\theta_y) + 2\overline{Q}_y(u_{o,y}\theta_x + v_{o,y}\theta_y) + 2\overline{S}_x(\theta_{x,x}\theta_x + \theta_{v,x}\theta_y)$$

$$+ 2\overline{S}_y(\theta_{x,y}\theta_x + \theta_{v,y}\theta_y) + 2\overline{P}^1_x(3u_{o,x}\zeta_x + 3v_{o,x}\zeta_y)$$

$$+ 2\overline{P}^1_y(3u_{o,y}\zeta_x + 3v_{o,y}\zeta_y) + 2\overline{S}^1_x(3\theta_{x,x}\zeta_x + 3\theta_{y,x}\zeta_y + \theta_x\zeta_{x,x} + \theta_y\zeta_{y,x})$$

$$+ 2\overline{S}^1_y(3\theta_{x,y}\zeta_x$$

$$+ 3\theta_{y,y}\zeta_y + \theta_x\zeta_{x,y} + \theta_y\zeta_{y,y}) + 2\overline{S}^2_x(3\zeta_{x,x}\zeta_x + 3\zeta_{y,x}\zeta_y)$$

$$+ 2\overline{S}^2_y(3\zeta_{x,y}\zeta_x + 3\zeta_{y,y}\zeta_y) \qquad (3.59)$$

This equation can be reduced to the form of

$$U_2 = \frac{1}{2}\{d\}^T[K_G]\{d\} \qquad (3.60a)$$

where,

$$[K_G] = \iint [G_s]^T[\tau][G_s]\,dA \qquad (3.60b)$$

and through arrangement,

$$[G_s]^T = \begin{bmatrix} 0 & 0 & \frac{\partial N_i}{\partial x} & \frac{\partial N_i}{\partial y} & 0 & 0 & 0 & 0 & 0 & 0 & 0 & 0 \\ 0 & 0 & 0 & 0 & \frac{\partial N_i}{\partial x} & \frac{\partial N_i}{\partial y} & 0 & 0 & 0 & 0 & 0 & 0 \\ 0 & 0 & 0 & 0 & 0 & 0 & \frac{\partial N_i}{\partial x} & \frac{\partial N_i}{\partial y} & 0 & 0 & 0 & 0 \\ N_i & 0 & 0 & 0 & 0 & 0 & 0 & 0 & \frac{\partial N_i}{\partial x} & \frac{\partial N_i}{\partial y} & 0 & 0 \\ 0 & N_i & 0 & 0 & 0 & 0 & 0 & 0 & 0 & 0 & \frac{\partial N_i}{\partial x} & \frac{\partial N_i}{\partial y} \end{bmatrix} \qquad (3.61c)$$

and the value of $[\tau]$ is

$$[\tau] = \begin{bmatrix} 0 & 0 & \overline{Q}_x & \overline{Q}_y & 0 & 0 & 0 & 0 & \overline{P}_x & \overline{P}_y & 0 & 0 \\ 0 & 0 & 0 & 0 & \overline{Q}_x & \overline{Q}_y & 0 & 0 & 0 & 0 & \overline{P}_x & \overline{P}_y \\ \overline{Q}_x & 0 & \overline{N}_x & \overline{N}_{xy} & 0 & 0 & 0 & 0 & \overline{M}_x & \overline{M}_{xy} & 0 & 0 \\ \overline{Q}_y & 0 & \overline{N}_{xy} & \overline{N}_y & 0 & 0 & 0 & 0 & \overline{M}_{xy} & \overline{M}_y & 0 & 0 \\ 0 & \overline{Q}_x & 0 & 0 & \overline{N}_x & \overline{N}_{xy} & 0 & 0 & 0 & 0 & \overline{M}_x & \overline{M}_{xy} \\ 0 & \overline{Q}_y & 0 & 0 & \overline{N}_{xy} & \overline{N}_y & 0 & 0 & 0 & 0 & \overline{M}_{xy} & \overline{M}_y \\ 0 & 0 & 0 & 0 & 0 & 0 & \overline{N}_x & \overline{N}_{xy} & 0 & 0 & 0 & 0 \\ 0 & 0 & 0 & 0 & 0 & 0 & \overline{N}_{xy} & \overline{N}_y & 0 & 0 & 0 & 0 \\ \overline{P}_x & 0 & \overline{M}_x & \overline{M}_{xy} & 0 & 0 & 0 & 0 & \overline{L}_x & \overline{L}_{xy} & 0 & 0 \\ \overline{P}_y & 0 & \overline{M}_{xy} & \overline{M}_y & 0 & 0 & 0 & 0 & \overline{L}_{xy} & \overline{L}_y & 0 & 0 \\ 0 & \overline{P}_x & 0 & 0 & \overline{M}_x & \overline{M}_{xy} & 0 & 0 & 0 & 0 & \overline{L}_x & \overline{L}_{xy} \\ 0 & \overline{P}_y & 0 & 0 & \overline{M}_{xy} & \overline{M}_y & 0 & 0 & 0 & 0 & \overline{L}_{xy} & \overline{L}_y \end{bmatrix} \qquad (3.62e)$$

c. Evaluating the third term of the Hamilton's principle:

$$\delta T = \frac{1}{2}\delta \int_v \left\{\dot{u}\right\}^T \rho \left\{\dot{u}\right\} dV \qquad (3.63)$$

$$= \frac{1}{2}\delta \int_v \rho \left[\left(\dot{u}\right)\left(\dot{u}\right) + \left(\dot{v}\right)\left(\dot{v}\right) + \left(\dot{w}\right)\left(\dot{w}\right)\right] dV \qquad (3.64)$$

But the generalized displacement,

$$u = u_o\,(x,y) + z\;\theta_x\,(x,y)\;\; f$$

$$v = v_o\,(x,y) + z\;\theta_y\,(x,y) \qquad (3.65)$$

$$w = w_o(x,y)$$

So,

$$\delta T = \frac{1}{2}\delta \int \int \rho \left[\left(\dot{u}_0 + z\dot{\theta}_x \right)\left(\dot{u}_0 + z\dot{\theta}_x \right) + \left(\dot{v}_0 + z\dot{\theta}_y \right)\left(\dot{v}_0 + z\dot{\theta}_y \right) + \left(\dot{w}_0 \right)\left(\dot{w}_0 \right) \right] dzdA \tag{3.67}$$

$$= \frac{1}{2}\delta \int I_P \left(\dot{u}_o \dot{u}_o + \dot{v}_o \dot{v}_o + \dot{w}_o \dot{w}_o \right) dV + \frac{1}{2}\delta \int I_{ci} \left(\dot{u}_o \dot{\theta}_x + \dot{\theta}_x \dot{u}_o + \dot{v}_o \dot{\theta}_y + \dot{\theta}_y \dot{v}_o \right) dV +$$

$$\frac{1}{2}\delta \int I_f \left(\dot{\theta}_x \dot{\theta}_y + \dot{\theta}_y \dot{\theta}_x \right) dV \tag{3.68}$$

where

$$I_p, I_c, I_f = \int_{-h/2}^{h/2} \left(\rho, \rho z, \rho z^2 \right) dz \tag{3.69}$$

Inserting the statement of shape function in equations *(8.34a-c)*, equation (3.68) can be rearranged in the following form.

$$\delta T = \frac{1}{2}\delta \{ \dot{d} \}^T [M] \{ \dot{d} \} \tag{3.70}$$

where

$$[M] = [N]^T [m] [N] \tag{3.71a}$$

where *[m]* is the mass matrix and *[N]* is the matrix of shape function.

$$[N]^T = \begin{bmatrix} 0 & 0 & \frac{\partial N_i}{\partial x} & \frac{\partial N_i}{\partial y} & 0 & 0 & 0 & 0 & 0 & 0 & 0 & 0 \\ 0 & 0 & 0 & 0 & \frac{\partial N_i}{\partial x} & \frac{\partial N_i}{\partial y} & 0 & 0 & 0 & 0 & 0 & 0 \\ 0 & 0 & 0 & 0 & 0 & 0 & \frac{\partial N_i}{\partial x} & \frac{\partial N_i}{\partial y} & 0 & 0 & 0 & 0 \\ N_i & 0 & 0 & 0 & 0 & 0 & 0 & 0 & \frac{\partial N_i}{\partial x} & \frac{\partial N_i}{\partial y} & 0 & 0 \\ 0 & N_i & 0 & 0 & 0 & 0 & 0 & 0 & 0 & 0 & \frac{\partial N_i}{\partial x} & \frac{\partial N_i}{\partial y} \end{bmatrix} \tag{3.71b}$$

and the value of *[m]* is

$$[m] = \begin{bmatrix} 0 & 0 & \overline{Q}_x & \overline{Q}_y & 0 & 0 & 0 & 0 & \overline{P}_x & \overline{P}_y & 0 & 0 \\ 0 & 0 & 0 & 0 & \overline{Q}_x & \overline{Q}_y & 0 & 0 & 0 & 0 & \overline{P}_x & \overline{P}_y \\ \overline{Q}_x & 0 & \overline{N}_x & \overline{N}_{xy} & 0 & 0 & 0 & 0 & \overline{M}_x & \overline{M}_{xy} & 0 & 0 \\ \overline{Q}_y & 0 & \overline{N}_{xy} & \overline{N}_y & 0 & 0 & 0 & 0 & \overline{M}_{xy} & \overline{M}_y & 0 & 0 \\ 0 & \overline{Q}_x & 0 & 0 & \overline{N}_x & \overline{N}_{xy} & 0 & 0 & 0 & 0 & \overline{M}_x & \overline{M}_{xy} \\ 0 & \overline{Q}_y & 0 & 0 & \overline{N}_{xy} & \overline{N}_y & 0 & 0 & 0 & 0 & \overline{M}_{xy} & \overline{M}_y \\ 0 & 0 & 0 & 0 & 0 & 0 & \overline{N}_x & \overline{N}_{xy} & 0 & 0 & 0 & 0 \\ 0 & 0 & 0 & 0 & 0 & 0 & \overline{N}_{xy} & \overline{N}_y & 0 & 0 & 0 & 0 \\ \overline{P}_x & 0 & \overline{M}_x & \overline{M}_{xy} & 0 & 0 & 0 & 0 & \overline{L}_x & \overline{L}_{xy} & 0 & 0 \\ \overline{P}_y & 0 & \overline{M}_{xy} & \overline{M}_y & 0 & 0 & 0 & 0 & \overline{L}_{xy} & \overline{L}_y & 0 & 0 \\ 0 & \overline{P}_x & 0 & 0 & \overline{M}_x & \overline{M}_{xy} & 0 & 0 & 0 & 0 & \overline{L}_x & \overline{L}_{xy} \\ 0 & \overline{P}_y & 0 & 0 & \overline{M}_{xy} & \overline{M}_y & 0 & 0 & 0 & 0 & \overline{L}_{xy} & \overline{L}_y \end{bmatrix} \qquad (3.71c)$$

d. Evaluating the fourth term of the Hamilton's principle:

Assuming three types of loading,

$$\delta W = \delta \int_A \{a\}^T \{f_s\} dA + \delta \int_V \{a\}^T \{f_v\} dV \qquad (3.72)$$

where $\{F_s\}$ and $\{F_V\}$ are surface and body loads. Using the statement of shape function in equations *(8.34a-c)*,

$$\delta W = \{\delta d\}^T \int_A [N]^T \{f_s\} dA + \{\delta d\}^T \int_V [N]^T \{f_v\} dV = \{\delta d\}^T \{F\}$$

(3.73)

So, combining equation *(3.52), (3.60a), (3.70)* and *(3.73)* the Hamilton's principle is reduced to

$$\frac{1}{2}\delta\{d\}^T \left([K_L] + [K_s] + [K_r] + \frac{1}{2}[N1] + \frac{1}{3}[N2] \right) \{d\} + \{\delta d\}^T \{P_o\} + \frac{1}{2}\delta\{d\}^T [K_G] \{d\} = \frac{1}{2}\delta \{\dot{d}\}^T [M]$$

$$\{\dot{d}\} + \{\delta d\}^T \int_A [N]^T \{f_s\} dA + \{\delta d\}^T \int_V [N]^T \{f_v\} dV \qquad (3.74)$$

With the application of Lagrange's equation, equation 3.74 can be simplified to the sought governing equation:G

$$[M]\{\ddot{d}\}+\left([K_L]+[K_s]+[K_r]+\frac{1}{2}[N1]+\frac{1}{3}[N2]+[K_G]\right)\{d\}=\{F\} \qquad (3.75)$$

Equation *(3.75)* can be reduced to governing equations of several structural problems:

Linear Stress and Deflection analysis:

$$([K_L]+[K_s]+[K_r])\{d\}=\{F\} \qquad (3.76)$$

Linear buckling analysis:

$$([K_L]+[K_s]+[K_r]+\lambda[K_G])\{d\}=0 \qquad (3.77)$$

where λ is the critical load coefficient.

$$([K_L]+[K_s]+[K_r]+\omega^2[M])\{d\}=0 \qquad (3.78)$$

where ω is the natural frequency of the plates.

3.6 Closure

Applying the constitutive relationship equations and implementing the FEM into the Hamilton's principle, we can derive the standard equations for both linear and non-linear structural behaviours while converting that equations into Lagrange's equation. This standard equation is then reduced to simple linear structural behaviour equations to be analysed in this thesis.

5.0 BUCKLING AND VIBRATION ANALYSIS OF SHAPE MEMORY ALLOY PLATES

5.1 Introduction

In this chapter, equations (3.77) and (3.78) were solved to study the effects of several parameters on the critical loads and free vibrations of SMA composites. The study is conducted on anti-symmetric angle ply composites. The effect of several parameters such as the geometric, mechanical and transformation effect on the SMA improvements of free vibrations and critical loads are studied. Relative critical loads and relative eigen frequencies are used to measure how much the effect of SMA in improving the buckling loads and free vibration of the SMA composite plates. In the following sections the buckling problem is discussed first followed by the results and discussions of the vibration problem.

5.2 Buckling of SMA plates

5.2.1 Convergence Test:

In this study, the convergence tests are conducted on three SMA composite plates to determine the appropriate mesh size for the buckling analysis while at the same time to provide the validation to the model developed. Similar to the convergence test for the vibration analysis, the SMA wires are not activated for this validation purpose. The results are compared to the analytical results that are calculated based on the classical lamination theory (CLT) and first order shear deformation theory (FSDT) of plates [23]. The results in table 5.1 show a quick convergence that occurs in the finite element analysis for all three SMA composites. It was decided in this study to use the 6x6 mesh.

Table 5.1 : Convergence test for simply supported anti-symmetric SMA composite plates.

Lay-ups	CLT[#]	FSDT[#]	2x2	3x3	4x4	5x5	6x6	7x7	8x8
$[0/(45/-45)_2/0]$	235.75	233.80	299.64	236.49	234.07	233.78	233.72	233.70	233.69
$[0/(45/-45)_4/0]$	264.43	261.98	329.14	264.70	262.29	261.99	261.92	261.88	261.88
$[0/(45/-45)_6/0]$	269.88	267.33	334.72	270.06	267.645	267.34	267.27	267.25	267.24

[#]Reddy, J.N. [23]

5.2.2 The effect of the thickness of the SMA layer

The objective here is initially to get a general idea on the required thickness of SMA layers with respect to the thickness of plate in order to give a certain impact to the buckling load of the SMA composite plate. Later, the effect of the ratios of thickness to side length of the plates are also studied. The SMA plates with configuration $[0/(45/-45)_5/0]$ are used in both studies.

Firstly the thickness of SMA layers are increased while the thickness of other layers stay constant. SMA with initial strain, $\varepsilon o = 0.001$ is used here. At the activation temperature of 60^0C, the Brinson's model will give the recovery stress of 91.6 MPa where full martensite transformation has occurred. The studies are conducted on all three types of boundary conditions. The plots of relative critical loads vs ratios of thickness of SMA layers to thickness of other layers (t_s/t) correspond to the three boundary conditions are shown in figure 5.1.

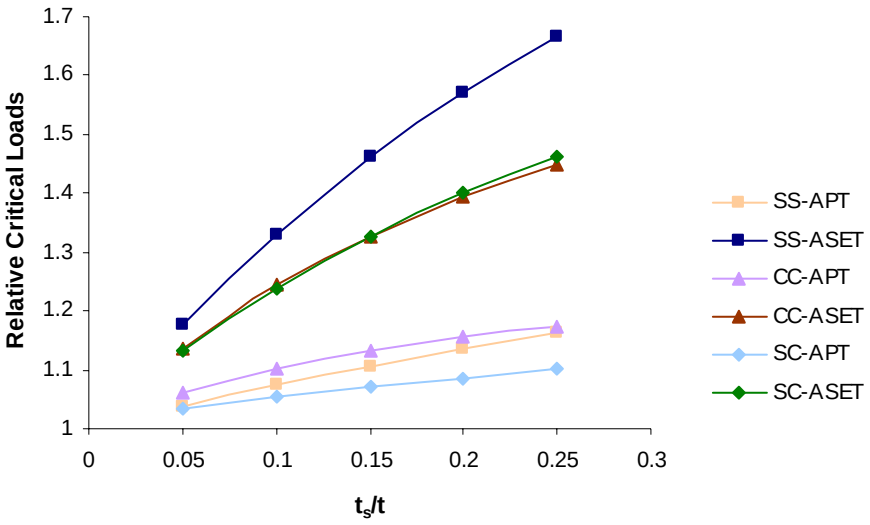

Figure 5.1: The effect of thickness of SMA layers on the relative critical loads

It shows in figure 5.1 that as the thickness of SMA layers is increased, the relative critical load will increase too for the all six cases. In easier words, the effect of SMA on the critical loads is increased with the increase of t_s/t. In the case of SS boundary condition, the increase of the critical load in the ASET improvement can be up to 1.7 times at SMA layer thickness equal to one fourth of the thickness of other layers. The increase of relative critical loads can be understood by the fact that as the t_s/t is increased, the volume fraction of the SMA is increased too. As a result the effect of the SMA in increasing the buckling load can be felt more. Figure 5.1 also shows that the effect of SMA is much more significant in the SS boundary condition. The SC and CC boundary conditions provides almost the same responses for ASET improvement. In any boundary conditions however, improvements made through ASET are always greater than the improvements made through APT. This is because in ASET the effect of recovery stress is considered

along with the effect of the increase in Young's modulus while in APT only the effect of the increase in Young's modulus is considered.

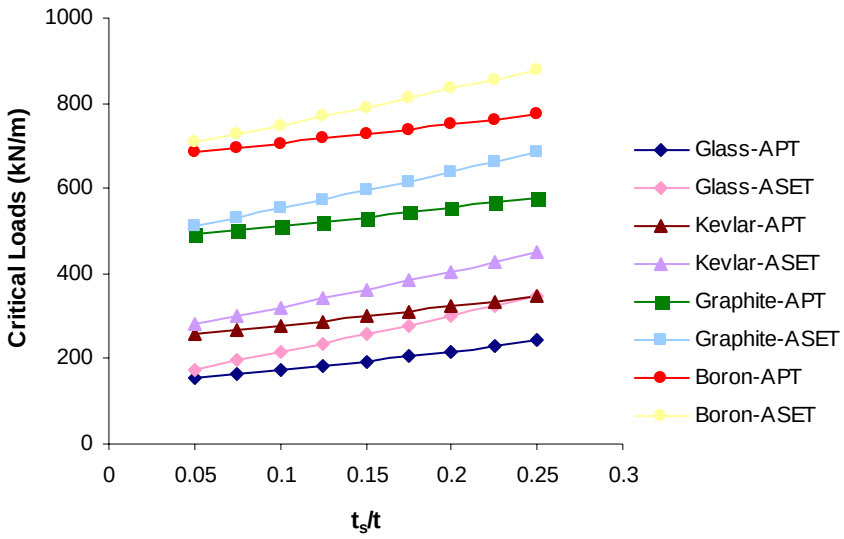

Figure 5.2: The effect of thickness of SMA layers on the critical loads for different fibres

The study was also conducted on different types of composite fibres to see the effect of different Young's modulus on the relative critical loads. Figure 5.2 shows that boron fibres provide the highest critical loads for SMA plates. The reason is obvious since the Young's modulus of boron is the highest among the Young's modulus of others in the group. In figure 5.3 however it can be seen that the effect of SMA is most significant if we use the glass fibres rather than other fibres. This can be easily understood as the ratio of Young's modulus of the glass fibre to the Young's modulus of Nitinol SMA is the lowest among ratios that involve other fibres. Furthermore as the ratio of t_s/t is increased, the effect of SMA on critical loads of glass fibre plates becomes greater compares to the effect of SMA on other fibre plates.

Next a study was conducted to see the effect of thickness to length ratio (TLR) on the APT and ASET improvements of the critical loads of SMA plates. Here, the thickness of

each SMA layer is set to remain constant at 0.6 mm while the thickness of other layers are varied according to the assigned values of TLR. The configuration of $[0/(45/-45)_5/0]$ is retained while SMA with initial strain, εo =0.001 that gives recovery stress of 91.6 MPa is also used.

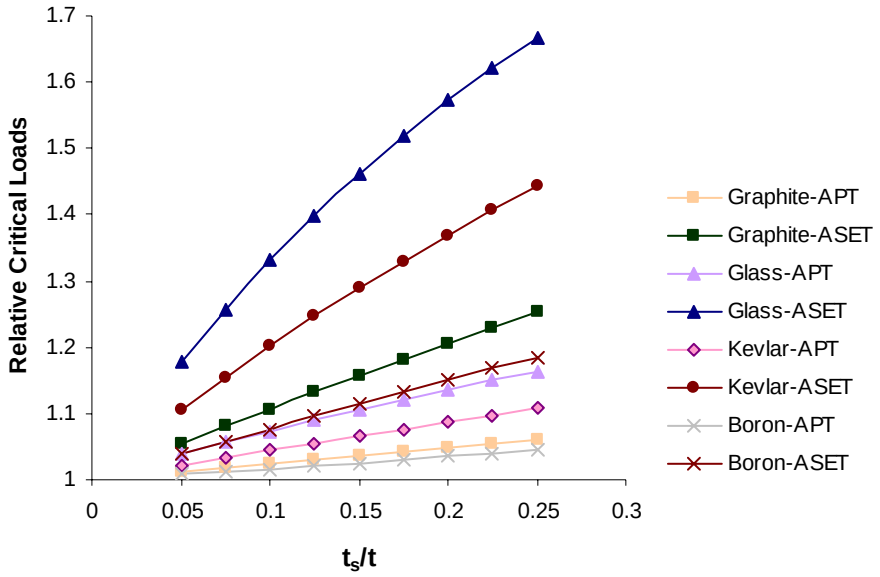

Figure 5.3 : The effect of thickness of SMA layers on the relative critical loads for different composite fibres

This study shows that the effect of SMA on the critical loads is decreased as the TLR is increased such as shown in Figure 5.4. This is due to the fact that as the thickness of the glass-epoxy layers is increased, the volume fraction of the SMA will be decreased. At high volume fractions of SMA, the increase in critical load after SMA activation is high. It should also be mentioned that while the relative critical loads are decreased with the increase of TLR, the critical loads are actually increased. The reason here is that the Young's modulus of glass is higher than the Young's modulus of the SMA and as the

volume fraction of the glass is increased, the critical loads are still increased regardless to the effect of the SMA.

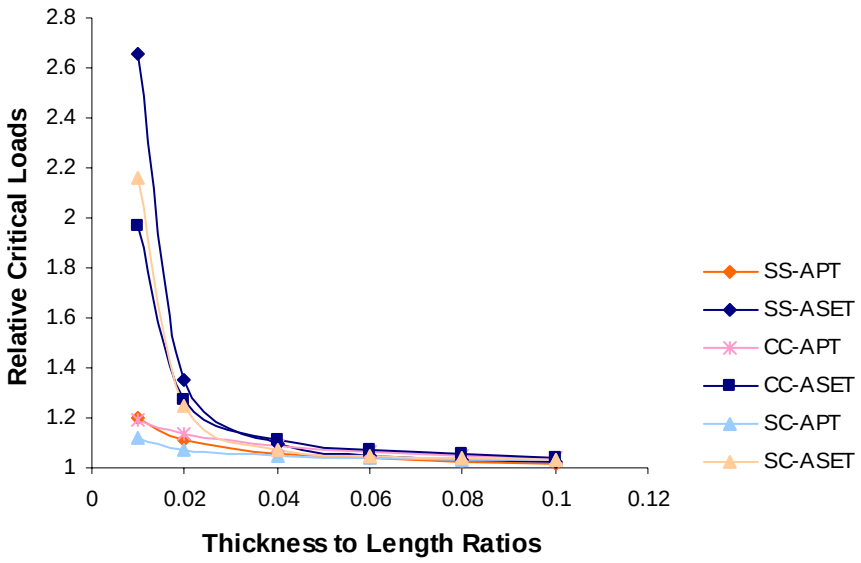

Figure 5.4: The effect of thickness to length ratio on the relative critical loads.

Figure 5.4 again shows that the effect of SMA is more significant for SS boundary condition while the CC and SC boundary conditions give almost the same responses for ASET improvement.

5.2.3 The effect of the volume fraction of Nitinol

The effect of volume fraction of SMA wires on the critical loads of the SMA composite plates can be studied by varying the volume fractions of the nitinol wires in the N-E layers while the volume fractions of glass fibres in the G-E layers are kept constant. Just like in the previous studies, SMA with initial strain of 0.005 m/m that gives recovery stress of 170.2 MPa at the activation temperature of 60^0C is used. The thickness of a N-E layer is 0.6 mm. The results of the effect of the volume fraction of the SMA on the relative critical loads can be seen in Figure 5.5.

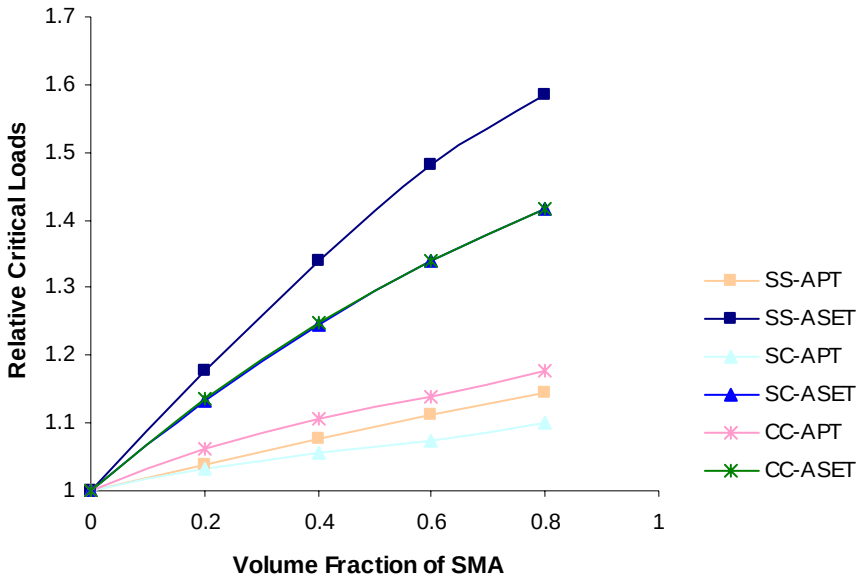

Figure 5.5: The effect of volume fraction of Nitinol fibres on critical loads

It shows that as the volume fraction of the SMA increases, the effect of SMA on the APT and ASET improvements increases too. This can be seen in the increase of the relative critical loads in the all six cases. As in the previous study, it should be mentioned that the actual critical loads are increased with the increase of the volume fraction of the SMA since the effective Young's modulus of the SMA plates will be increased too. Notice also that the improvement made by APT is very small compare to the improvement made by ASET. Furthermore, the effect of boundary condition is similar to the one shown in previous studies where the effect is more significant in the SS boundary condition as compared to the other two boundary conditions.

5.2.4 The effect of the number of layers

In this study, SMA layers remain the outermost layers with a constant thickness of 0.6 mm per layer. However the number of inner G-E layers is varied for the same total thickness of 8 mm. This means that n in the configuration $[0/(45/-45)_n/0]$ is set to vary from 1 to 9 for the same amount of thickness. The objective here is to see the effect of

bending-extension coupling stiffness that presents in the anti-symmetric composites on the APT and ASET improvements of the SMA composites.

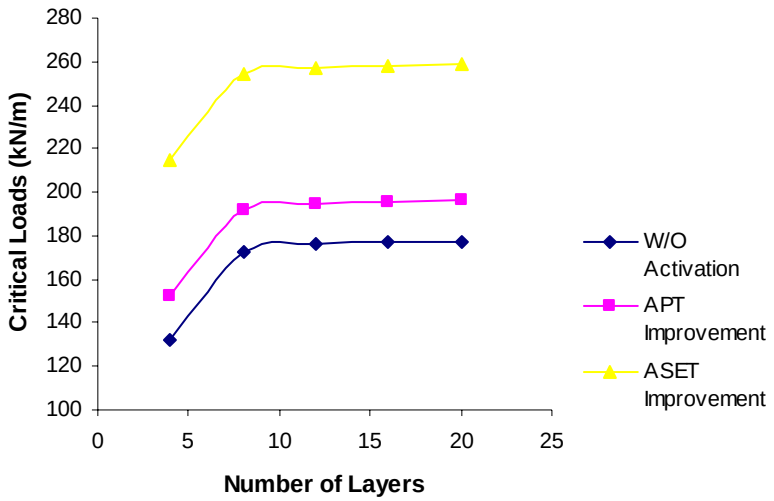

Figure 5.6: The effect of number of layers on critical loads of SS SMA composite plates

It is well known that this coupling stiffness reduces buckling loads of anti-symmetric composite plates and this coupling stiffness will reduce to zero with the increase in the number of layers [23]. Figures 5.6 and 5.7 show how the actual critical loads and the relative critical loads, respectively vary with the change in the number of layers. It can be seen in figure 5.6 that critical loads are increased with the increase of the number of layers for SS plates before SMA activation and after activation corresponds to APT and ASET improvements. It shows that with higher bending-stretching coupling stiffness values, plates with lower number of layers have lower critical loads. The values of this coupling stiffness is reduced to almost zero when the number of layers is about 8. As such the critical loads correspond to number of layers greater than 8 remains almost constant.

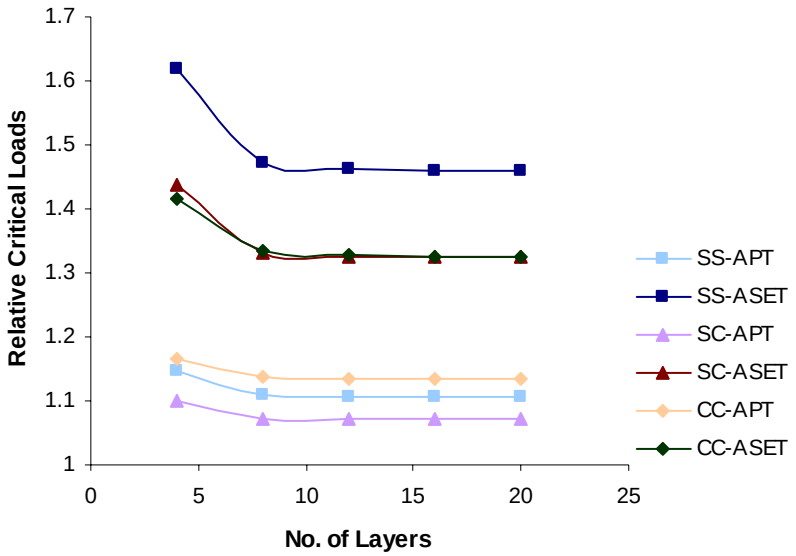

Figure 5.7: The effect of number of layers on relative critical loads of SMA composite plates

Figure 5.7 shows that the effect of SMA is reduced with the increase of the number of layers. It shows that the present of coupling stiffness is in fact enhances the effect of SMA in improving the critical loads. As in figure 5.6, the effect of coupling is reduced to almost zero when the number of layers is about 8. It can also be seen that the effect of boundary condition remains consistent where SS boundary condition gives the highest effect on the relative critical loads while the SS and CC boundary conditions show almost the same responses in the ASET improvement cases.

5.2.5 The transformation effect

In this section, the martensite transformation behaviour of SMA is studied through its effect on the critical loads of the SMA plates. The transformation effects to be considered here are the activation temperature and the amount of initial strain. To study the effect of activation temperatures on the APT and ASET improvements of SMA composites, the Brinson's model is used to determine the recovery stresses and the corresponding Young's modulus of SMA at several temperatures during the transformation process.

Data in table 5.2 shows the amount of recovery stress, σ_1^r, SIM volume fraction, ξ_s and Young's modulus, E_s at several activation temperatures, T_{act} for SMA with initial strain, εo =0.001. Full stress recovery is assumed here. These data shows, while the activation temperature is increased as the martensite transformation is progressing, the Young's modulus and the corresponding recovery stress are increased too. Recall from table 2.3, the austenite start temperature, A_s and the austenite finish temperature, A_f are 37.2^0C and 47.0^0C respectively. However, with the effect of stress, the actual austenite start temperature, A_{sm} and the austenite finish temperature, A_{fm} become 38.2^0C and 58.2^0C respectively [17]. Figure 5.8 shows the effect of increasing activation temperatures on the APT and ASET improvements of critical loads for the three cases of boundary conditions.

Table 5.2: The restrained recovery stress results based on Brinson's model at εo =0.001

T_{act} (^{0}C)	σ_1^r (MPa)	ξ_s	E_s (GPa)
20	0	0.01724	33
30	5.5	0.01724	33
40	12.92	0.01628	35.05
50	61.23	0.00441	60.23
60	91.6	0	69.6
70	97.1	0	69.6

It can be seen from figure 5.8 that as the temperatures are increased, the relative critical loads are increased for all APT and ASET cases where the effect of SMA is greater between temperature of 40^0C and 60^0C. These are the range of temperatures where stress is mostly recovered and Young's modulus is increased quickly as the martensite transformation takes place within this range. Notice the small effect of SMA can be seen even before the transformation starts due to the temperature effect that results in the presence of stress.

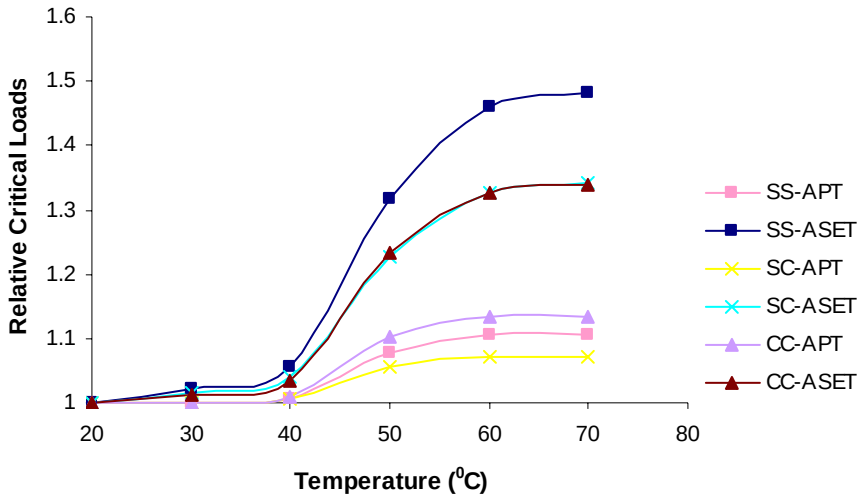

Figure 5.8 : The effect of activation temperatures on relative critical loads

Figure 5.8 also shows that the effect of SMA in ASET improvement is more significant for SS boundary condition while the effect of SMA in ASET improvement for SC and CC boundary conditions shows almost similar responses just as in the previous studies.

In studying the effect of initial strains on the APT and ASET improvements of SMA composites, the Brinson's model is used to determine the recovery stresses and the corresponding Young's modulus of the SMA for several values of initial strains at a fixed temperature of 55^0C. Data in table 5.3 shows the amount of recovery stress, σ_1^r, SIM volume fraction, ξ_s and Young's modulus, E_s for several initial strains, e_0 for SMA at T_{act} = 55^0C. It can be seen from table 4 that the increase in initial strain will result in the increase in recovery stress and the decreased in the Young's modulus. This is due to the fact that a higher initial strain value require a higher temperature for the transformation to complete. As a result at a fixed temperature of 55^0C, the transformation that occur is less complete as the initial strain is increased. This behaviour patterns can be seen in figure 5.9 that shows the effect of initial strains to the relative critical loads.

Table 5.3 : The restrained recovery stress results based on Brinson's model at $T_{act} = 55^0C$

e_0 (^0C)	σ_1^r (MPa)	E_s (GPa)
0.001	86.49	68.82
0.003	118.84	55.10
0.005	128.53	49.28
0.008	135.95	44.93
0.01	139.08	43.20

In figure 5.9, the reduction of Young's modulus is obvious when the effect of SMA in APT improvement can be seen to be declining as the initial strain is increased. However since the recovery stress is increased, the effect of SMA in the ASET improvement can be seen to increased as the initial strain is increased. Typically, the effect of SMA is at the greatest in the case of SS boundary condition.

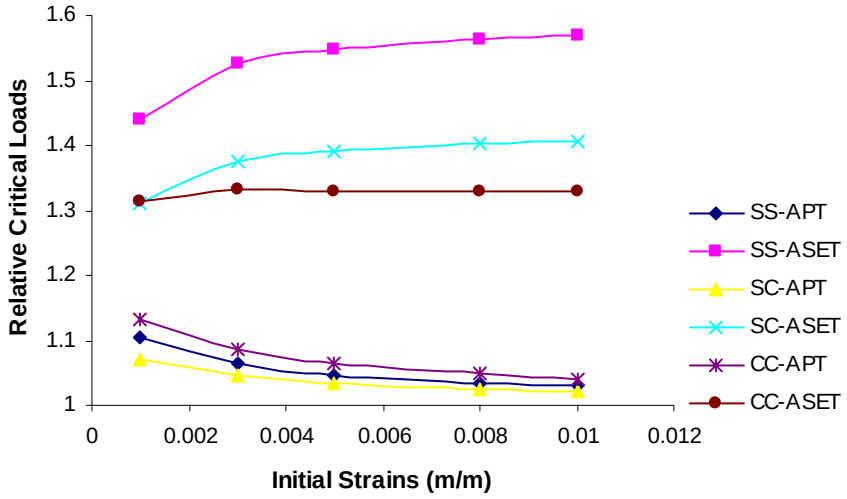

Figure 5.9 : The effect of initial strains on relative critical loads

5.2.6 The effect of SMA fibres orientation angles

The effect of SMA orientation angles on the improvement of critical loads can be studied by changing the angle of orientations of the SMA fibres. It is interesting to compare the effect of the orientation angles of the SMA fibres between the cases of anti-symmetric and symmetric composites. As such the configurations of $[0/(\theta/-\theta)_4/0]$ and $[0/(\theta/-\theta)_2]_s$

correspond to anti-symmetric and symmetric composites are used here. Both composites have the same number of layers. The angle of θ varies from 0^0 to 90^0.

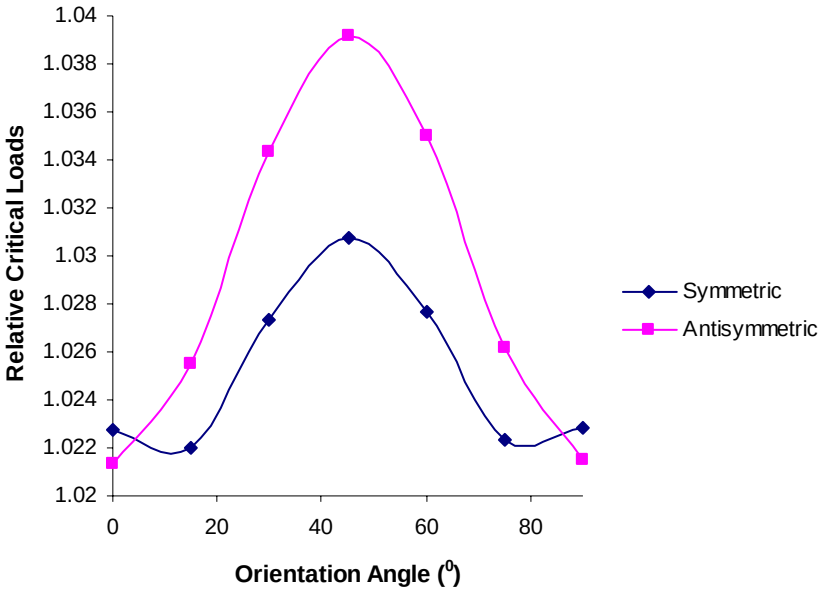

Figure 5.10: The effect of orientation angles on the relative critical loads for APT improvement.

SMA with initial strain of 0.005 m/m are used in this study. At the activation temperature of 60^0C, the Brinson's model will give in the SMA recovery stress of 170.2 MPa while the Young's modulus is 53.58 GPa. Figure 5.10 and 5.11 show the change of relative critical loads as the orientation angles of the SMA fibres are varied for APT and ASET improvements respectively.

It can be seen in figure 5.10 that the relative critical loads are maximum at 45^0C for both symmetric and anti-symmetric composites. Notice the difference between the two curves at temperatures between 0 and 15 degree and 75 and 90 degrees. Furthermore the maximum relative critical load for anti-symmetric composite is higher than the maximum relative critical load for symmetric composite.

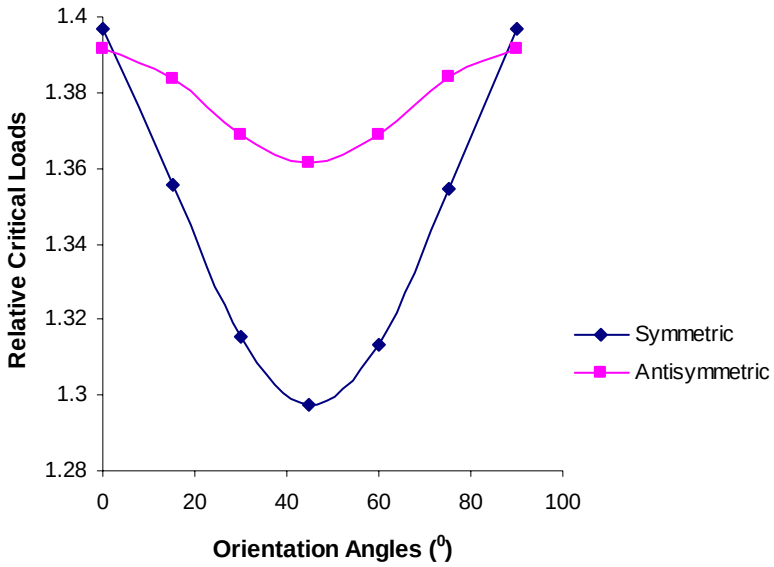

Figure 5.11: The effect of orientation angle on the relative critical loads for ASET improvement.

The effect of orientation angles is strongly influenced by the change of Young's modulus and the presence of recovery stress. In the case of APT improvement, only the change in the Young's modulus is considered. With the existence of recovery stress in ASET improvement, the trend for the effect of orientation angle has reversed to curves with minimum values such as shown in figure 5.11. Now the minimum relative critical load value for the symmetric composite is lower than that of the anti-symmetric composite. The switch from concave up curve to concave down curve as the recovery stress effect is added can be explained in the following study. Assuming at a fully transformed state (austenite, E=69.9 GPa), for different values of initial strains, we can have a set of corresponding values of recovery stresses.

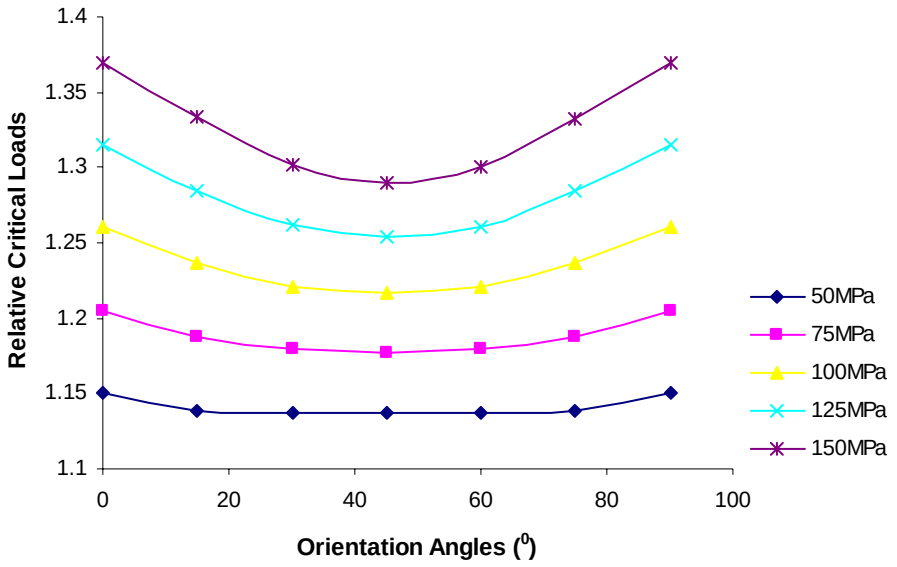

Figure 5.12: The effect of orientation angle on the relative critical loads for different values of recovery stress in the ASET improvement of symmetric composites.

Figure 5.12 shows that as the recovery stress effect is increased to the symmetric SMA composite, the relative critical loads vs orientation angle curve changes from having a maximum value to having a minimum value quite early i.e. only after the recovery stress is about the value of 75 MPa. In contrast, the anti-symmetric SMA composite requires a higher value of recovery stress of 125 MPa for the relative critical loads vs orientation angle curve to change from having a maximum value to having a minimum value such as shown in figure 5.13.

In the case of APT improvement, the curves will remain in having a maximum value for the increase of the Young's modulus. This can be seen in the following study on SMA composites with a pre-strained SMA of ε_0=0.005 m/m. Obtaining through the Brinson's model, table 5.4 shows the results of the martensite transformation process in the restrained recovery process of SMA composites.

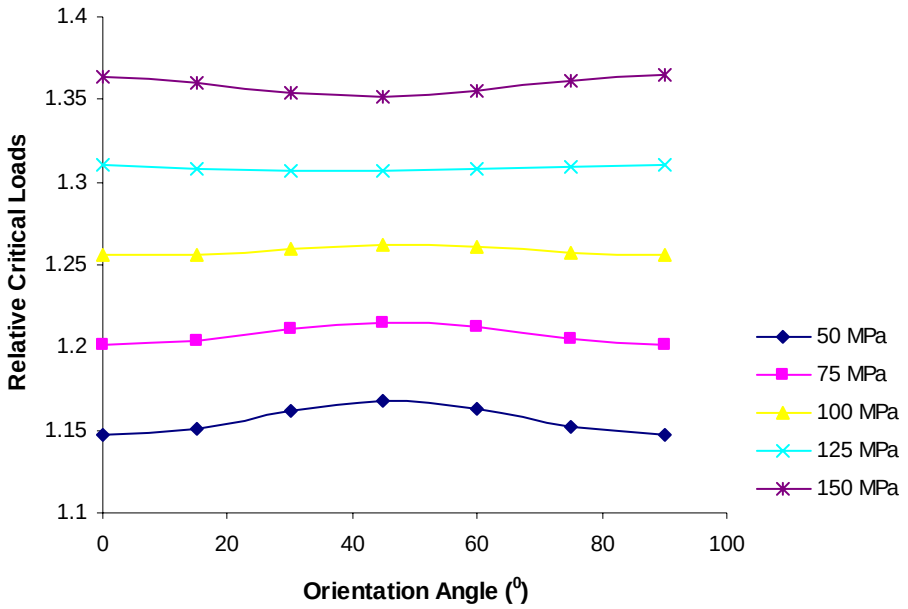

Figure 5.13: The effect of orientation angle on the relative critical loads for different values of recovery stress in the ASET improvement of anti-symmetric composite.

Table 5.4: The restrained recovery stress results based on Brinson's model at $\varepsilon o = 0.005$

T_{act} (^{0}C)	σ_1^r (MPa)	ξ_s	E (GPa)
30	5.5	0.0862	33
40	16.40	0.0834	34.20
50	87.82	0.0586	44.72
60	170.23	0.0382	53.38
70	254.67	0.0214	60.52
80	337.79	0.0072	66.57
90	386.5	0	69.6

With these data, the critical loads are determined in the APT improvement method for the symmetric composites. Figure 5.14 shows that the relative critical loads vs orientation angle curves remain to have a maximum value for the whole range of temperatures.

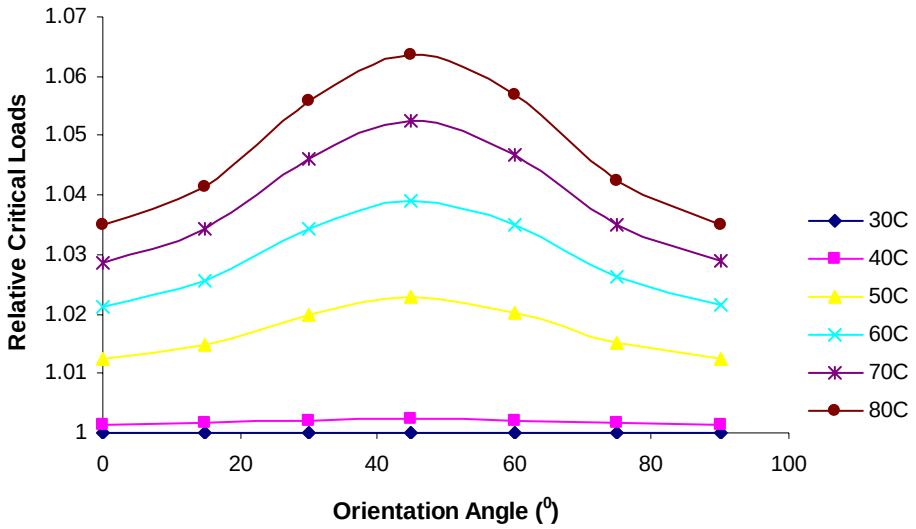

Figure 5.14: The effect of orientation angle on the relative critical loads for different values of temperature in the APT improvement.

As a conclusion to this section , the curves of relative critical loads vs orientation angles for APT improvement remain to have a maximum value at 45^0 even for an increase values of Young's Modulus. However the curves of relative critical loads vs orientation angles for ASET improvement change from having a maximum value to having a minimum value at the same 45^0 as the recovery stress is increased.

5.2.7 The effect of the locations of the SMA layers

In this study, two SMA layers are located symmetrically with respect to mid- surface of the SMA composite as in previous studies. However the distance between the two SMA layers is now varied to see its effect on the critical loads of the SMA composite plates. Here the fully recovered SMA with initial strain of 0.001 m/m that gives recovery stress of 91.6 MPa and Young's modulus of 69.6 GPa is used. The thickness of the SMA layers remain 0.6mm each.

Figure 5.15 shows that in cases of no activation of SMA wires (NA), APT and ASET improvements, as the distance between SMA layers are increased, the actual critical loads are decreased.

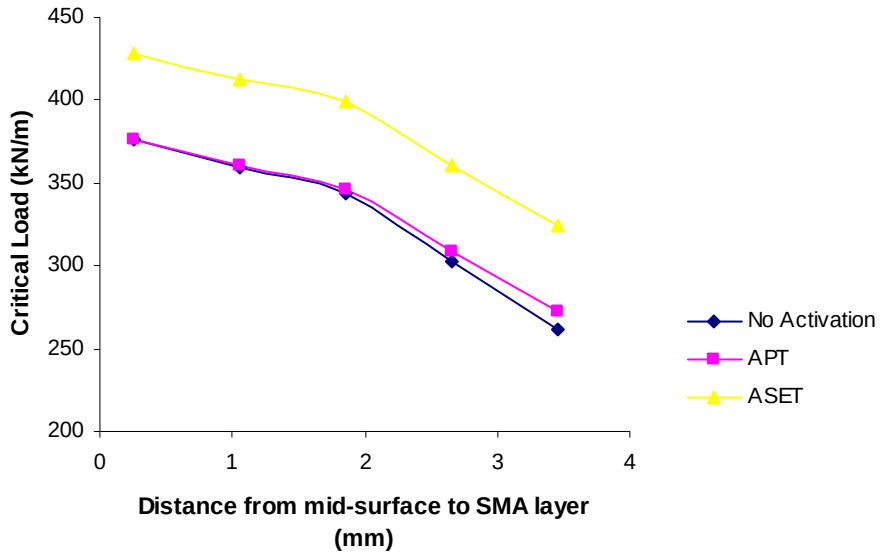

Figure 5.15: The effect of the distance between SMA layers on critical loads

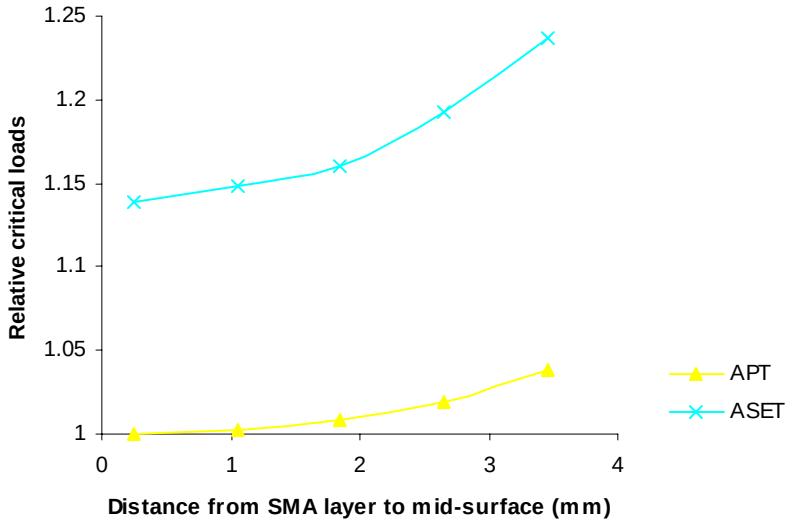

Figure 5.16: The effect of the distance between SMA layers on relative critical loads

On the other hand, the effect of SMA on critical loads of the SMA composites is increased with the increase of the distance between SMA layers. This can be seen from

the increase of the relative critical loads in figure 5.16 for the cases of APT and ASET improvements.

5.2.8 Conclusion to the buckling analysis

A simple linear finite element model for SMA composite plates was developed to study the effect of SMA on critical loads of composite plates. The effect of recovery stress in this model is represented by the additional geometric stiffness matrix. The values of SMA Young's modulus and recovery stress were pre-determined from the Brinson's model through either constrained or controlled recovery assumptions. Studies were conducted to see the effect of geometric, mechanical and transformation factors on the APT and ASET improvements of critical loads of SMA composite plates. It can be concluded that

1. The effect of SMA on the critical loads is increased with the increase of the ratio of SMA thickness to thickness of other layers. In the case of simply supported boundary condition, the increase of the critical load can be up to 1.7 times at SMA thickness equal to one fourth of the total thickness of other layers. Thus in terms of the required thickness of SMA layers to give an impact on the critical loads of composite plates, the ASET improvement of the critical loads of SMA plates can be considered as a good method.
2. Even though Boron fibre gives the highest critical loads of the SMA composite plates, it is the glass fibre that responses the greatest to the effect of SMA on the critical loads of the composite plates. This is because the ratio of the Young's modulus of the glass fibre to the Young's modulus of nitinol is the lowest of all ratios that involve other fibres.

3. The increase in the thickness to length ratio of the G-E layers will result in the decrease of the effect of SMA on the critical loads of the SMA plates. This is due to the increase of the volume fraction of the glass fibre as the thickness to length ratio is increased. Even though the relative critical loads are decreased, the actual critical loads are increased since the volume fraction of the glass fibres is increased.
4. The effect of the volume fraction of the nitinol in the SMA layers is quite significant where at the SMA volume fraction of 0.5, the relative critical load is about 1.5.
5. The presence of coupling stiffness of the composite enhances the effect of SMA even though it lowers the critical loads of the SMA plates. This can be concluded when the relative critical loads are decreased when the number of layers of the SMA plates is increased while in reverse, the critical loads are increased as the number of layer is increased.
6. In general as the activation temperature is increased, the effect of SMA on buckling loads is increased too since the Young's modulus of the SMA and the recovery stress are increased. However the effect of SMA can be seen to increase greatly between certain SMA activation temperatures where martensite transformation occurs greatly.
7. The increase of initial strains of the SMA at a fixed value of an activation temperature will cause the increase in the recovery stress and the decrease in the Young's modulus. As a result, the relative critical loads for APT improvement are seen to be decreasing as the initial strains are increased while the relative critical loads for ASET improvement are increased as the initial strains are increased.
8. The effect of orientation angle is strongly influenced by the change of Young's modulus and the presence of recovery stress. In APT improvement, the relative

critical loads are maximum at the angle orientation of 45^0 for both symmetric and anti-symmetric composites. With the addition of the recovery stress effect in ASET improvement, the relative critical loads vs orientation angle curve changes from having a maximum value to having a minimum values as the recovery stress is increased. The change occurs earlier at 75MPa for symmetric composite while for anti-symmetric composite the change occurs at a higher value of 125 MPa.

9. The change in the distance between the two SMA layers affects the critical loads and the relative critical loads. While the critical loads are decreased as the distance is increased, the relative critical loads are increased.
10. In all cases, the SMA effect in ASET improvement is much more significant than the SMA effect in the APT improvement.
11. The simply supported boundary condition provide the much more significant effect of the SMA on the critical loads as compared to the effects provided by the other two boundary conditions.

The simple finite element model was able to show the influence of SMA in the buckling improvement of laminated SMA plates.

5.3 Vibration of SMA plates

5.3.1 Convergence Test:

In this study, the convergence tests are conducted on a SMA composite plate to determine the appropriate mesh size for the free vibration analysis. It is also to provide the validation to the finite element model developed. The eigen frequencies of up to sixth mode are determined. The SMA wires are not activated for this purpose of validation. The results are compared to the analytical results that are calculated based on the classical

lamination theory (CLT) and first order shear deformation theory (FSDT) of plates [23]. The results in table 5.5 show quite a slow convergence that occurs in the free vibration finite element analysis for higher modes of vibrations. It was decided in this study to used the 8x8 mesh.

Table 5.5: Convergence test for anti-symmetric angle-ply composite plates ($[0/(45/-45)_4/0]$).

Modes	CLT[#]	FSDT[#]	2x2	3x3	4x4	5x5	6x6	7x7	8x8	9x9	10x10
I	135.99	135.35	153.0	136.2	135.5	135.4	135.37	135.36	135.36	135.36	135.36
II	309.38	306.24	596.8	324.7	309.6	307.4	306.75	306.5	306.39	306.35	306.3
III	320.15	316.79	596.8	335.3	320.3	318.0	317.33	317.08	316.95	316.9	316.86
IV	543.55	533.7	1089	671.2	558	538.8	535.38	534.45	534.09	533.92	533.84
V	571.79	561.8	1838.4	688.1	590.5	572.5	566.89	564.55	563.42	563.02	562.47
VI	602.56	591.42	4315.9	701.6	621.5	602.9	596.9	594.39	593.19	592.72	592.15

[#]Reddy, J.N. [23]

5.3.2 The effect of the thickness of the SMA layer

Similar to the buckling analysis, the objective here is initially to get a general idea on the required thickness of SMA layers with respect to the thickness of plate in order to give a certain impact to the eigen frequencies of the SMA composite plate. So the study on the effect of the ratio of SMA layer thickness to thickness of other layers (t_s/t) is first conducted. The effect of the ratios of thickness to side length ratio (TLR) of the plates are studied later. The same SMA plates with configuration $[0/(45/-45)_5/0]$ and SMA wires with initial strain, εo =0.001 are used here where at the activation temperature of 60^0C, the Brinson's model will give the recovery stress of 91.6 MPa. Figures 5.17 and 5.18 shows the effect of thickness on the APT and ASET improvements respectively of the relative eigen frequencies of the SS SMA composite plates.

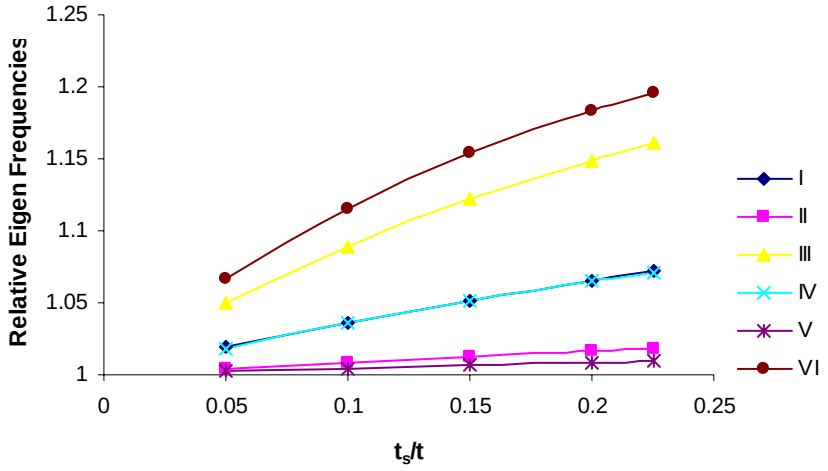

Figure 5.17: The effect of thickness of SMA layers on the APT improvement of relative eigen frequencies of SS SMA composite plates

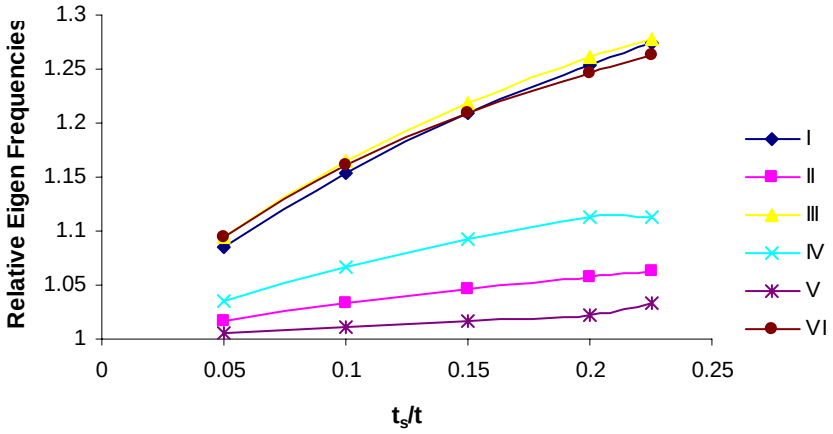

Figure 5.18: The effect of thickness of SMA layers on the ASET improvement of relative eigen frequencies of SS SMA composite plates

The plots show that the responses of the relative eigen frequencies to the thickness of SMA layers are varies among different modes for both APT and ASET cases. In general, the responses are greater for frequencies of modes 1 and IV and modes III and VI. The frequencies of modes II and V seem to show little response on the increase in thickness of the SMA layers. For example, the increase of the eigen frequencies for mode III and

VI can be up to 1.25 times at SMA layer thickness equal to one fifth of the thickness of other layers.

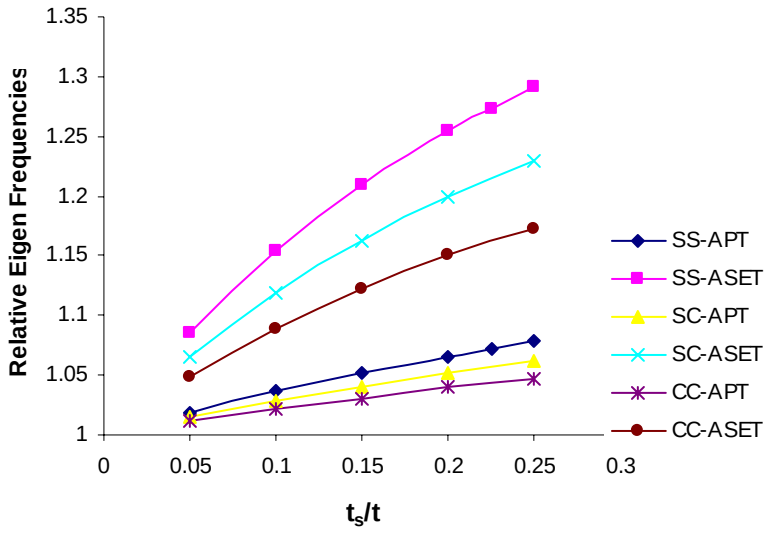

Figure 5.19: The effect of thickness of SMA layers and boundary conditions on the APT and ASET improvements of relative eigen frequencies mode I of angle-ply composite plates

Figure 5.19 shows the effect of thickness of SMA layers on the APT and ASET improvements of relative eigen frequencies mode I of SMA composite plates with different boundary conditions. It shows that the effect of SMA on eigen frequencies is at the greatest for the SS boundary condition and at the smallest for CC boundary condition. Furthermore, for all three boundary conditions, the ASET improvements are greater than the APT improvements as expected.

Figures 5.20 and 5.21 show the effect of thickness of SMA layers on APT and ASET improvement, respectively, of eigen frequencies mode I and II of simply supported SMA composite plates with different composite fibres. Four types of fibres are used: glass, kevlar, graphite and boron.

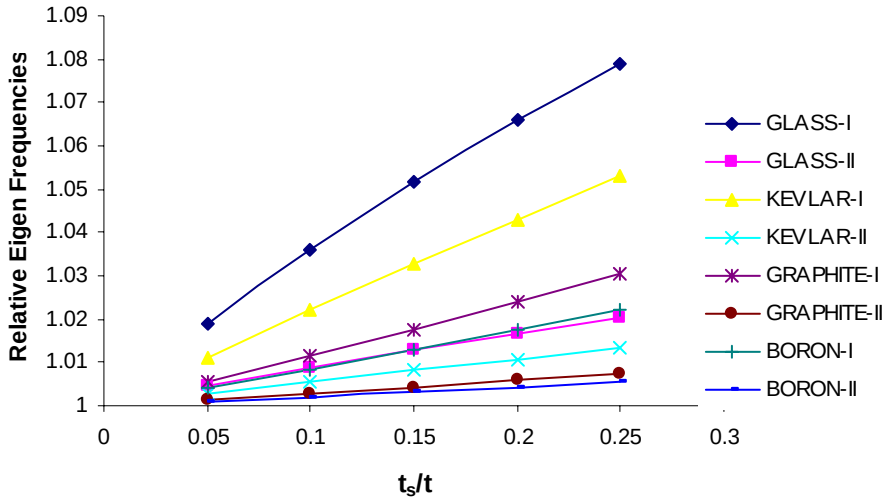

Figure 5.20: The effect of thickness of SMA layers on the APT improvement of eigen frequencies mode I and II of SS SMA composite plates with different composite fibres

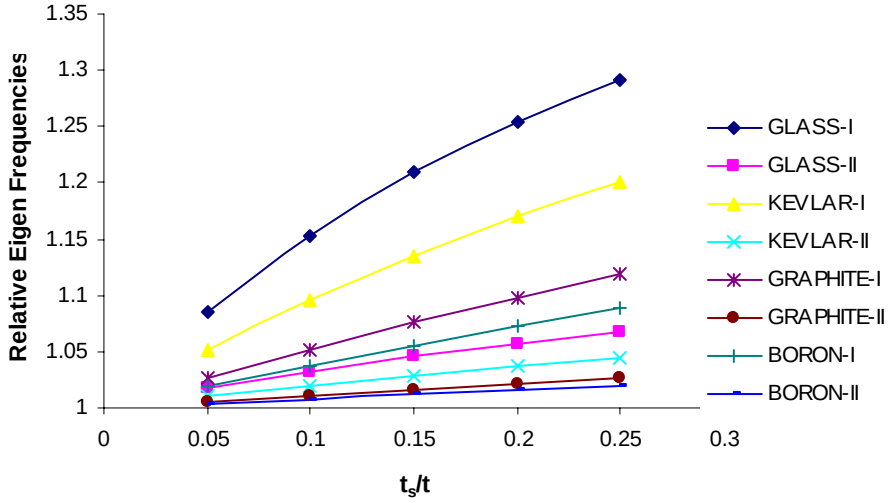

Figure 5.21: The effect of thickness of SMA layers on the APT improvement of eigen frequencies mode I and II of simply supported SMA plates with different composite fibres

These plots show that the effect of SMA is most significant if we use the glass fibre rather than other fibres. As in the buckling analysis, this can be easily understood as the ratio of Young's modulus of the glass fibre to the Young's modulus of Nitinol SMA is the lowest among ratios that involve other fibres. Furthermore as the ratio of t_s/t is increased, the effect of SMA on critical loads of glass fibre plates becomes greater

compares to the effect of SMA on other fibre plates. Both figures 5.20 and 5.21 also show that the effect of SMA is significant in the eigen frequency mode I while the effect is small in the eigen frequency mode II.

To study the effect of TLR on the APT and ASET improvements of the eigen frequencies, the specifications of the SMA plates that were used in the study of the same effect on buckling analysis are retained here. This means that the SMA plate configuration of $[0/(45/-45)_5/0]$ and SMA with initial strain, $\varepsilon o = 0.001$ that gives the recovery stress of 91.6 MPa are used. The thickness of each SMA layer is set to remain at 0.6 mm while the thickness of other layers are varied according to the values of TLR. Figure 5.22 to 5.25 give the results of the effect of the TLR on the APT and ASET improvements of eigen frequencies correspond to SS, SC and CC boundary conditions.

From the plots, it can be stated that in general as the TLR are increased, relative eigen frequencies are decreased at the same time. This can be easily understood by the fact that as the thickness of the plate increases, the volume fraction of the SMA will be decreased so that the effect of SMA is decreased too.

There are several trends that can be observed in these results. Firstly the effect of SMA seems to be of a similar level for certain modes of frequencies. For example, typical couples with similar level of responses are frequencies of modes I and IV, II and V and III and VI. Frequency couples of modes I and IV and III and VI seem to have greater responses as compared to the couple of mode II and V. The couple of modes I and IV seems to have almost exact responses between them in the case of APT improvement of SS SMA composite plates.

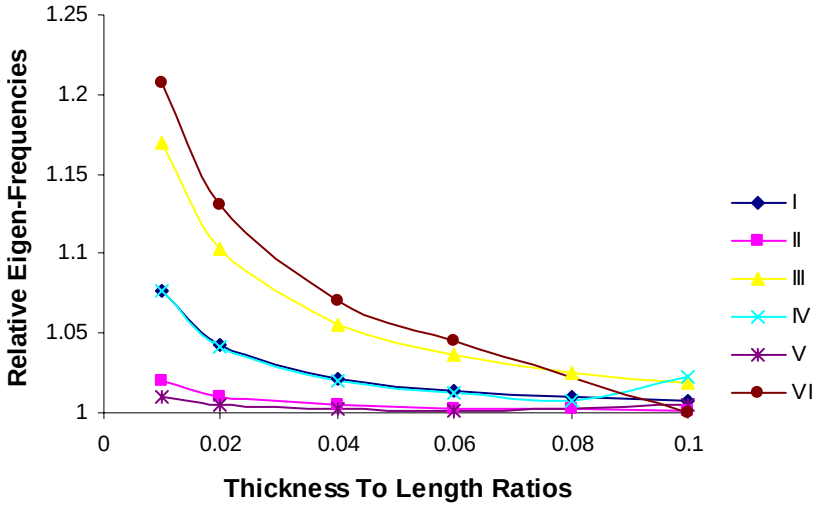

Figure 5.22: The effect of thickness to length ratio on the APT improvement of relative eigen frequencies of SS SMA composite plates

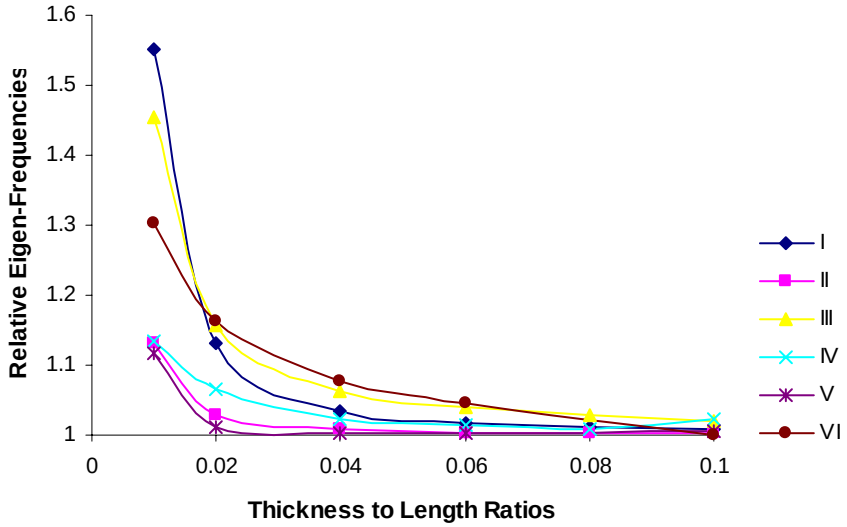

Figure 5.23: The effect of thickness to length ratio on the ASET improvement of relative eigen frequencies of SS SMA composite plates.

Furthermore, the effect of SMA as stated previously is the greatest for the case of SS boundary condition and the smallest for the case of CC boundary conditions. For example, the relative eigen frequency of mode I is close to 1.6 for SS boundary condition, 1.45 for SC boundary condition and only 1.35 for CC boundary condition.

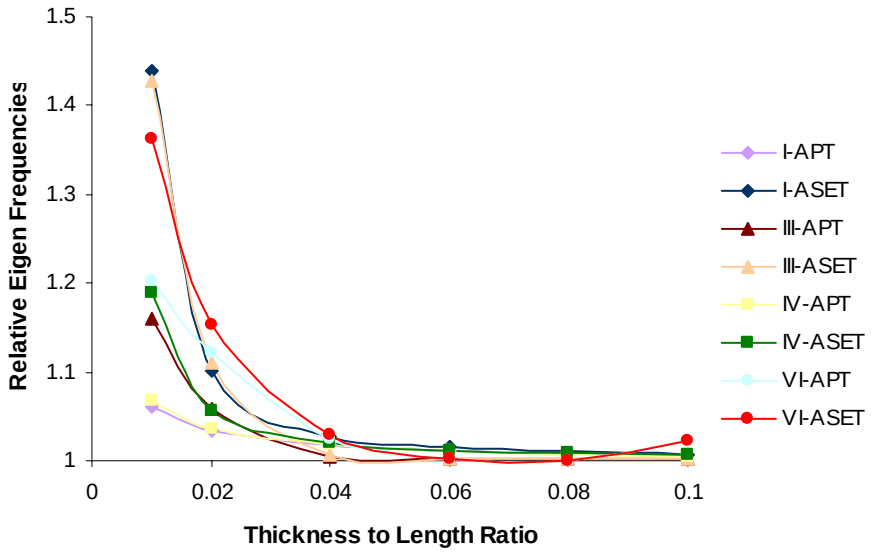

Figure 5.24: The effect of thickness to length ratio on the APT and ASET improvement of relative eigen frequencies of SC SMA composite plates .

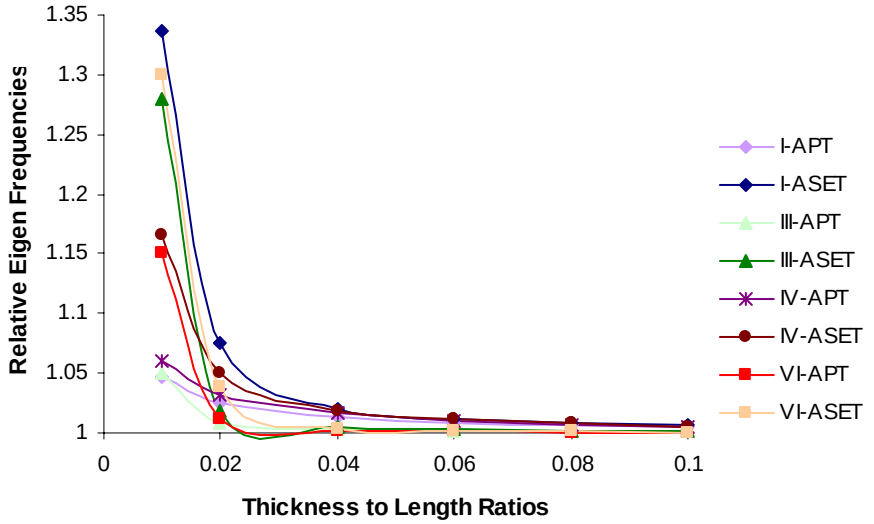

Figure 5.25: The effect of thickness to length ratio on the APT and ASET improvement of relative eigen frequencies of CC SMA composite plates .

Thirdly, as expected the effect of TLR on the ASET improvement is in general always greater than the effect of TLR on APT improvement. This is due to the consideration of both the change in Young's modulus and the recovery stress that we made in the ASET study while only the increase in the Young's modulus is considered in the APT study.

5.3.3 The effect of the volume fraction of Nitinol

The effect of the volume fraction of SMA wires on the eigen frequencies of the SMA composite plates can be studied by varying the volume fraction of the nitinol wires in the N-E layers while the volume fraction of glass fibres in the G-E layers is kept constant. Just like in the buckling study, SMA with initial strain of 0.005 m/m that gives recovery stress of 170.2 MPa at the activation temperature of 60^0C is used. The thickness of a N-E layer is 0.6 mm. The results of the effect of the volume fraction of the SMA on the APT and ASET improvements of eigen frequencies can be seen in Figure 5.26 to 5.29 for the three boundary conditions.

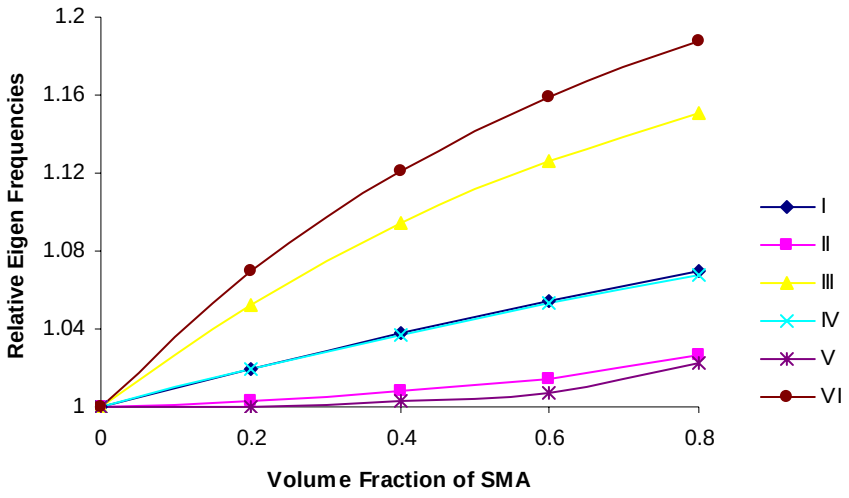

Figure 5.26: The effect of volume fraction of Nitinol fibres on APT improvement of eigen frequencies of SS SMA composite plates

From these plots, it can be stated that the effect of volume fraction of SMA wires on the relative eigen frequencies of the SMA plates is in reverse to the effect of TLR on the relative eigen frequencies. It shows that as the volume fraction of the SMA increases, the effect of SMA on the APT and ASET improvements increases too.

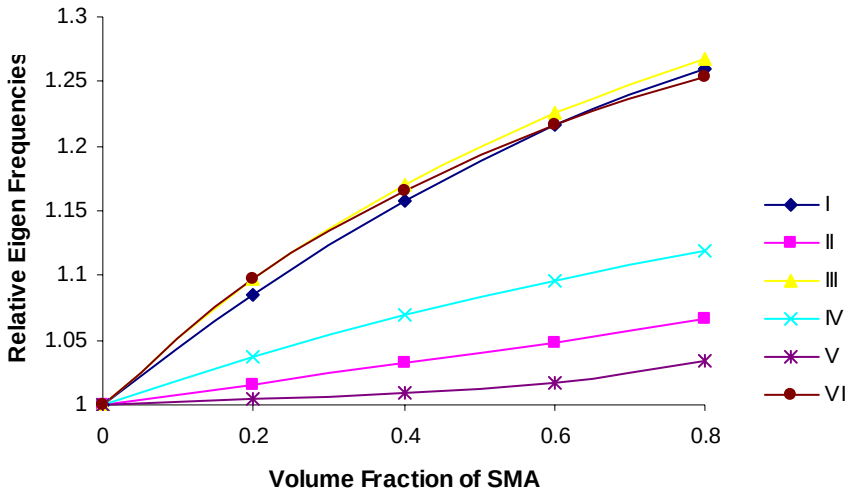

Figure 5.27: The effect of volume fraction of Nitinol fibres on ASET improvement of eigen frequencies of SS SMA plates

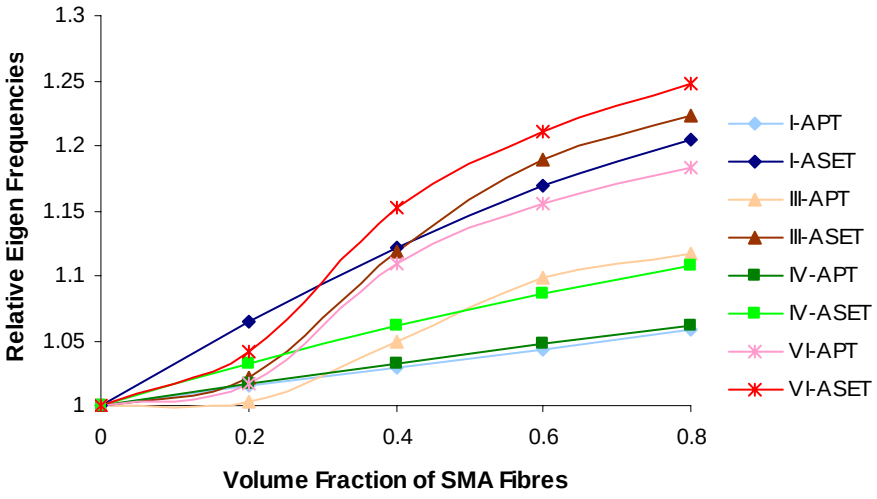

Figure 5.28: The effect of volume fractions of Nitinol fibres on APT and ASET improvements of eigen frequencies of SC SMA composite plates

The trends that were observed in the previous study can be seen here. For example, typical couples with similar level of responses such as frequencies of modes I and IV, II and IV and III and VI can again be observed here. As expected, frequency couples of modes I and IV and II and IV seem to have greater responses as compared to the couple

of mode II and IV. The couple of I and IV in the case APT improvement of SS SMA plates gives the almost exact response between the two. Furthermore the effect of SMA seems to be greater in the case of SS boundary condition.

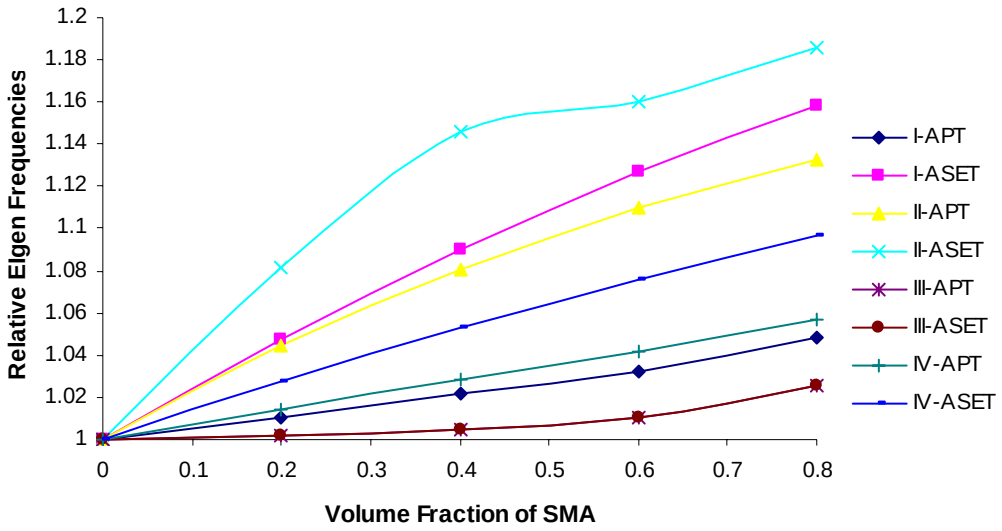

Figure 5.29: The effect of volume fractions of Nitinol fibres on APT and ASET improvements of eigen frequencies of CC SMA plates

Figure 5.29 shows that for CC boundary condition, at lower relative eigen frequencies values as a whole as compared to the SS and SC boundary conditions, mode II seems to be more dominant.

5.4.4 The effect of the number of layers

In this study, as in the buckling analysis, the n in the configuration $[0/(45/-45)_n/0]$ is set to vary from 1 to 9 for the same amount of 8mm thickness while the thickness of a SMA layer is set to 0.6mm. This is in order to see the effect of bending-extension coupling stiffness that presents in the anti-symmetric composites on the APT and ASET improvements of the SMA composites. Figures 5.31 and 5.31 show the effects of the number of layers on the APT and ASET improvements respectively on the relative eigen

frequencies of the SMA composite plates. Only the SS boundary condition is implemented in this study.

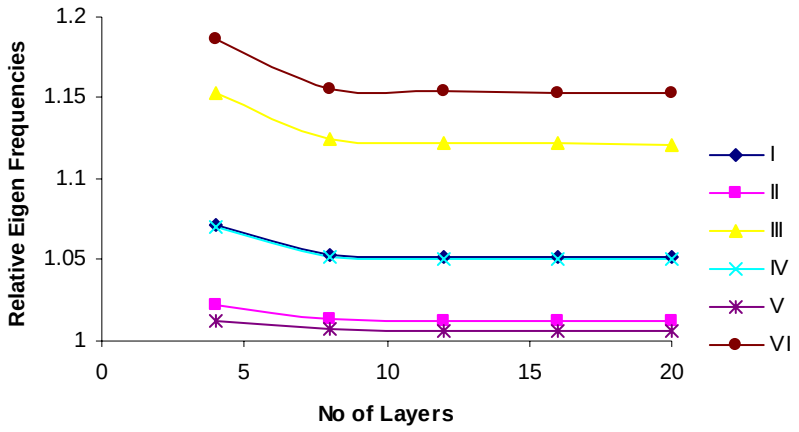

Figure 5.30: The effect of number of layers on APT improvement of relative eigen frequencies of SS SMA composite plates.

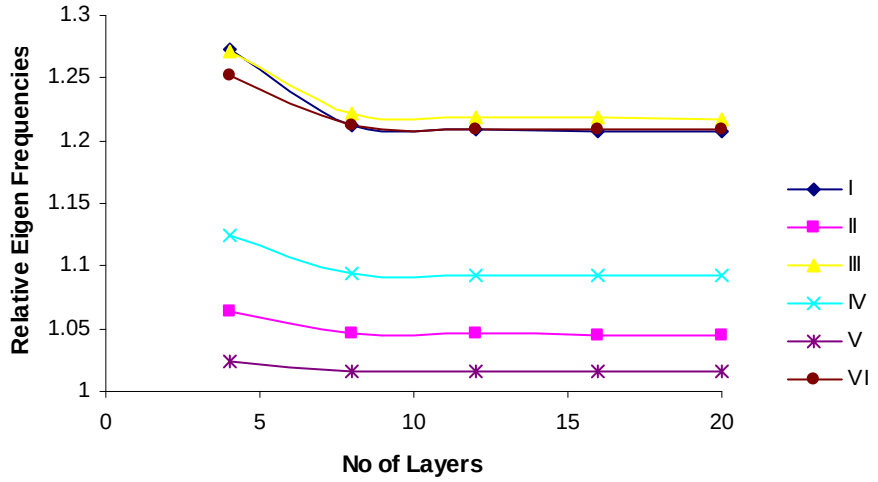

Figure 5.31: The effect of number of layers on ASET improvement of relative eigen frequencies of SS SMA composite plates.

Similar to the effect of the number of layers on critical loads, the existence of bending-stretching coupling increases the effect of SMA on the eigen frequencies of the SMA composite plates. This can be observed in figures 5.30 and 5.31 that as the number of layers is increased i.e. as the bending-stiffness coupling is reduced, the relative eigen

frequencies are reduced too. As in the analysis of buckling, the effect of coupling is reduced to almost zero when the number of layers is about 8. The typical trend of couples of modes of frequencies with similar level of response remain consistent here for the SS boundary condition. It shows that frequency couples of modes I and IV and II and IV seem to have greater responses as compared to the couple of mode II and IV. Furthermore the couple of modes 1 and IV shows almost the exact response in the case of APT improvement.

5.2.5 The transformation effect

In this section, the martensite transformation behaviour of SMA is studied through its effect on the eigen frequencies of the SMA plates. The transformation effects to be considered here are the activation temperature and the amount of initial strain. As in the buckling analysis, data in table 5.2 that shows the amount of recovery stress, σ_1^r, SIM volume fraction, ξ_s and Young's modulus, E_s at several activation temperatures, T_{act} for SMA with initial strain, εo =0.001 is used here. Figure 5.32 to 5.37 shows the effect of increasing activation temperatures on the APT and ASET improvements of eigen frequencies for the three cases of boundary conditions.

It can be seen from figures 5.32 to 5.37 that as the temperatures are increased, the relative eigen frequencies are increased for all APT and ASET cases where the effect of SMA is greater between temperature of 40^0C and 60^0C. These are the range of temperatures where stress is mostly recovered and Young's modulus is increased quickly as the martensite transformation takes place within this range. Notice also as in the buckling analysis, the small effect of SMA can be seen even before the transformation starts due to the temperature effect that results in the presence of stress.

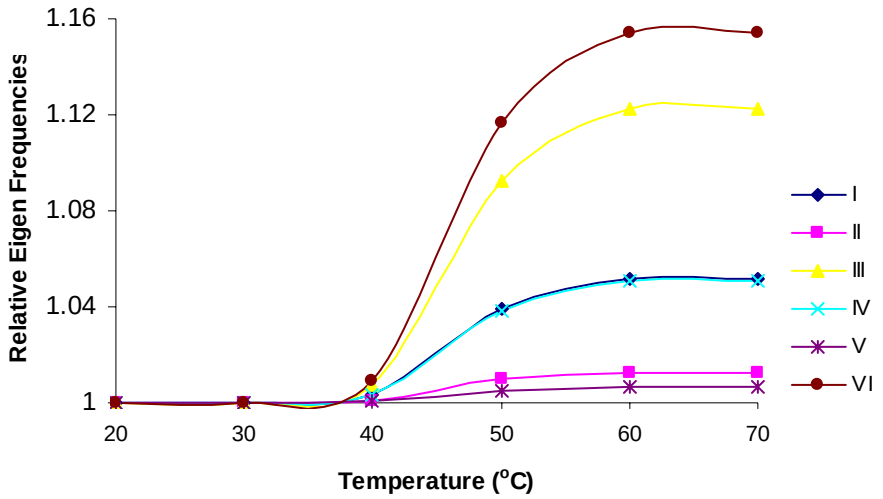

Figure 5.32 : The effect of activation temperatures on APT improvement of relative eigen frequencies for SS SMA composite plates

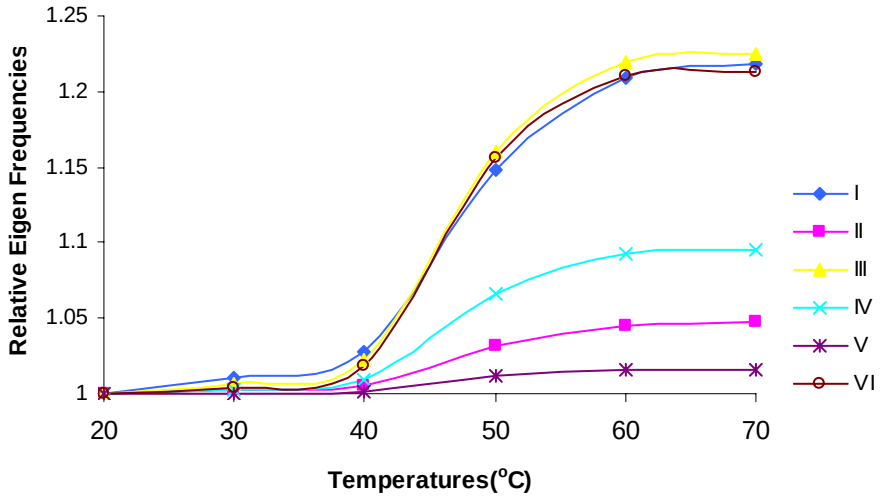

Figure 5.33 : The effect of activation temperatures on ASET improvement of relative eigen frequencies for SS SMA composite plates

The typical trend of responses mentioned previously can be observed again here. That is, firstly there exists couples of modes of frequencies with similar level of response. Secondly couples of I and IV and III and VI have greater responses than the couple of modes II and V except for the CC boundary condition where the response of the couple of mode II and V seems to be dominant.

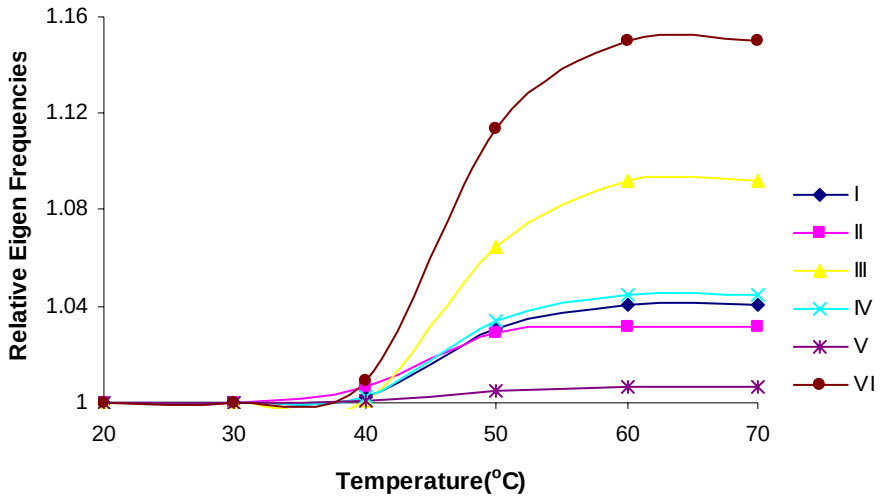

Figure 5.34 : The effect of activation temperatures on APT improvement of relative eigen frequencies for SC SMA composite plates

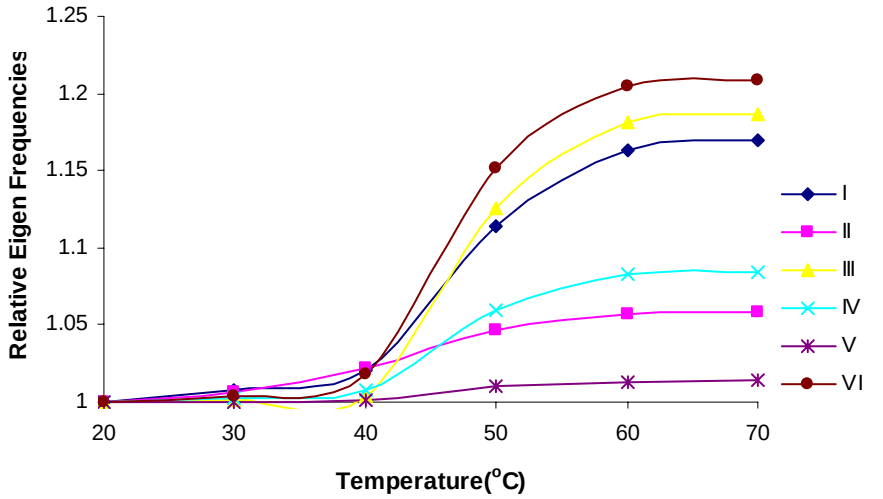

Figure 5.35 : The effect of activation temperatures on ASET improvement of relative eigen frequencies for SC SMA composite plates

Furthermore Figure 5.32 to 5.37 also shows that the effect of SMA in ASET improvement is more significant for SS boundary condition while the effect of SMA in ASET improvement for SC and CC boundary conditions shows almost similar responses just as in the previous studies.

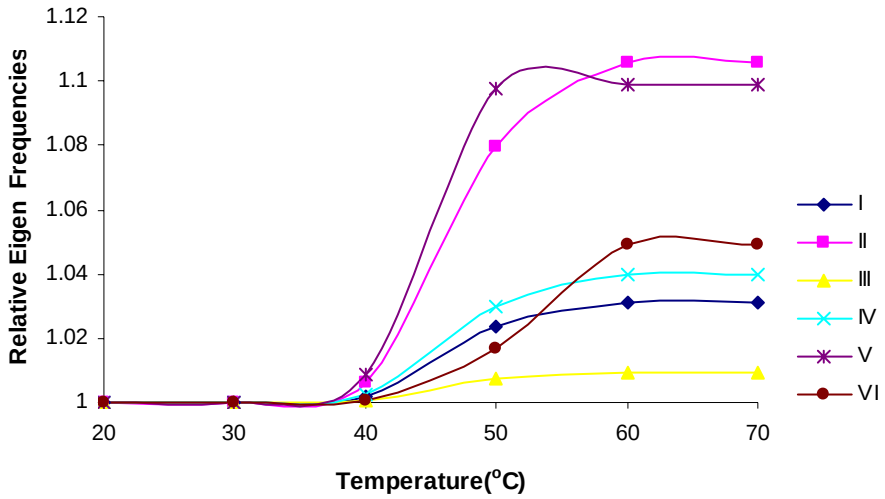

Figure 5.36 : The effect of activation temperatures on APT improvement of relative eigen frequencies for CC SMA composite plates

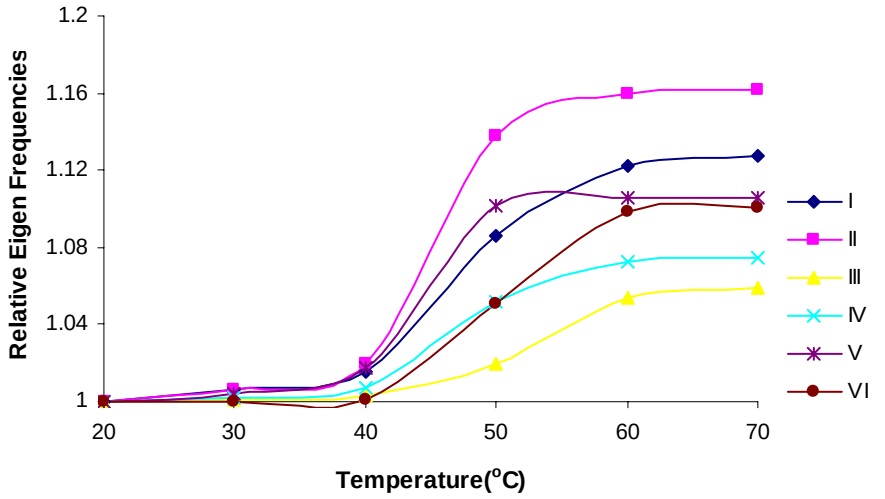

Figure 5.37 : The effect of activation temperatures on ASET improvement of relative eigen frequencies for CC SMA composite plates

In studying the effect of initial strains on the APT and ASET improvements of SMA composites, as in the buckling studies, data in table 5.3 shows the amount of recovery stress, σ_1^r, SIM volume fraction, ξ_s and Young's modulus, E_s for several initial strains, e_0 for SMA at $T_{act} = 55^0$C. As a reminder, it can be seen from table 5.3 that the increase in initial strain will result in the increase in recovery stress and the decreased in the Young's

modulus. This is due to the fact that a higher initial strain value requires a higher temperature for the transformation to complete. As a result at the fixed temperature of 55^0C, the transformations that occur are actually less complete as the initial strains are increased. This behaviour pattern can be seen in figure 5.38 to 5.43 that show the effect of initial strains to the relative eigen frequencies.

In figure 5.38 the reduction of Young's modulus is obvious when the effect of SMA in APT improvements can be seen to be declining as the initial strain is increased in the case of SS SMA composite plates. The same thing can be said to figures 5.40 and 5.42, for the case of SC and CC SMA composite plates, respectively.

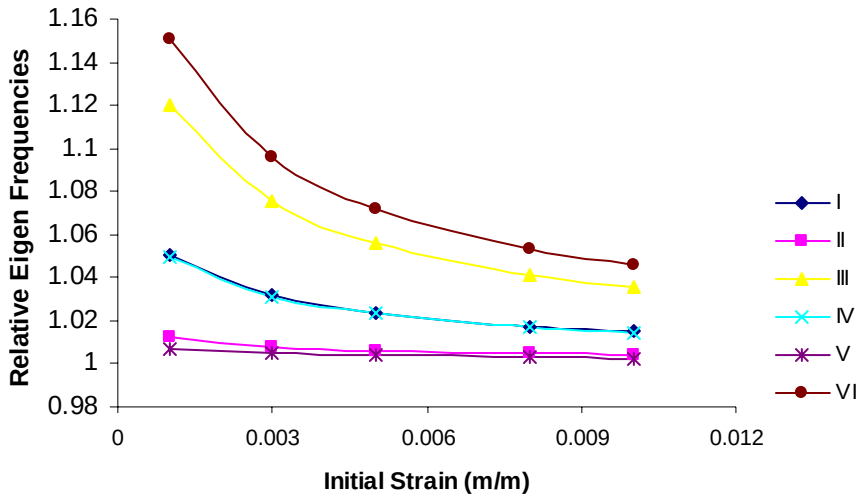

Figure 5.38 : The effect of initial strains of the SMA wires on the APT improvement of relative eigen frequencies for SS SMA composite plates

However since the recovery stress is increased as the initial strain is increased and with the decrease in the Young's modulus at the same time, the effect of SMA in the ASET improvement can be seen to either increase or decrease as the initial strain is increased. This fact can be seen in figure 5.39, 5.41 and 5.43 for the cases of SS, SC and CC boundary conditions respectively. In most cases the mode I is increased while mode III

and IV are decreased as the initial strain is increased. Other modes seem to have little effect.

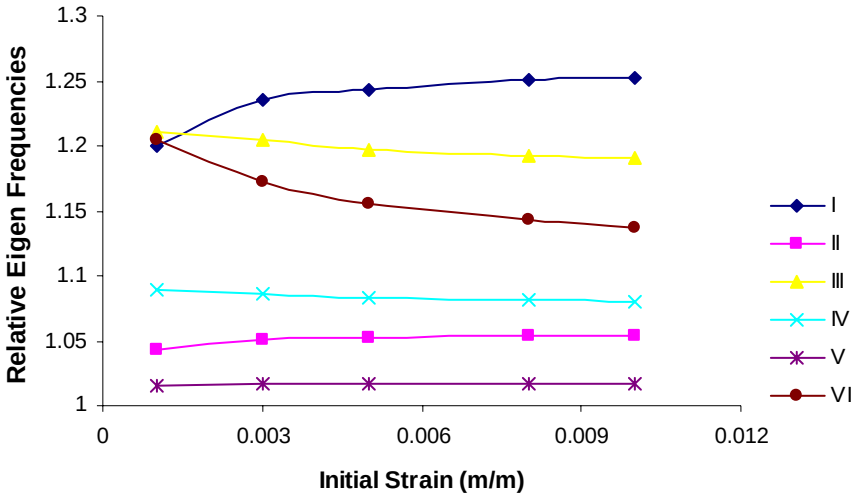

Figure 5.39 : The effect of initial strains of the SMA wires on the ASET improvement of relative eigen frequencies for SS SMA composite plates

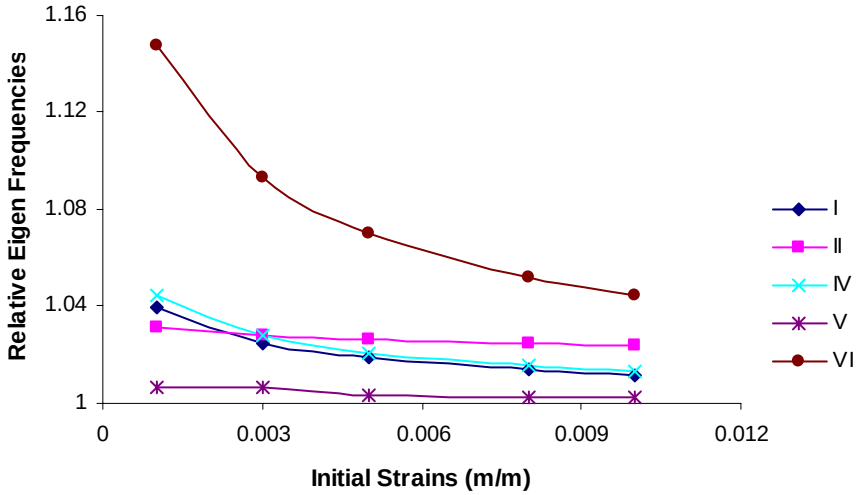

Figure 5.40 : The effect of initial strains of the SMA wires on the APT improvement of relative eigen frequencies for SC SMA composite plates

Typically, the effect of SMA is at the greatest in the case of SS boundary condition where for ASET improvement of mode I, the relative eigen frequencies can be up to 1.25 as compare to only 1.2 and 1.15 for the case of SC and CC boundary conditions respectively.

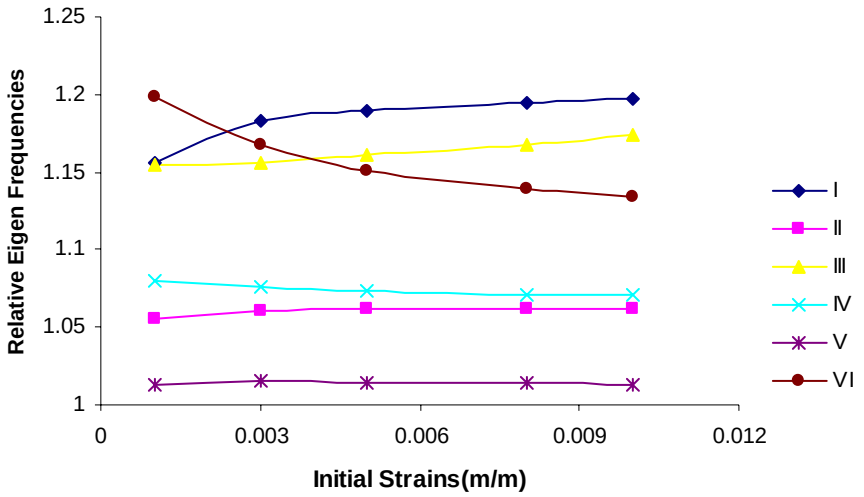

Figure 5.41 : The effect of initial strains of the SMA wires on the ASET improvement of relative eigen frequencies for SC SMA composite plates

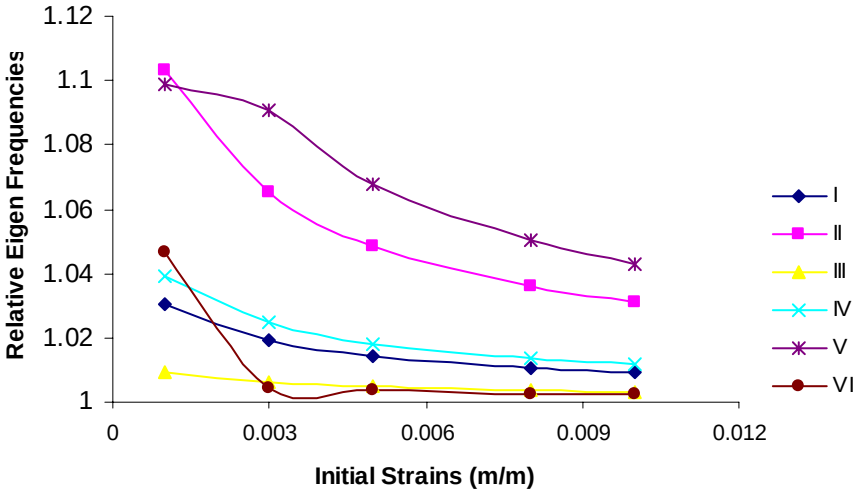

Figure 5.42 : The effect of initial strains of the SMA wires on the APT improvement of relative eigen frequencies for CC SMA composite plates

Figure 5.43 shows that as in the previous study the more dominant effect of SMA on the relative eigen frequencies of mode II and IV.

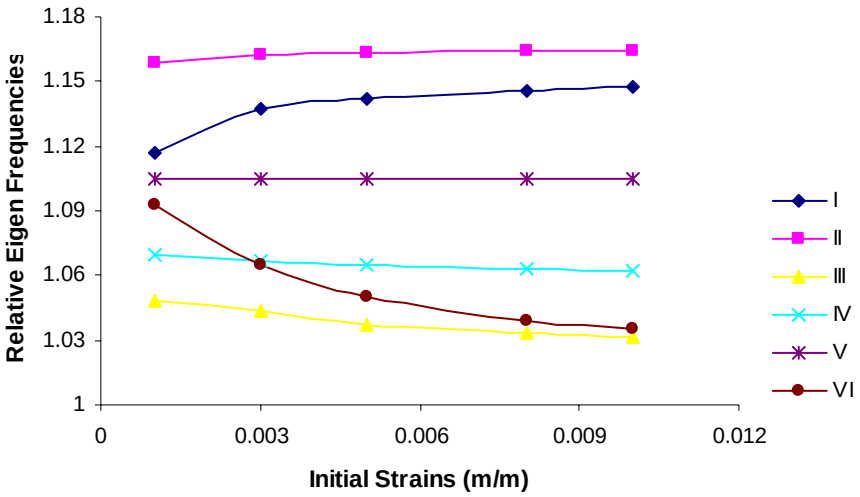

Figure 5.43 : The effect of initial strains of the SMA wires on the ASET improvement of relative eigen frequencies for CC SMA composite plates

5.3.6 The effect of SMA fibres orientation angles

As in the case of buckling analysis, the effect of SMA orientation angles on the improvement of relative eigen frequency can be studied by changing the angle of orientations of the SMA fibres. Here the effects of the orientation angles of the SMA fibres in the cases of anti-symmetric and symmetric composites are also studied. Again the configurations of $[0/(\theta/-\theta)_4/0]$ and $[0/(\theta/-\theta)_2]_s$ correspond to anti-symmetric and symmetric composites are used here. Both composites have the same number of layers. The angle of θ varies from 0^0 to 90^0 and only SS boundary condition is applied here.

The effect of orientation angle is strongly influenced by the change in Young's modulus and the presence of recovery stress. For APT improvement where only the effect of Young's modulus takes place, figure 5.44 shows that the mode I relative eigen frequencies are maximum at 45^0 for both symmetric and antisymmetric composite. Notice the difference between the two curves at temperatures between 0 and 15 degrees and 75 and 90 degrees. Furthermore the maximum relative eigen frequency for

antisymmetric composite is higher than the maximum relative eigen frequency for symmetric composite. Figure 5.45 and 5.46 show the effect of the angle orientation of the SMA wires to the first sixth relative eigen frequency modes for antisymmetric and symmetric composite respectively, in the case of APT improvement.

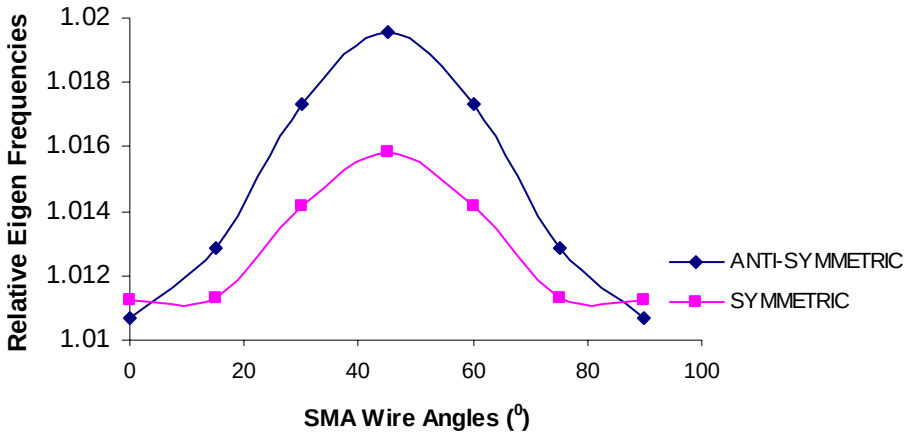

Figure 5.44: The effect of orientation angle on the APT improvement of mode I relative eigen frequencies for SS SMA composite plates.

With the existence of recovery stress in the ASET improvement, the trend for the effect of orientation angle has reversed to curves with minimum values such as shown in figure 5.47. Now the minimum eigen frequency value for the symmetric composite is lower than that of the antisymmetric composite. Figure 5.48 and 5.49 show the effect of the angle orientation of the SMA wires to the first sixth relative eigen frequency modes for antisymmetric and symmetric composite respectively, in the case of ASET improvement.

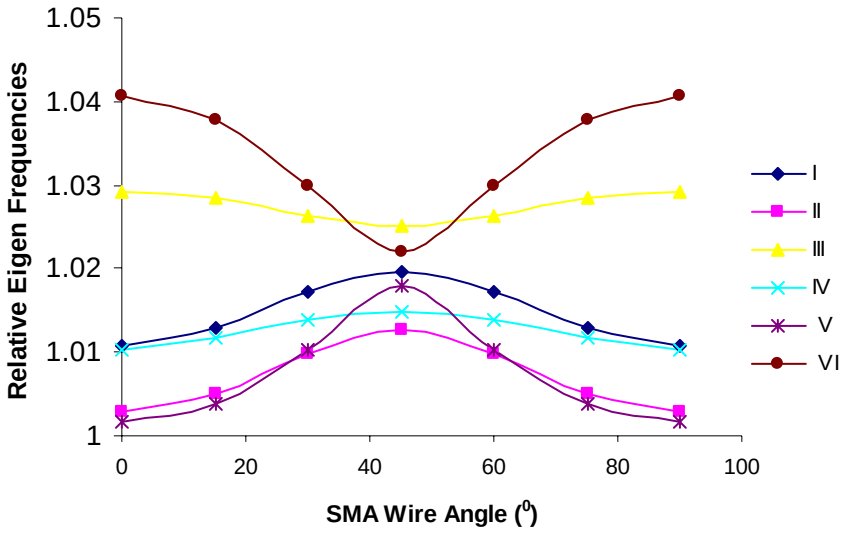

Figure 5.45: The effect of orientation angle on the APT improvement of the relative eigen frequencies for SS antisymmetric SMA composite plates.

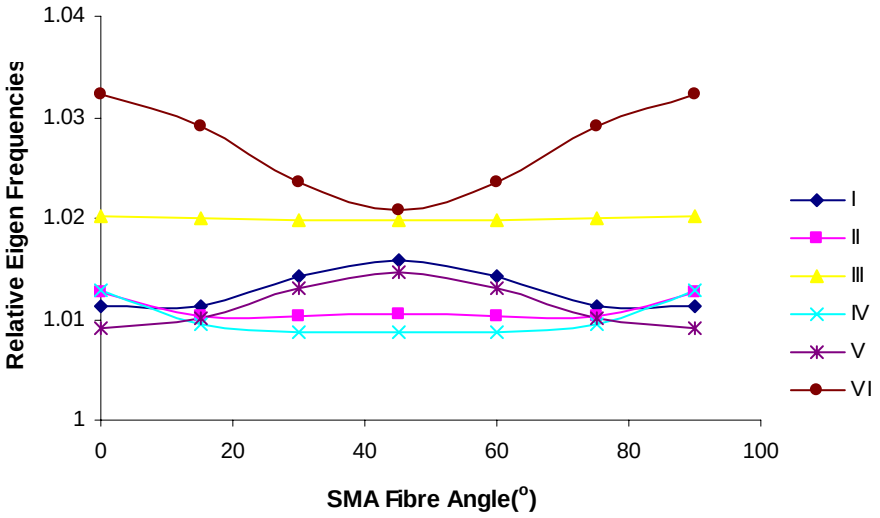

Figure 5.46: The effect of orientation angle on the APT improvement of the relative eigen frequencies for SS symmetric SMA composite plates

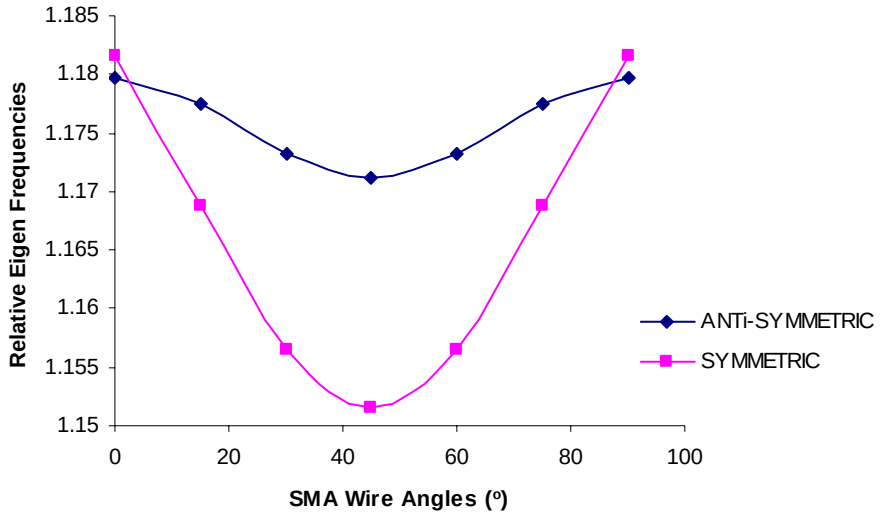

Figure 5.47: The effect of orientation angle on the ASET improvement of mode I relative eigen frequencies of SS SMA composite plates.

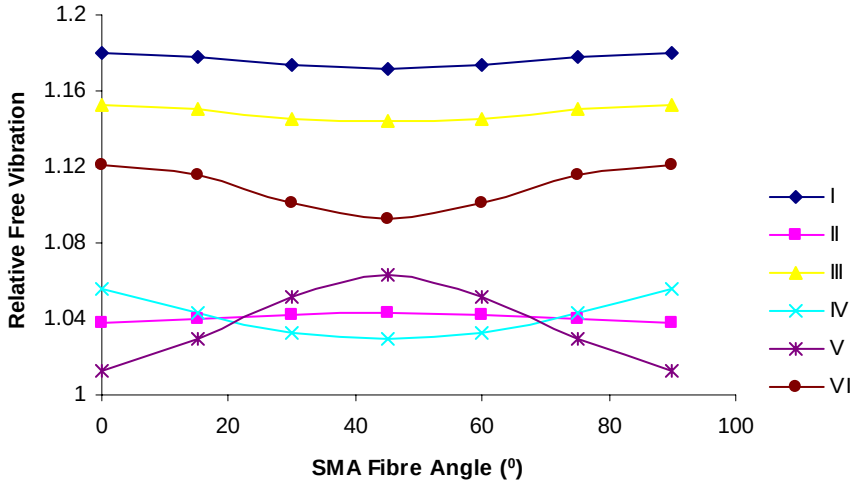

Figure 5.48: The effect of orientation angle on the ASET improvement of the relative eigen frequencies for SS antisymmetric SMA composite plates

The switch from concave up curve to concave down curve as the recovery stress effect is added such as shown in figures 5.44 and 5.47 can be understood in the following study.

Assuming at fully transformed state (E=69.9 GPa), for different values of initial strains, we can have a set of corresponding values of recovery stresses.

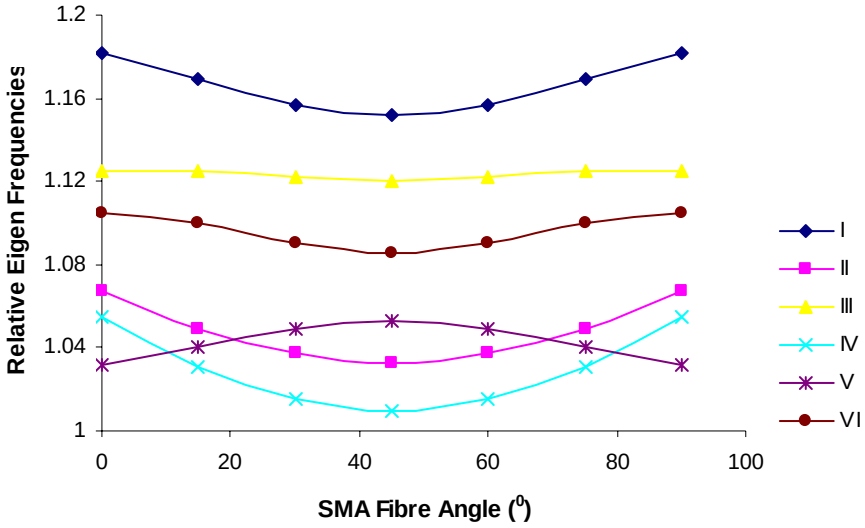

Figure 5.49: The effect of orientation angle on the ASET improvement of the relative eigen frequencies for SS symmetric SMA composite plates

Figure 5.50 shows that as the recovery stress is added to the symmetric SMA composite, the relative eigen frequencies vs orientation angle curve changes from having concave up to concave down quite early i.e. only after the recovery stress is equal to 75 MPa. In contrast, the antisymmetric SMA composite requires a higher value of recovery stress of 125 MPa for the relative eigen frequencies vs orientation angle curve to change from having concave up to concave down curve such as shown in figure 5.51.

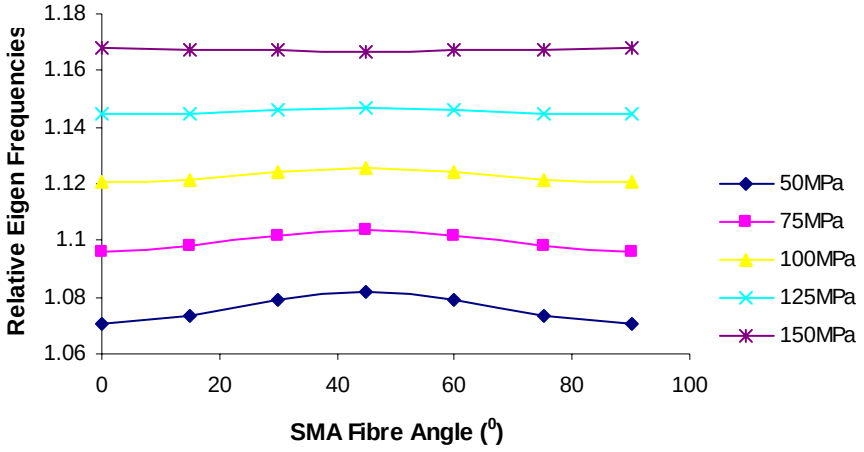

Figure 5.50: The effect of orientation angle on the ASET improvement of the mode I relative eigen frequencies of the SS antisymmetric SMA composite plates for different values of recovery stresses.

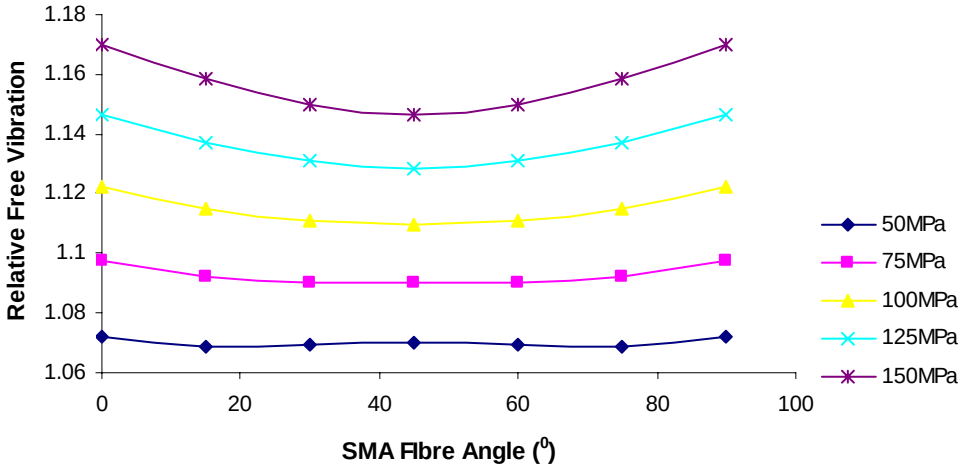

Figure 5.51: The effect of orientation angle on the ASET improvement of the mode I relative eigen frequencies of the SS symmetric SMA composite plates for different values of recovery stress.

5.2.7 The effect of the locations of the SMA layers

In this study, two SMA layers are located symmetrically with respect to mid- surface of the SMA composite as in previous studies. However the distance between the two SMA layers is now varied to see its effect on the eigen frequencies of the SMA composite

plates. Here the fully recovered SMA with initial strain of 0.001 m/m that gives recovery stress of 91.6 MPa and Young's modulus of 69.6 GPa is used.

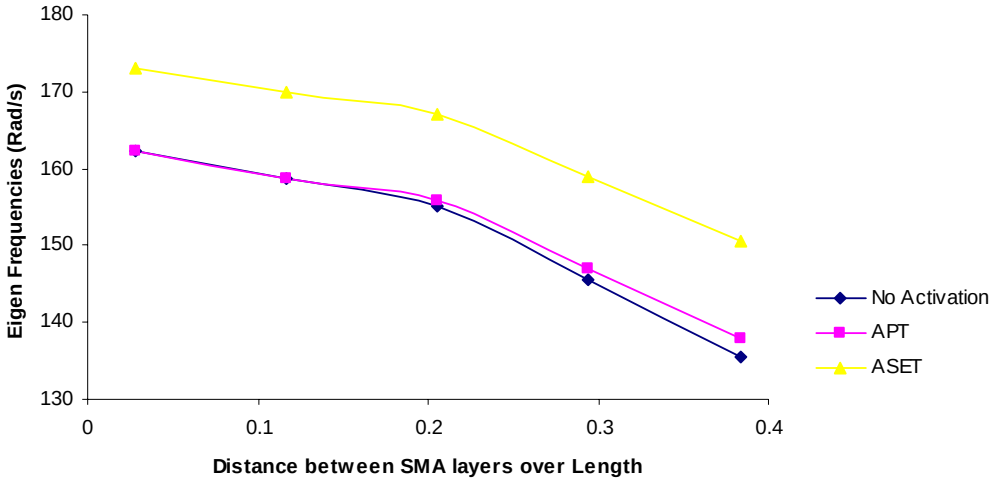

Figure 5.52: The effect of the distance between SMA layers on mode I eigen frequency for SS antisymmetric SMA composite plates

Figure 5.52 shows that in each cases of no activation, APT and ASET improvements, as the distance between SMA layers are increased, the eigen frequencies are decreased. However at the same time, the relative eigen frequencies are increased as the distance between SMA layers are increased. This can be seen in figure 5.53 and 5.54 where this behaviour is followed by all six modes of eigen frequencies in the APT and ASET improvements respectively.

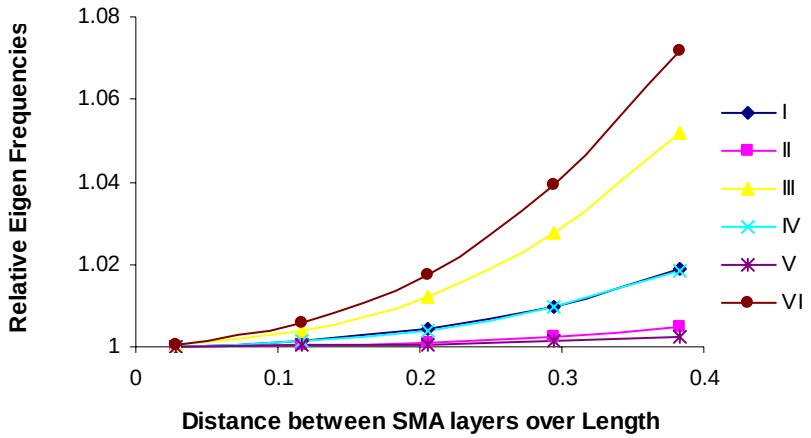

Figure 5.53: The effect of the distance between SMA layers on the APT improvement of the first six eigen frequencies for SS antisymmetric SMA composite plates

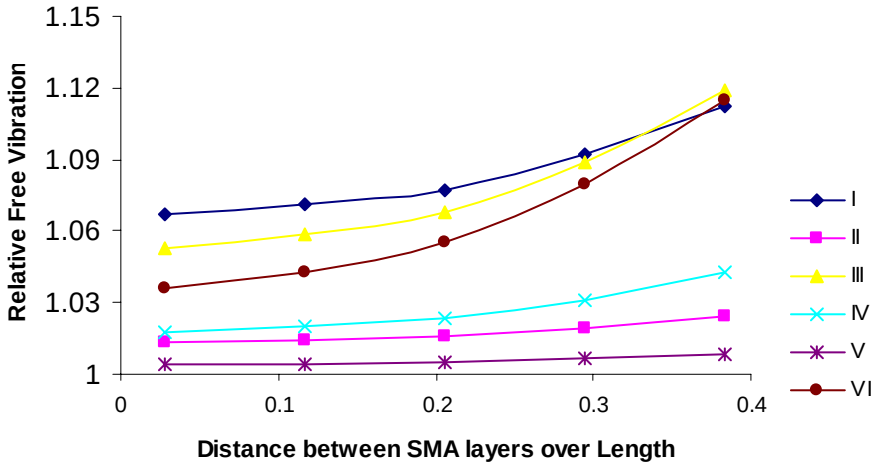

Figure 5.54: The effect of the distance between SMA layers on the ASET improvement of the first six eigen frequencies for SS antisymmetric SMA composite plates

5.2.8 Conclusion to the vibration analysis

A simple linear finite element model for SMA composite plates was developed to study the effect of SMA on free vibrations of composite plates. As in buckling analysis, an additional geometric stiffness matrix is used to represent recovery stress in this model while the values of SMA Young's modulus and recovery stress were pre-determined from the Brinson's model through either constrained or controlled recovery assumptions. Studies were conducted to see the effect of geometric, mechanical and transformation

factors on the APT and ASET improvements of relative eigen frequencies of SMA composite plates. Several conclusions can be made here.

1. In general it can be stated that there are three trends of response behaviour of the relative eigen frequencies (TRREF). Firstly the effect of SMA seems to be of a similar level for certain modes of frequencies. Typical couples with similar level of responses are frequencies of modes I and IV, II and V and III and VI.
2. Secondly, frequency couples of modes I and IV and III and VI seem to have greater responses as compared to the couple of mode II and V in SS and SC boundary condition while in CC boundary condition, the couple of modes II and V seems to be dominant .
3. Thirdly, the couple of modes I and IV seems to have almost exact responses between them in the case of APT improvement of SS SMA composite plates.
4. In general as the ratios of SMA thickness to thickness of other layers are increased, the relative eigen frequencies are increased too, following the three TRREF. For example, the increase of the eigen frequencies for mode III and VI can be up to 1.25 times at SMA layer thickness equal to one fifth of the thickness of other layers.
5. The glass fibre responses the greatest to the effect of SMA on the eigen frequencies of the SMA composite plates. This is because as in the buckling analysis the ratio of the Young's modulus of the glass fibre to the Young's modulus of nitinol is the lowest of all ratios that involve other fibres.
6. In general, following the three TRREF, the increase in the thickness to length ratio of the G-E layers will result in the decrease of the effect of SMA on the eigen

frequencies of the SMA plates. This is due to the increase of the volume fraction of the glass fibre as the thickness to length ratio is increased.

7. It can be stated that the effect of volume fraction of SMA wires on the relative eigen frequencies of the SMA plates is in reverse to the effect of TLR on the relative eigen frequencies. Again, following the TRREF, it shows that as the volume fraction of the SMA increases, the effect of SMA on the APT and ASET improvements increases.
8. The presence of coupling stiffness of the composite enhances the effect of SMA on the eigen frequencies of SMA composite plates. As the number of layers is increased i.e. as the bending-stiffness coupling is reduced, the relative eigen frequencies are reduced too. The TRREF are still followed for the case of SS boundary condition
9. In general, following the three TRREF as the activation temperature is increased, the effect of SMA on eigen frequencies is increased too since the Young's modulus of the SMA and the recovery stress are increased. However the effect of SMA can be seen to increase greatly between certain SMA activation temperatures where martensite transformation occurs greatly.
10. As in buckling analysis, the increase of initial strains of the SMA at a fixed value of an activation temperature will cause the increase in the recovery stress and the decrease in the Young's modulus. As a result, the relative eigen frequencies for APT improvement are seen to be decreasing as the initial strains are increased while the relative eigen frequencies for ASET improvement can be increased or decreased as the initial strains are increased.
11. The effect of orientation angle on the relative eigen frequencies is strongly influenced by the change of Young's modulus and the presence of recovery stress. In APT

improvement, the relative eigen frequencies of mode I are maximum at the angle orientation of 45^0 for both symmetric and anti-symmetric composites. With the addition of the recovery stress effect in ASET improvement, the relative eigen frequencies of mode I vs orientation angle curve changes from having a maximum value to having a minimum values as the recovery stress is increased.

12. The change in the distance between the two SMA layers affects the eigen frequencies and the relative eigen frequencies. While the eigen frequencies of mode I are decreased as the distance is increased, the relative eigen frequencies are increased.
13. In all cases, as in the buckling analysis, the SMA effect in ASET improvement is much more significant than the SMA effect in the APT improvement.

Finally it can be concluded here that the simple finite element model was able to show the influence of SMA in the free vibration improvement of SMA composite plates.

CHAPTER 6

CONCLUSION AND RECOMMENDATION

6.1 Conclusion

A finite element program was developed to study buckling behaviour of laminated composite plate. Critical buckling loads were calculated through the eigen-value analysis employing the inverse power method. The post-buckling responses were obtained by applying the Newton-Raphson algorithm onto the non-linear formulation that includes the von-Karman non-linear terms. Buckling behaviour of the laminated composite plate was studied by varying factors such as plate thickness, angle of lamination, fiber orientation, boundary condition and level of anisotropy. Several buckling behaviour can be concluded based on this study.

- The effect of extensional-bending coupling is significant as it causes the difference between the behaviour of the symmetric and anti-symmetric composites. The existence of coupling effects will weaken the composite. In general, for two composites that differ only for being symmetric and anti-symmetric, the symmetric composite will have a higher buckling load. However, this is only true for composites with small number of layers (2 – 4 layers). The coupling effect rapidly decreases as the number of layer increases.
- Buckling load decreases at quite a rapid rate as the thickness is decreased. As the aspect ratio changes from the ratio of 10 to 20, the increase of the non-

dimensionalised buckling load is 27.3%. The increase however decline to 9.7% moving from the ratio of 20 to 30.

- The effect of lamination angle is great so a designer can tailor the property of a composite by controlling the angle of lamination. Knowing the meaning of each term in the A, B, D, E, F and G matrices the designer can control the required properties to the desired level. In the case of buckling of anti-symmetric composite in this study, the optimum lamination angle that givesthe composite the highest buckling load is 45^0.
- The stiffness of the composite can also be controlled by controlling the Young Modulus of the fibre and the matrix. Increasing the level of anisotropy will increase the stiffness of the composite and the coupling effects as well.
- The non-linear responses in most cases in this study show very close agreement to the eigen-value analysis conducted. Angle-ply composites weather symmetric or anti-symmetric posses stable post-buckling behaviour. However the non-linear response for anti-symmetric cross-ply composite does not show a clear bifurcation point. The effect of coupling seems to relax the stress, making the curve looks like having imperfection from the beginning of the curve.
- The post-buckling behaviour shows similar patterns for thin or thick composites. While the buckling loads for angle-ply composites are very sensitive to imperfection, the anti-symmetric cross-ply composites show the opposite behaviour. In all cases where bifurcation points are clear, the non-linear curves show little effect of pre-buckling deformation unless imperfection is present.

6.2 Recommendations

The work in this thesis can be extended to include other factors.

- Fibre reinforced composite is well known to posses at least one material non-linearity in the shear direction. Thus the effect of material non-linearity should be studied especially in matrix-dominated composites where high ductility is desired. The study on buckling analysis that includes the effect of material non-linearity is rather rare.
- The effect of damages such as delamination of layers of composites on buckling and post-buckling behaviour can be significant. The addition of this factor will be useful to the industry.
- Similar studies on the buckling and post-buckling behaviour can be conducted using different geometries such as shells and corrugated shape. These two geometries offer wide applications in the industries today.
- The study of buckling and post-buckling can be extended to other materials such as smart materials. The advantages offer by smart materials are getting popularly utilised that studies on failures such as buckling should be conducted.
- The study should also be extended to include hygro-thermal effects especially the moisture effect, as it is relevant considering the weather where the structure is used.

1. Jones, R.M. 1974. *Mechanics of Composite Materials*, New York: McGraw-Hill Book Company.
2. Hyer, M.W. 1998. *Stress Analysis of Fibre-Reinforced Composite Materials*, New York: McGraw-Hill Book Company
3. Mantovanni, D. 2001. SMA: properties and biomedical applications, JOM. 52 : 36-44.
4. Jia, J. and Rogers, C.A. 1992. Formulation of a mechanical model for composites with embedded SMA actuators, *J. Mech. design*. 114 : 670-676.
5. Otsaka, K. and Kakeshita, T. 2002. Science and technology of SMA: New developments, MRS Bulletin. 2 : 91-100.
6. Wei, Z.G., Tang, C.Y. and Lee, W.B. 1997. Design and fabrication of intelligent composites based on SMA, *J. Mater. Proc. Technol*. 69 : 68-74.
7. Y. Liu, Detwinning process and its anisotrophy in SMA, Proceedings of SPIE, 2001, 4234, 82-93.
8. Thompson, S.P. & Loughlan, J. 2001, Enhancing the post-buckling response of a composite panel structure utilising shape memory alloy actuators- a smart structural concept. *Composite structures*, 51: 21– 36.
9. Michaud, V. 2003. Can shape memory alloy composites be smart?. *Scripta Materialia.* Vol 50(2); 249-253.
10. M.V. Gandhi, B.S. Thompson, Smart materials and structures, Chapman & Hall, 2000.
11. Jones, R. M. 1973. Buckling and vibration of unsymmetrically laminated cross-ply rectangular plates. *AIAA Journal*, 11(12): 1626-1632.
12. Whitney, J.M. 1987. *Structural Analysis of Laminated Anisotropic Plates*, Lancaster: Technomic Publishing Co.
13. Srinivas, S. & Rao, A.K. 1970. Bending, vibration and buckling of simply supported thick orthotropic rectangular plates and laminates. *International Journal of solid & Structures*, 6: 1463-1481
14. Pagano, N. J. 1969. Exact solutions for composite laminates in cylinderical bending. *Journal of Composite Materials*, 3(3): 398-411
15. Kam, T.Y. & Chang, R.R. 1992. Finite element analysis of shear deformable laminated composite plates. *Composite Material Technology*, 45 : 133-139.
16. Leissa, A.W. 1995. Buckling and post-buckling theory for laminated composite plates. Turvey, G.J. & Marshal, I.H. (edit). *Buckling and Post-buckling of Composite Plates*: 1-29. London: Chapman & Hall.
17. Lo, K.H., Christensen, R.M. & Wu, E.M. 1977. A higher order theory of plate deformation. *Journal of Applied Mechanics*, Dec 77: 669-676.
18. Reddy, J.N. 1984. A simple higher-order theory for laminated composite plates. *Journal of Applied Mechanics*, 51: 745-752.
19. Reddy, J.N. 1989. On refined computational models of composite laminates plates. *International Journal of Numerical Methods in Engineering*, 27: 361-382.
20. Moita, J.S., Soares, C.M. & Soares, C.A. 1995. Buckling and dynamic behaviour of laminate composite plates using a discrete higher order displacement model. *Advances analysis and design of composites*, Edinburg : Civil-Comp Press.
21. Zabaras, N. & Pervez, T. 1990. Viscous damping approximation of laminated anistropic composite plates using the finite element method. *Computer methods in applied mechanics and engineering*, 81: 291-316.
22. Phan, N.D. & Reddy, J.N. 1989. Analysis of laminated composite plates using a higher-order shear deformation theory. *International Journal for Numerical Methods in Engineering*, 21: 2201-2219.

23. Noor, A.K. & Peters, J.M. 1989. Buckling and post-buckling analysis of laminated anisotropic structures. *International Journal for Numerical Methods in Engineering*, 27 : 383-401.
24. Reddy J.N. & Khdeir, A.A. 1989. Buckling and vibration of laminated composite plates using various Plate Theories. *AIAA Journal*, 27(12) : 1808-1723.
25. Kozma, F. & Ochoa, O. 1986. Buckling of composite plates using shear deformable finite elements. *AIAA Journal*, 24 : 1721-1723.
26. Luccioni, L.X. & Dong, S.B. 1998. Levy-type finite element analyses of vibration and stability of thin and thick laminated composite rectangular plates. *Composite Part B*, 29B : 459-475.
27. Shankara, C.A. & Iyengar, N.G. 1993. A finite element model for the thermo-mechanical buckling analysis of composite plates. *Composite Material Technology*, 53 : 293-301.
28. Chen, R.R. & Mei, C. 1994. Thermo-mechanical buckling and post-buckling of composite plate using MIN3 Eeement. Noor, A.K. (edit). *Buckling and Postbuckling of Composite Structure* : 39-53. New York : ASME Press
29. Reddy, J.N. 1984. A Refined nonlinear theory of plates with transverse shear deformation. *International Journal of Solids and Structures*, 20(9-10) : 881-896.
30. Chandrashekhara, K. & Bangera, K.M. 1991. Geometrically nonlinear analysis of cross-ply composite beams under transverse loading. *Composite Material Technology*, 37 : 237-241.
31. Kapania, R.K. & Raciti, S. Recent advances in analysis of laminated beams and plates, Part 1: Shear effects and buckling. *AIAA Journal*, 7(7) : 923-934.
32. Noor, A.K. 1994. Finite element buckling and postbuckling analysis of composite structure. Turvey, G.J. & Marshal, I.H. (edit). *Buckling and Post-buckling of Composite Plates*: 1-29. London : Chapman & Hall.
33. Stein, M. 1983. Post-buckling of orthotropic composite plates loaded in compression. *AIAA Journal*, 21(12) : 1729-1735.
34. Zhang, Y. & Matthews, F.L. 1984. Post-buckling behaviour of anisotropic laminated plates under pure shear and shear combined with compressive loading. *AIAA Journal*, 22(2) : 281-286.
35. Shiau, L.C. & Wu, T.Y. 1995. Application of the finite element method to post-buckling analysis of laminated plates. *AIAA Journal*, 33(12) : 2379-2385.
36. Barbero, E.J. & Reddy, J.N. 1990. Non-linear analysis of composite laminates using a generalised laminated plate theory. *AIAA Journal*, 38(11) : 1987-1994.

37. Otsaka, K. and Wayman, C.M. 1998. Mechanism of shape memory effect and superelasticity in Shape Memory Materials, Ed. K. Otsaka, C.M. Wayman, 27-49.
38. Funakubo, H. 1987. Shape memory alloys, Gordon and Breach Science Publication, Amsterdam.
39. Xu, Y., Otsuka, K., Yoshida, H., Nagai, H., Oshi, R., Horikawa, H. and Kishi, T. 2002. A new method for fabricating SMA/SFRP smart hybrid composites. *Intermetallics.* 10: 361-369.
40. Humbeeck, J.V. Non-medical applications of shape memory alloys, *Materials Science and Engineering A*, 273-275: 134-148.
41. Birman, V. 1997. Review of mechanics of shape memory alloy structures. *Applied mechanics review*, 50 (11) : 629-645.
42. Wada B.K., Fanson J.L. & Crawley E.F. 1990. Adaptive Structures. *Journal of intelligent material systems structures*, 1 : 157-174.

43. Rogers, C.A. 1993. Intelligent Material Systems - The Dawn of a New Materials Age. *Journal of Intelligent Material Systems and Structures*. 4(1): 4-12.
44. Tanaka, K. 1990. A phenomenological description on thermomechanical behaviour of SMA, *J. App. Mecha.* 112 :158-163.
45. Liang, C. and Rogers, C.A. 1990. One-dimensional thermo-mechanical constitutive relations for shape memory materials, *J. Intel. Mater. Sys. Struct.* 1 : 207-1234.
46. Brinson, L.C. 1990. Constitutive behaviour of SMA: One-dimensional thermo-mechanical derivation with non-constant material functions and redefined martensite internal variable, *J. Mater. Devices.* 1: 729-743.
47. Ford, D.S., Hebda, D.A. and White, S.R. 1995. Constitutive and transformation behaviour of TWSM Nitinol. *Active Materials and Smart Structures.* 2427:218-233.SPIE.
48. Lagoudas, D.C. & Tadjbakhsh, I.G. 1992. Active flexible rods with embedded SMA fibres. *Smart Material Structure*. 1: 162-167.
49. Bhattacharyya, A. & Lagoudas D.C. 1997. A stochastic thermodynamics model for a gradual thermal transformation of SMA polycrystals. S*mart material structures.* 6: 235-250.
50. Lagoudas D.C. & Bhattacharyya, A. 1998. Modelling of thin layer extensional thermoelectric SMA actuators. *International journal of solid and structures.* 35: 331-362.
51. Shu, G.S., Lagoudas D.C., Hughes, D. & John, W.T. 1997. Modelling of a flexible beam actuated by SMA wires. S*mart material structures.* 6: 265-277.
52. Achenbach, M. 1989. A model for an alloy with shape memory. *International Journal for Plasticity*. 5: 371-395.
53. Achenbach, M. & Müller, I. 1982. A model for shape memory. *J de Phys Colloque C4*. 12: 163-167.
54. Müller, I & Xu, H. 1991.On the pseudo-elastic hysteresis, *Acta Metallurgica et Materialia.*. 39(3): 263-271.
55. Seelecke, S. 2002. Modeling the dynamic behavior of shape memory alloys. *International Journal of Non-Linear Mechanics*. 37(8): 1363-137.
56. Rogers, C.A., Liang, C. and Jia, J. 1991. Structural modification of simply supported laminated plates using embedded shape memory alloy fibres. *Computer and structures.* Vol 38 (5-6); 569-580.
57. Yoshida, I., Ono, T. and Asai, M. 2000. Internal friction of Ti-Ni alloys, *J. Alloys Compound.* 310: 339-343.
58. Zak, A., Cartmell, M.P. and Ostachowicz, W. 2003. Dynamics of a multilayered composite plates with SMA wires. *Journal of Applied Mechanicss*. 470 313– 327.
59. Song,G., Kelly, B. and Agrawal, B.N. 2000. Active position control of a SMA wire actuated composite beam, *Smart Mat. Struc.* 9 : 711-716.
60. Icardi, U. 2001. Large bending actuator made with SMA contractile wires: theory, numerical simulation and experiments, *Comp. Eng.: Part B.* 32 : 259– 267.
61. Wang, G. and Shahinpoor, M. 1997. Design, prototyping and computer simulations of a novel large bending actuator made with a shape memory alloy contractile wire, *Smart Mat. Struc.* 6 : 214-221.
62. B.J. de Blonk, D.C. Lagoudas, Actuation of elastomeric rods with embedded two-way SMA actuators, Smart Mat. Struc. 7 (1998) 771-783.
63. S.G. Shu, D.C. Lagoudas, D. Hughes, J.T. Wen, Modelling of a flexible beam actuated by SMA. Smart Mat. Struc. 6 (1997) 265-277.

64. Moallem, M. 2003. Deflection control of a flexible beam using SMA actuators, *IOP*. 12 : 1023-27.
65. Seelecke, S. 1997. Control of beam structures by shape memory wires, Proceedings of the 2nd Sci. Conf. on Smart Mechanical Systems – Adaptronics, 33-42.
66. Chaudhry, Z. and Rogers, C.A. 1991. Bending and shape control of beams using SMA actuators, *J. Intel. Mat. Sys. Struct.* 2 : 581-602.
67. Chaudhry, Z and Rogers, C.A. 1991. Response of composite beams to an internal actuator force. J. of Mech. Design – Trans. of the ASME., 114, 343-348.
68. Baz, A., Chen,T. and Ro, J. 2000. Shape control of nitinol reinforced composite beams, *Comp. Engin.: Part B.* 31: 631-642.
69. Choi, S. and Lee, J.J. 1998. The shape control of a composite beam with embedded SMA wire actuators, *Smart Mat. Struc.* 7 :759-770.
70. Choi, S., Lee, J.J., Seo, D.C. and Choi, S.W. 1999. The active control of laminated composite beams with embedded SMA wires. *Composite Struc.* 47 :679– 686.
71. C. Kim, B.S. Park, N.S. Goo, Shape changes by coupled bending and twisting of SMA embedded composite beams, Smart Mat. Struc. 11 (2002) 509-526.
72. Chandra. R. 20001. Active shape control of composite blades using shape memory actuation. Smart Mat. Struc. 10 : 1018-1024.
73. Roglin, Hanagud. A helicopter with adaptive rotor blades for collective control, Smart Mat. Struc. 5 (1996) 76-88.
74. Brinson, L.C. and Lammering, R. 1992. FEA of the behaviour of SMA and their applications, Int. J. Sol. Struc. 30 : 3261-3280.
75. M.M. Ghomshei, A. Khajepour, N. Tabandeh, K. Behdinan, Finite element modeling of SMA composite actuators: Theory and experiment, J. Intel. Mat. Sys. Struc. 12 (1996) 761-773.
76. J. Epps, Chandra. SMA actuation for active tuning of composite beams, Smart Mat. Struc. 6 (1997) 251-264.
77. Baz,A., Poh, S., Ro,J. and Gilheany, J. 1995. Control of natural frequencies of nitinol reinforced composites beams, J. Sound Vib. 185: 171-185
78. K.T. Lau, L.M. Zhou, X.M. Tao, Control of natural frequencies of a clamped-clamped composite beam with embedded SMA wires, Compos. Struc. 58(2002) 39– 47.
79. X.Y. Tsai, L.W. Chen, Dynamic stability of SMA wire reinforced composite beam, Compos. Struc. 56 (2002) 235-241.
80. M.M.R. Rasani, Free vibration modelling of a thin plate internally constrained through a SMA wire. A Master Thesis, University Kebangsaan Malaysia, 2002.
81. Baz,A., Iman, K. and Mc Coy, J. 1990. Active vibration control of flexible beams using SMA, *J. Sound Vib.* 140 :437-456.
82. K.T. Lau, Vibration characteristics of SMA composite beams with different boundary conditions, Mater. Design. 23 (1990) 741-749.
83. Baz,A., Poh, S. and Gilheany, J. 1993. A multimode distributed sensors for vibrating beams, *J. Sound Vib.* 165:481-495
84. E.R. Oberaigner, F.D. Fischer, K. Tanaka, On the Optimal Damping of a Vibrating SMA Rod, J. Eng. Mat. Tech. 124 (2002) 97-102.
85. Q. Chen, C. Levy, Active vibration control of elastic beam by means of SMA layers, Smart Mat. Struc. 5 (1996) 400-406.
86. Q. Chen, C. Levy, Vibration analysis and control of flexible beam by using smart damping structures, Compos. Part B: Eng. 30 (1999): 395-406.

87. Baz, A., Ro, J., Mutua, M. and Gilheany, J. 1992. Active buckling control of nitinol-reinforced composite beams, SPIE conference, 10, 167-176
88. S. Choi, J.J. Lee, D.C. Seo, S.W. Choi, The active buckling control of laminated composite beams with embedded SMA wires, Compos. Struc. 47 (1999) 679–686.
89. Choi, S. Lee, J.J. and Seo, D.C. 2000. Study on the buckling and postbuckling control of composite beams with embedded NiTi actuators, *J. Compos. Mat.* 34:1494-1510.
90. Thompson, S.P. & Loughlan, J. 2000. The control of the post-buckling response in thin composite plates using smart technology. *Thin walled structures*. 36: 231–263.
91. Loughlan, J., Thompson, S.P. & Smith, H. 2002. Buckling control using embedded shape memory actuators and the utilisation of smart technology in future aerospace platforms. C*omposite structures*. 58: 319– 347.
92. Zhong, Z.W., Chen, R.A. & Mei, Chuh. 1994. Buckling and post-buckling of shape memory alloy fiber-reinforced composite plates. : Buckling and postbuckling of composite structures ASME AD-vol 41 / PVP-Vol. 293: 115-133.
93. Cross, W.B., Kariotis, A.H. and Stimler, F.J. 1970. Nitinol Characterization Study, NASA,CR-1433,Hampton,Virginia,1970.
94. Duan, B., Tawfik, M., Goek, S.N., Ro, J.J. & Mei, C. 2002. Analysis and control of large thermal deflection of composite plates using shape memory alloy. *Proceedings of SPIE - The International Society for Optical Engineering*, 3991 :346-357
95. Duan, B., Tawfik, M., Goek, S.N. , Ro, J.J. & Mei, C. 2002. Vibration of laminated composite plates embedded with shape memory alloy at elevated temperatures *Proceedings of SPIE - The International Society for Optical Engineering*, 3991 :366-376.
96. Tawfik, M. 1999. Suppression of post-buckling deflection and panel-flutter shape memory alloy. Master Thesis, Old Dominion University.
97. K. Otsaka, K. C.M. Wayman, Mechanism of shape memory effect and superelasticity in Shape Memory Materials, Ed. K. Otsaka, C.M. Wayman, 1998, 27-49.
98. Y. Huo, I. Müller, S. Seelecke, Phase transition and hysteresis in Lecture Notes in Mathematics, Ed. A. Visintin, Springer Verlag, 1993, 89-148.
99. Hornbogen, SMA in Advanced structural and functional materials, Ed. W.G.J. Bunk, 1991, 133-163.

100.
101.
102. E.
103.

104. Müller, I and Seelecke, S. 2001. Thermodynamic aspects of shape memory alloys. *Mathematical and Computer Modelling*. 34(12-13): 1307-1355.
105. Thompson, S.P. and Loughlan, J. 1997. Adaptive post-buckling response of carbob fibre composite plates employing SMA actuators. C*omposite structures*. 38; 667– 678
106. J.D. Jonnalagada, N.R. Sottos, M.A. Qidwai, D.C. Lagoudas, Transformation of embedded SMA ribbons, J. Intel. Mat. Sys. Struc. 9 (1998) 1-23

107. P. Sittner, R. Stalmans, Developing hybrid polymer composites with embedded SMA wires, JOM. 52 (2000) 15-20.
108. Y. Zheng, L. Cui, Y. Li, R. Stalmans, Partial transformation behavior of prestrained
109. K.A. Tsoi, R. Stalmans, J. Schrooten, Transfor-mational behaviour of constrained SMA, Acta Materialia. 50 (2002) 3535-3544.
110. Thompson, S.P. & Loughlan, J. 2001. Enhancing the post-buckling response of a composite panel structure utilising shape memory alloy actuators- a smart structural concept. C*omposite structures*. 51: 21– 36.

111. Zak, A., Cartmell, M.P., Ostachowicz, W.M.& Wiercigroch, M. 2003. One-dimensional shape memory alloy models for use with reinforced composite structures. *Smart Materials and Structures*. 12: 338– 346.
112. Zienkiewicz, O.C. & Taylor, R.L. 1989 & 1991. *The Finite Element Method*: Vols *1 and 2*, New York : McGraw-Hill Book Company.
113. Rogers, C.A. 1990. Active vibration and structural acoustic control of shape memory alloy hybrid composites: experimental results. *Journal of Acoustical Society of America.* 88:2803-2811.
114. Owen, D.R.J. & Hinton, E. 1980. *Finite Elements in Plasticity : Theory and Practice.* Swansea : Pineridge Press Limited .
115. Reddy,J.N. 2003.Mechanics of Laminated Composite Plates and Shells.:CRC Press.